Title	Study of solid electrolyte and solid-oxide galvanic-cells at steelmaking temperatures(Dissertation_全文)
Author(s)	Iwase, Masanori
Citation	Kyoto University (京都大学)
Issue Date	1979-03-23
URL	http://dx.doi.org/10.14989/doctor.r3816
Right	
Type	Thesis or Dissertation
Textversion	author

STUDY OF SOLID ELECTROLYTE AND SOLID-OXIDE GALVANIC CELLS AT STEELMAKING TEMPERATURES

BY

MASANORI IWASE

SEPTEMBER, 1978

CONTENTS

CHAPTER 1.

GENERAL INTRODUCTION

CHAPTER 2.

ELECTROCHEMICAL MEASUREMENTS OF STANDARD FREE ENERGIES OF FORMATION OF NiO, CoO AND MoO_2

CHAPTER 3

ELECTROCHEMICAL MEASUREMENTS OF OXYGEN IN LIQUID IRON, NICKEL AND IRON-NICKEL ALLOYS

CHAPTER 4

OXYGEN PERMEABILITY OF CALCIA-STABILIZED ZIRCONIA

CHAPTER 5

CHAPTER 1

GENERAL INTRODUCTION

The all crystalline inorganic compounds are inherently non-stoichiometric[1]. Stoichiometric compounds may be described in terms of isolated point defects, such as interstitial ions or vacancies in the lattice, and much is known regarding their effects on the electrical properties. An important system in which large deviations from stoichiometry determines the properties of materials is calcia-stabilized zirconia. The electrochemical measurement of oxygen potential in the present study is based on the conduction of oxygen ion in the calcia-stabilized zirconia.

ZrO_2 is stable in the monoclinic structure at room temperature[2] and is transformed into a tetragonal form at about 1323 K being accompanied by a volume contraction amounting 9 %. This undesirable thermal contraction can be eliminated by the addition of bivalent or trivalent oxides into the pure ZrO_2 and it will be expected that ZrO_2 have cubic structure[3]. The added oxide for this object and ZrO_2 thus treated are called a stabilizer and a stabilized zirocnia, respectively. The phase diagram of the system $CaO-ZrO_2$

shows that this system has cubic structure in some composition and temperature range, indicating that CaO can form a solid solution with ZrO_2[4-8]. In this case, chemical defects are necessary in order to preserve electrical neutrality in the solid solution. The probable structure model in such a case is an oxygen vacancy model : all metal ions being fixed at the normal lattice points. The validity of this model was experimentally demonstrated by Hund[9] by comparing the calculated density based on this model with that obtained by pychnometric measurement.

The existence of the oxygen-ion vacancy suggests the appearance of oxygen-ion conduction by vacancy mechanism in these solid solutions. It has been recognized that ionic conduction in calcia-stabilized zirconia is mainly due to oxygen-ion and the contribution of cationic conduction is negligibly small[10-13].

However, the electronic conduction in calcia-stabilized zirconia can not be neglected in some cases. The introduction of electronic defects into the electrolyte structure can be described as

$$O_2(g) + 2\,V_O^{\bullet\bullet} = 2\,O_O + 4\,h^{\bullet}, \quad [1]$$

$$2\,O_O = O_2(g) + V_O^{\bullet\bullet} + 4\,e', \quad [2]$$

where $V_O^{\bullet\bullet}$ is an oxygen-ion vacancy in normal site occupation with "plus" two charge relative to normal lattice site, O_O is an oxygen ion on an oxygen site, $h^{\bullet}$ is a positive hole, and e' is an excess electron (14). The concentration of the excess electron and positive hole must be affected by the surrounding oxygen partial pressure. When these concentrations are low and the interaction between the species in eqs.[1] and [2] is negligible, the application of mass action law to eqs. [1] and [2] yields in terms of concentration instead of activities;

$$\frac{[O_O]^2 [h^{\bullet}]^4}{[V_O^{\bullet\bullet}]^2 \; P_{O_2}} = K_h , \quad [3]$$

$$\frac{P_{O_2} \; [V_O^{\bullet\bullet}]^2 \; [e']^4}{[O_O]^2} = K_e , \quad [4]$$

where K_h and K_e are the equilibrium constants for the reactions [1] and [2], respectively.

The $P_{O_2}^{1/4}$ and $P_{O_2}^{-1/4}$ dependencies for the p-type and n-type electronic conductivity, $\sigma_{\oplus}$ and $\sigma_{\ominus}$, would be expected from eqs.[3] and [4], respectively

$$\sigma_{\oplus} = \sigma_{\oplus}^{\circ} P_{O_2}^{1/4} , \qquad [5]$$

$$\sigma_{\ominus} = \sigma_{\ominus}^{\circ} P_{O_2}^{-1/4} , \qquad [6]$$

where $\sigma_{\oplus}^{\circ}$ and $\sigma_{\ominus}^{\circ}$ are the p-type and n-type electronic conductivities at P_{O_2} = 1 atm, respectively.

The total conductivity of mixed conductor is the sum of the partial conductivities of ions, excess electron and positive hole, and hence

$$\sigma_t = \sigma_{ion} + \sigma_{\oplus} + \sigma_{\ominus} . \qquad [7]$$

From the definition of transference number it follows that

$$t_{ion} = \frac{\sigma_{ion}}{\sigma_{ion} + \sigma_{\oplus} + \sigma_{\ominus}} . \qquad [8]$$

Eq.[8] may be expressed in terms of the oxygen partial pressure. If the specific values of P_{O_2} at which the ionic conductivity of the electrolyte equals to the p-type and n-type electronic conductivities are designated by $P_{\oplus}$ and $P_{\ominus}$, respectively[15,16], the introduction of eqs.[5] and [6] into eq.[8] gives

$$t_{ion} = [\ 1 + (\frac{P_{O_2}}{P_{\oplus}})^{1/4} + (\frac{P_{O_2}}{P_{\ominus}})^{-1/4}\ ]\ . \qquad [9]$$

A solid galvanic cell consists of solid-oxide electrolyte separating two electrode compartments with definite oxygen partial pressure, P'_{O_2} and P''_{O_2}. Two metal electrodes are in contact with the interfaces of the electrolyte. Such cell is represented by

metallic lead/P'_{O_2}/ZrO_2(CaO)/P''_{O_2}/ metallic lead .

Wagner[17] has derived a general formula for the e.m.f. of the galvanic cell with electrolyte that exhibits mixed ionic and electronic conduction;

$$E = \frac{1}{4F} \int_{\ln P'_{O_2}}^{\ln P''_{O_2}} t_{ion}\ d(\ln P_{O_2}) . \qquad [10]$$

The introduction of eq.[9] into [10], followed by integration, gives (15,16)

$$E = \frac{RT}{F} \left[\ln \frac{P_{\oplus}^{1/4} + P_{O_2}'^{1/4}}{P_{\oplus}^{1/4} + P_{O_2}''^{1/4}} + \ln \frac{P_{\ominus}^{1/4} + P_{O_2}''^{1/4}}{P_{\ominus}^{1/4} + P_{O_2}'^{1/4}} \right] . \qquad [11]$$

Patterson (18) has made a comprehensive survey of the literature concerning the conduction properties of ZrO_2-CaO and other electrolytes and has provided estimates for the limits of the electrolytic domain in which the ionic conductivitiy is larger than the p-type and n-type electronic conductivities. The results of his assesment are shown in Fig.1.1. As shown in this figure, the contribution of p-type electronic conduction in usual metallurgical experiments is negligible, whereas the n-type electronic conduction should significantly affect the measured e.m.f. of the solid galvanic cell as discussed in the latter section.

The present paper consists of four chapters including chapter 1. The chapter 2 describes the electrochemical measurement of standard free energies of formation of NiO, CoO and MoO_2. The chapter 3

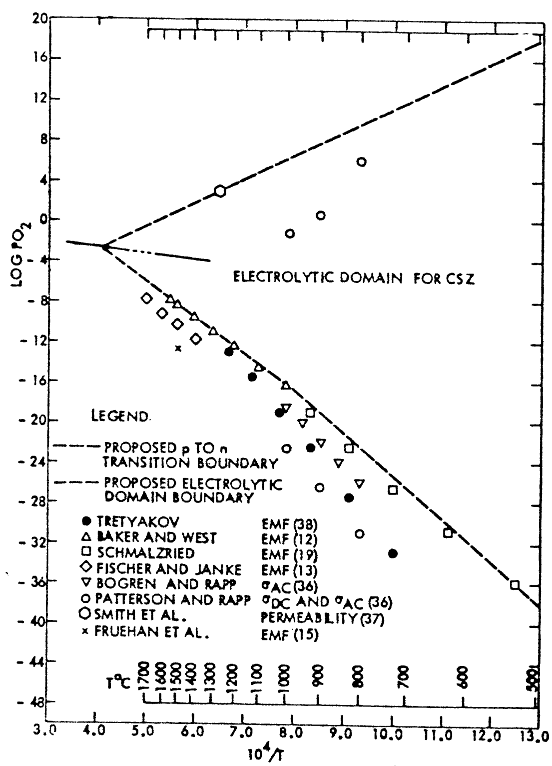

Fig.1.1 Electrolytic domain for calcia-stabilized zirconia after Patterson(18).

includes the electrochemical measurement of oxygen in liquid iron, nickel and iron-nickel alloys. The interaction parameters for oxygen in these melts were determined by means of solid-oxide galvanic cell. In chapter 4, oxygen permeability of solid-oxide electrolyte will be mainly described.

REFERNCES

1. C. Wagner and W. Schotky : Z. Phys. Chem., B11 (1931), 97-103.

2. O.Ruff and F. Ebert : Z. anorg. Chem., 180(1929), 19.

3. E. Ryshkewitch ; "Oxide Ceramics", Academic Press, New York, (1960), p.353.

4. D. Duwez, F. Odell and F. M. Brown : J. Amer. Ceram. Soc. 35(1952), 109.

5. A. Diezel and H. Torber ; Ber. Dtch. Keram. Ges., 30(1953),47.

6. A. Cocco ; Chim. Industria(Milano), 41(1959), 882.

7. R. Roy ; Bull. Soc. Chim. France, (1965), 1148.

8. T. Noguchi, M. Mizuno and M. R. Corn ; Solar Energy, 11(1967), 145.

9. F. Hund ; Z. Phys. Chem., 199(1952), 142.

10. W. D. Kingery, J. Pappis, M. E. Dotty and D. C. Hills; J. Amer. Ceram. Soc., 42(1959), 393.

11. K. Kiukkola and C. Wagner ; J. Electrochem. Soc., 104(1957), 379.

12 J. Weisbart and R. Ruka ; " Fuel Cells " vol.2, edited by G. J. Young, Reinhold Pub. Corp., New York, (1963), p.37.

13. S. F. Palguev and A. D. Nuijimin ; Electrochem. Molten. Solid Electrolyte, 1(1961), 90.

14. F. A. Kröger and H. J. Vink ; "Solid State Physics" vol. 3, edited by F. Seitz and D. Turnbull, Academic Press, New York, (1960), p.310.

15. H. Schmalzried ; Ber. Bunsenges. Phys. Chem., 66 (1962), 572.

16. H. Schmalzried ; Z. Phys. Chem., 38(1963), 87.

17. C. Wagner ; Z. Phys. Chem., B21(1933), 25-41.

18. J. M. Patterson ; J. Electrochem. Soc., 118(1971), 1033-1039.

CHAPTER 2

ELECTROCHEMICAL MEASUREMENTS OF STANDARD FREE ENERGIES OF FORMATION OF NiO, CoO and MoO_2

2.1 Introduction

The Ni-NiO, Co-CoO and Mo-MoO_2 systems are of importance because they are considered for reference electrodes of solid-oxide galvanic cell, by which dissolved oxygen in liquid metals such as Cu, Ni, Co and Fe can be electrochemically measured. However, calculation of equilibrium oxygen potential in these systems at high temperature is often handicapped by the lack of reliable thermodynamic data on free energies. The standard free energies of formation of these oxides have been calculated from enthalpies and heat capacities measured by calorimeter or from gas-metal equilibrium measurements. Quite often the high-temperature heat capacities are obtained by extra-polation from lower temperature or are estimated using semi-empirical rules. Calculations based on carolimetric data or gas-metal equilibrium measurements include rather wide error limits of free energies. For example, the free energies of formation of NiO, CoO and MoO_2 given by Kubaschewski et al.[1] have an estimated uncertainty of $\pm$ 4.2, $\pm$ 4.2 and $\pm$ 12.6 kJ mol-oxide^{-1}, respectively.

A solid-oxide galavanic cell can be used for the determination of standard free energies of formation of these oxides with a higher degree of accuracy. The pioneering work of Kiukkola and Wagner[2] has demonstrated the usefulness of calcia-stabilized zirconia as solid electrolyte. The cells used in the present study are

cell(I) Pt/air/ZrO_2(CaO)/Ni-NiO/Pt,

cell(II) Pt/Ni-NiO/ZrO_2(CaO)/ZrO_2(CaO) powder/Co-CoO/Pt,

cell(III) Pt/Co-CoO/ZrO_2(CaO) powder/ZrO_2(CaO)/Mo-MoO_2/Pt,

cell(IV) Pt/air/ZrO_2(CaO)/Mo-MoO_2/Mo.

Since the contribution of electronic conduction is negligible in the present experimental condition[3], the e.m.f.'s of cell(I), (II), (III) and (IV) are given by

$$E(I) = [RT \ln 0.2093 - 2\Delta G^\circ(NiO)] / 4F, \quad [1]$$

$$E(II) = [\Delta G^\circ(NiO) - \Delta G^\circ(CoO)] / 2F, \quad [2]$$

$$E(III) = [2\Delta G^\circ(CoO) - \Delta G^\circ(MoO_2)] / 4F, \quad [3]$$

$$E(IV) = [RT \ln 0.2093 - \Delta G^\circ(MoO_2)] / 4F - E(t), \quad [4]$$

where E(I), E(II), E(III) and E(IV) are electromotive force of the cells(I),(II), (III) and (IV), respectively, R is the gas constant, T is temperature, F is the Faraday constant, E(t) is the thermoelectromotive force between Pt and Mo, and $\Delta G^\circ(NiO)$, $\Delta G^\circ(CoO)$ and $\Delta G^\circ(MoO_2)$ are the standard free energies of formation of NiO, CoO and MoO_2, respectively.

2.2 Experimental

2.2.1 Solid Electrolyte

The solid-oxide electrolyte used was a tubular zirconia, stabilized by 11 mol% of CaO and commercially available form Nippon Chemical Ceramics Co Ltd. The tube can be described as having one closed end, an ID of 9 mm, an OD of 13 mm and a length of 100 mm or 500 mm. All tubes were previously checked for gastightnes at room temperature. The chemical composition and mai physical properties of the zirconia tube are listed in TABLE 1.

2.2.2 Materials

The molybdenum dioxide was obtained as an intermediate product of hydrogen reduction of MoO_3 of 99.42 wt% purity. The major impurities in resulting MoO_2 powder are 0.17 wt% N.V.R., 0.015 wt% Fe, 0.002 wt% Cu, and a slight amount of MoO_3. Molybdenum powde of 99.5 wt% purity was thoroughly mixed with MoO_2 powder in about 4:1 volume ratio. Prior to the experiments, these mixtures were put in a silica tube, heated in vacuum at 1373 K for 24 hrs, and quenched in water. X-ray analysis of the resulting powder mixture indicated only Mo + MoO_2. Other materials were supplied from Nakarai Chemical Co. Ltd.

TABLE 1 The chemical composition and physical properties of calcia-stabilized zirconia

SiO_2	TiO_2	Al_2O_3	Fe_2O_3	CaO
1.50* ~ 1.58	0.14* ~ 0.24	0.46* ~ 0.71	0.17* ~ 0.20	5.80* ~ 5.93

MgO	Na_2O	K_2O	ZrO_2
0.67* ~ 0.92	tr ~ 0.02	tr	90.98* ~ 91.62

Apparent specific gravity = 5.39

Bulk specific gravity = 5.36 ~ 5.39

Apparent porosity = approximately 0 ~ 0.6 %.

* wt pct.

2.2.3 Experimental Apparatus and Procedure

a. Cells (I) and (IV)

The schematic diagram of cells (I) and (IV) is shown in Fig. 2.1. A tubular zirconia of 500 mm long was used for these cells as electrolyte. A platinum gauze was sintered on the outer bottom of the tube by means of platinum black at 1273 K for 48 hrs. A Pt-PtRh13 thermocouple was spot-welded on the platinum gauze and the Pt wire of the couple was used as electrical lead to the outer electrode. A 4:1 volume ratio of powder mixture of Mo-MoO_2 or Ni-NiO was tightly packed in the zirconia tube with a small amount of water and/or methyl alcohol as binder. Electrical leads to Mo-MoO_2 and Ni-NiO electrodes were accomplished by Mo wire and Pt wire, respectively. The inner electrode was tightly pressed against the inner bottom of the zirconia tube by means of a metal spring between an alumina pushing-rod and the top of the zirconia tube as shown in Fig.2.1.

The assembled cell was first evacuated in order to remove methyl alcohol and water, heated very slowly to avoid thermal cracking of the zirconia tube in a SiC resistance furnace having a homogeneous temperature zone of 80 mm long within $\pm$ 1 K, and then purified

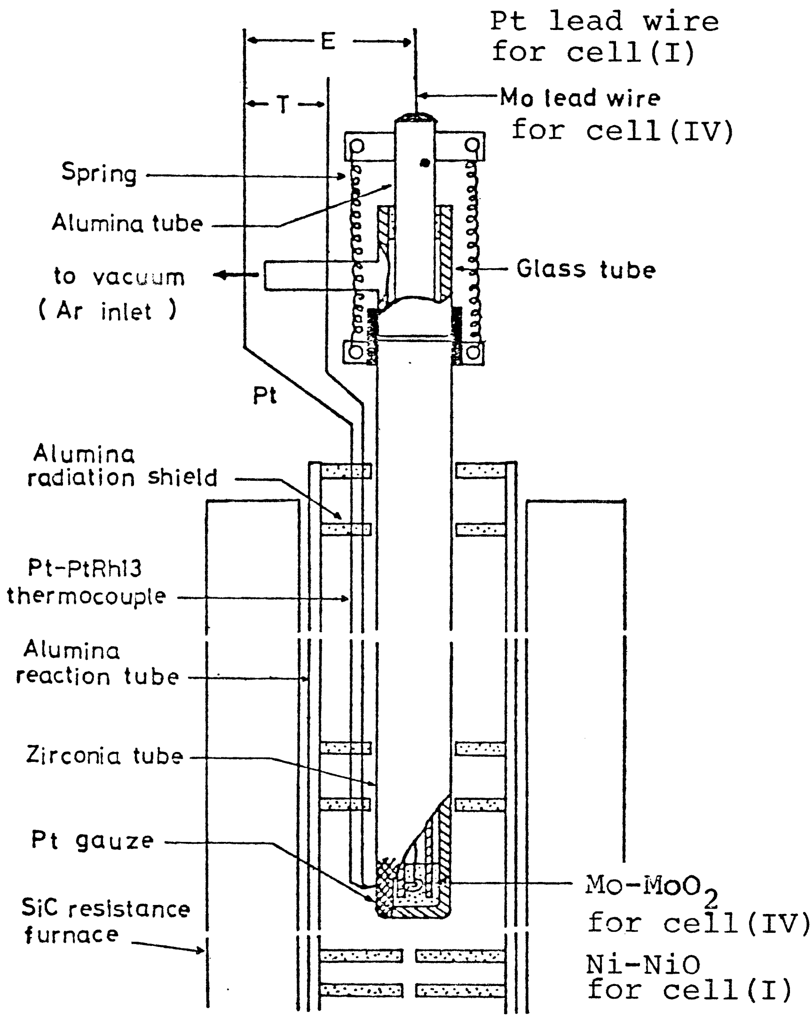

Fig.2.1 Schematic diagram of cells(I) and (IV)

argon was led into the zirconia tube. The purification train for argon consisted of silica-gel, phosphorous pentoxide and magnesium chips kept at 723 K. During the e.m.f. measurements at 973 to 1723 K for cell (I), and at 1273 to 1883 K for cell(IV), the inside of the zirconia tube was filled with purified argon whose pressure was 6670 Pa on gauge higher than the atmospheric pressure. Temperature was measured by Pt-PtRh13 thermocouple, and controled within $\pm$ 1 K by using a saturable reactor. Prior to the measurements of e.m.f., thermoelectromotive force between Mo and Pt was measured at the same condition as the e.m.f. measurements. The e.m.f. was measured by digital voltmeter with an internal impedance of 10^8 ohm. Reproducibilities and reversibilities of cell potential were generally inferred from the high linearity between e.m.f. and temperature which was not affectd by temperature cycling. Further check of reversibilities of the cell was made by passing a small external current in either direction for a few seconds. In each case, the e.m.f. was found to return to the original value. To avoid induction noise from the furnace, the electric current for the furnace was momentarily disconnected without any change of temperature. In all cases, the cell potentials were confirmed to be unaffected by induction noise.

b. Cells (II) and (III)

The schematic diagram of cells (II) and (III) is shown in Fig. 2.2. The cell consists of two half cell compartments separated by the zirconia tube of 100 mm long. The inner electrode compartment contains a 4:1 volume ratio of powder mixture of Mo-MoO_2 or Ni-NiO which was tightly packed in the solid electrolyte tube with a small amount of water and/or methyl alcohol as binder.

The alumina crucible of outer electrode compartment contains Co-CoO powder mixture in 4:1 volume ratio which is contacted with zirconia tube via a layer of calcia-stabilized zirconia powder having a thickness of 3 to 5 mm. The zirconia tube was cemented to the alumina crucible by zirconia cement, by which the outer electrode compartment was sealed from furnace atmosphere. The zirconia tube was tightly pressed against the outer electrode by means of a metal spring between alumina pushing-rod and the top of the furnace. Platinum wire of 0.5 mm dia. was used as lead wires to both electrodes. The experimental procedure for cells (II) and (III) was similar to that for cells (I) and (IV).

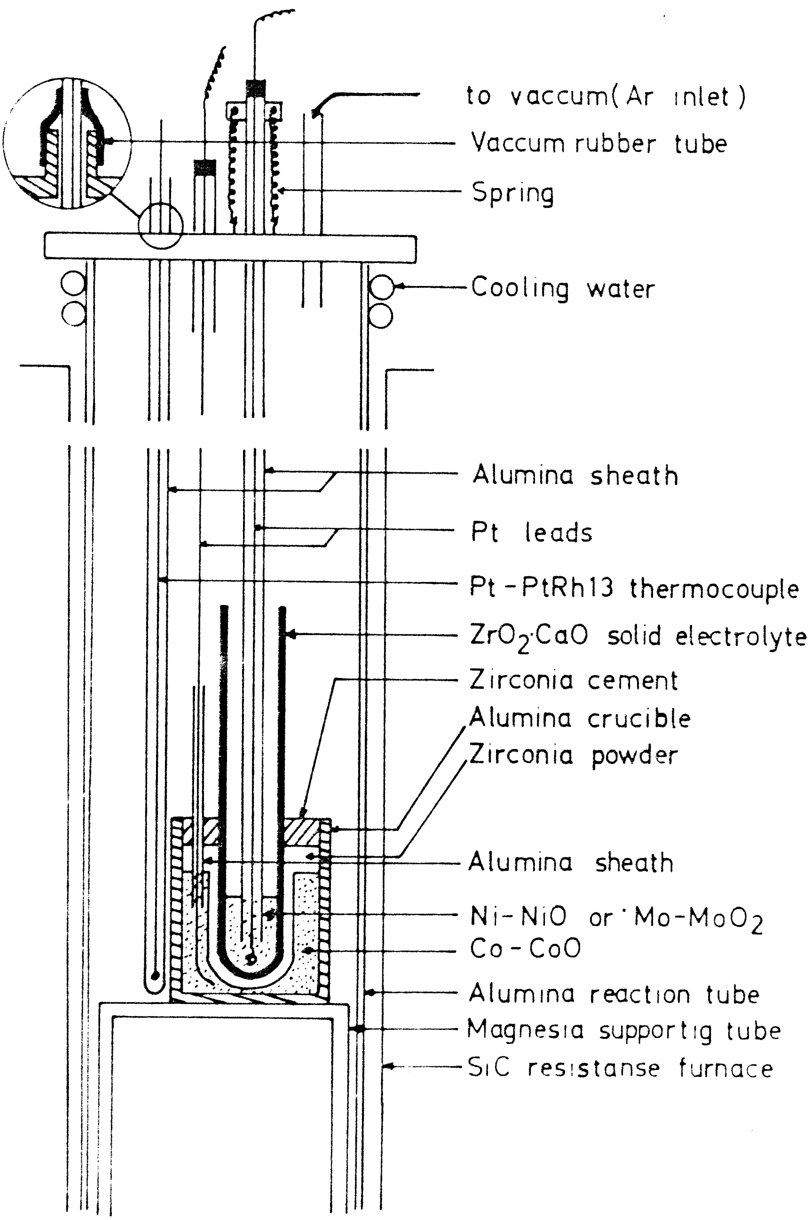

Fig. 2.2 Schematic diagram of cells (I) and (III).

Cells in which Co-CoO powder mixture was directly contacted with the zirconia tube were used in several initial experimental runs. In this case, however, an experimental difficulty was experienced. The e.m.f of the cell in this type dropped steadily after it was held above 1623 K for an extended period of time (about 3 to 5 hrs), and after experiments the penetration of a bluish layer from outer electrode(Co-CoO) to the inner electrode($Mo-MoO_2$ or Ni-NiO) through the solid electrolyte was observed. The phases present in the bluish layer were examined by X-ray diffraction, and only cubic ZrO_2, Co and CoO were identified. Though the zirconia tubes were of high density and were impervious at room temperature, they may become slightly porous at experimental temperature, and Co and/or CoO may diffuse to the outer electrode compartment through micropores without any chemical reactions. For this reason, the layer of zirconia powder, which would delay the penetration of Co and/or CoO from the outer electrode, was applied to cells(II) and (III) in order to overcome the above mentioned experimental difficulty. Thus the e.m.f.'s of cells(II) and (III) could be reversibly measured over 30 hrs above 1623 K. However prolonged e.m.f. measurements above 1623 K over 40 hrs were impossible because the penetration of Co and/or

CoO reached to the inner electrode compartment.

2.3 Results and Discussion

2.3.1 Standard Free Energy of Formation of Nickel Oxide

The e.m.f.'s of cell (I) are shown in Fig.2.3. By using the least squares method, the line in this figure was represented as

$$E(I)/mV = 1195 - 0.463\ (T/K) \pm 1.8 \qquad [4]$$

from 973 to 1723 K.

The standard deviations of the coefficients in this equation are, respectively, $\pm$ 0.9 mV and $\pm$ 0.0007 mV K^{-1}. Introduction of eq.[4] into [1] yields

$$\Delta G^\circ(NiO)/kJ\ mol\text{-}NiO^{-1} = -\ 230.7 + 0.008489\ (T/K) \pm 0.4 \qquad [5]$$

from 973 to 1723 K.

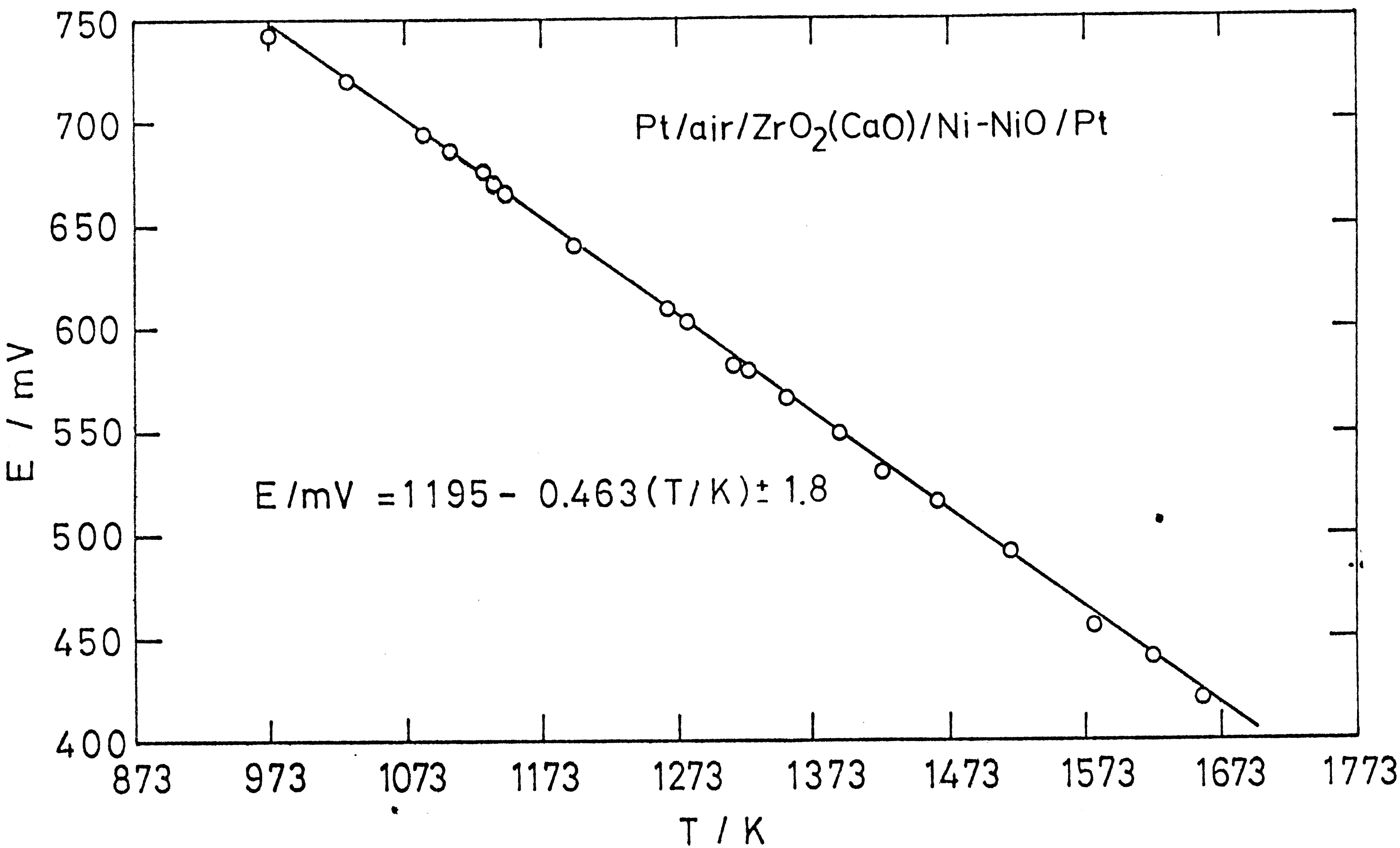

Fig. 2.3 Relation between e.m.f. and temperature for cell(I)

2.3.2 Standard Free Energy of Formation of Cobalt Oxide

The cell voltage, E(II), for cell(II) was measured in the temperature range from 1478 to 1717 K. The results are shown in Fig.2.4. The equation for the line in this figure as determined by the method of least squares is

$$E(II)/mV = -7.2 + 0.0755\ (T/K) \pm 0.4 \qquad [6]$$

from 1473 to 1723 K.

The standard deviations of the coefficients in this equation are, respectively, $\pm$ 0.3 mV and $\pm$ 0.0002 mV K^{-1}. Introduction of eqs.[5] and [6] into eq.[2] yields

$$\Delta G^\circ(CoO)/kJ\ mol\text{-}CoO^{-1} = -229.0 + 0.06832\ (T/K) \pm 0.4$$

from 1473 to 1723 K.

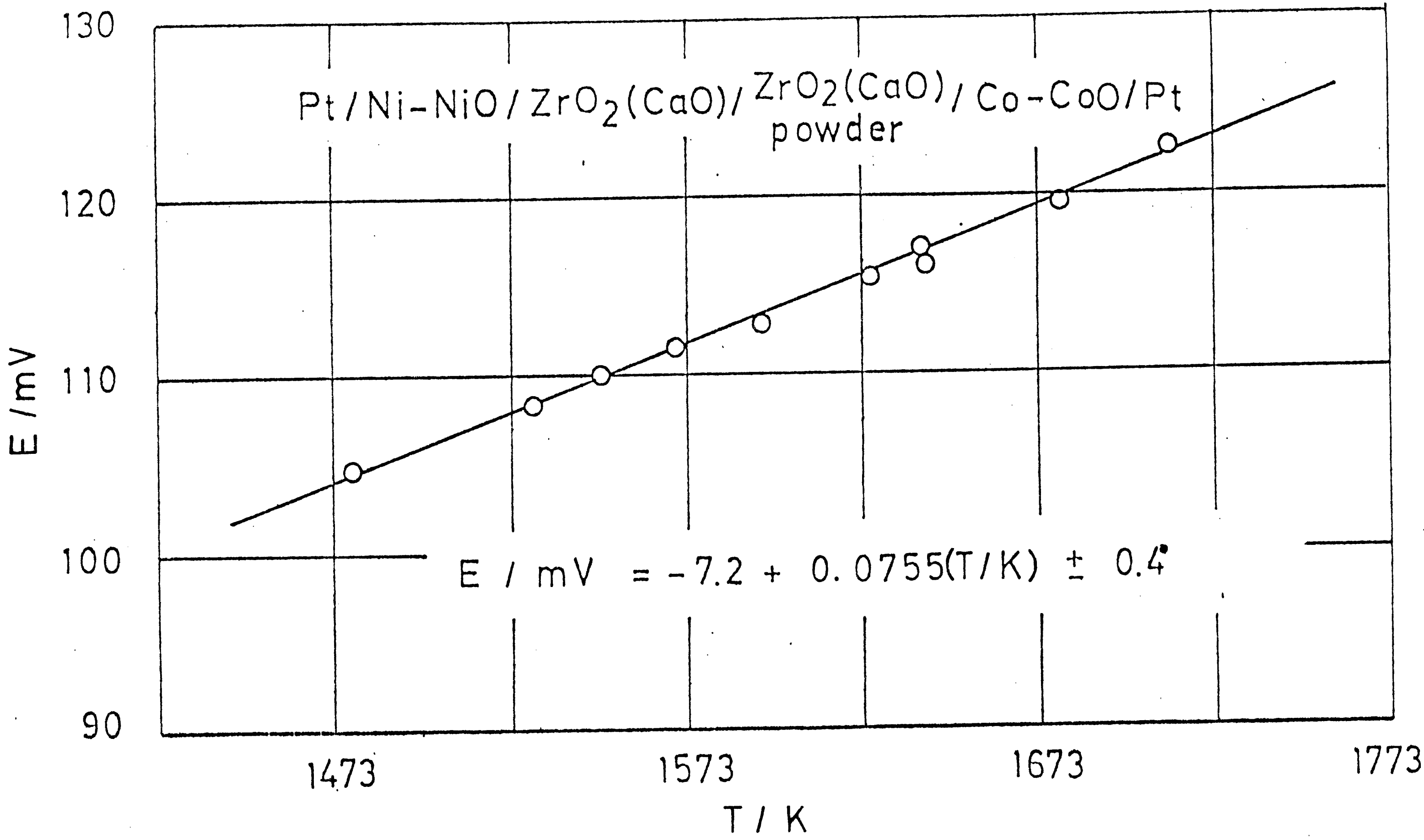

Fig. 2.4 Relation between e.m.f. and temperature for cell(II).

2.3.3 Standard Free Energy of Formation of Molybdenum Dioxide

The cell voltage, E(III), for cell(III) was measured in the temperature range from 1528 to 1716 K. The results are shown in Fig.2.5. The least squares method gave an equation for the line in this figure;

$$E(\mathrm{III})/\mathrm{mV} = 238.1 - 0.0445\ (T/K) \pm 0.6 \qquad [8]$$

from 1523 to 1723 K.

The standard deviations of the coefficients in eq.[8] are, respectively, $\pm$ 0.8 mV and $\pm$ 0.0072 mV K^{-1}. Introduction of eqs.[7] and [8] into eq.[3] yields

$$\Delta G°(MoO_2)/\mathrm{kJ\ mol\text{-}MoO_2}^{-1} = -\ 549.9 + 0.1538\ (T/K) \pm 0.9\ . \qquad [9]$$

from 1523 to 1723 K.

The cell voltage, E(IV), for cell(IV) was measured in the temperature range from 1213 to 1823 K. In the case of cell(IV), the time necessary to attain a steady e.m.f. at a constant temperature was quite short. The results are shown in Fig.2.6, where the black points indicate the e.m.f. values measured in equilibrium and

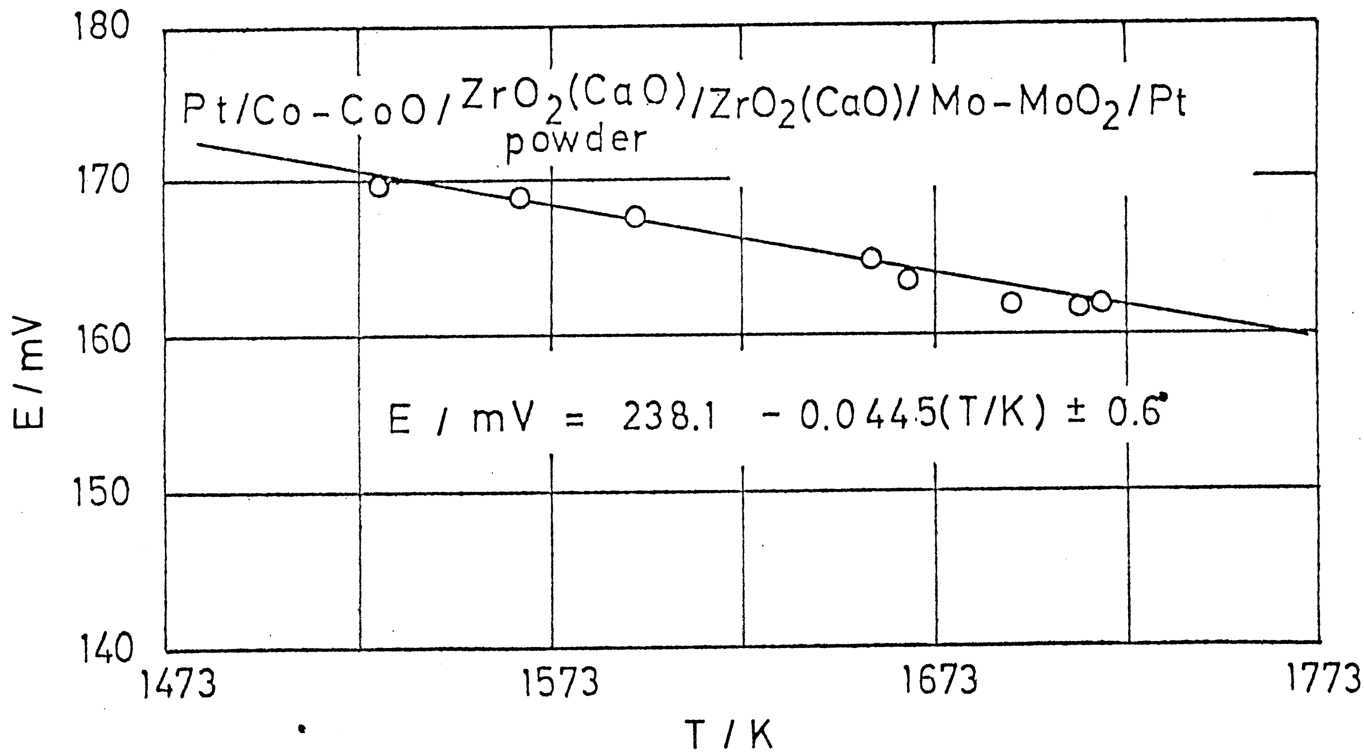

Fig. 2.5 Relation between e.m.f. and temperature for cell(III)

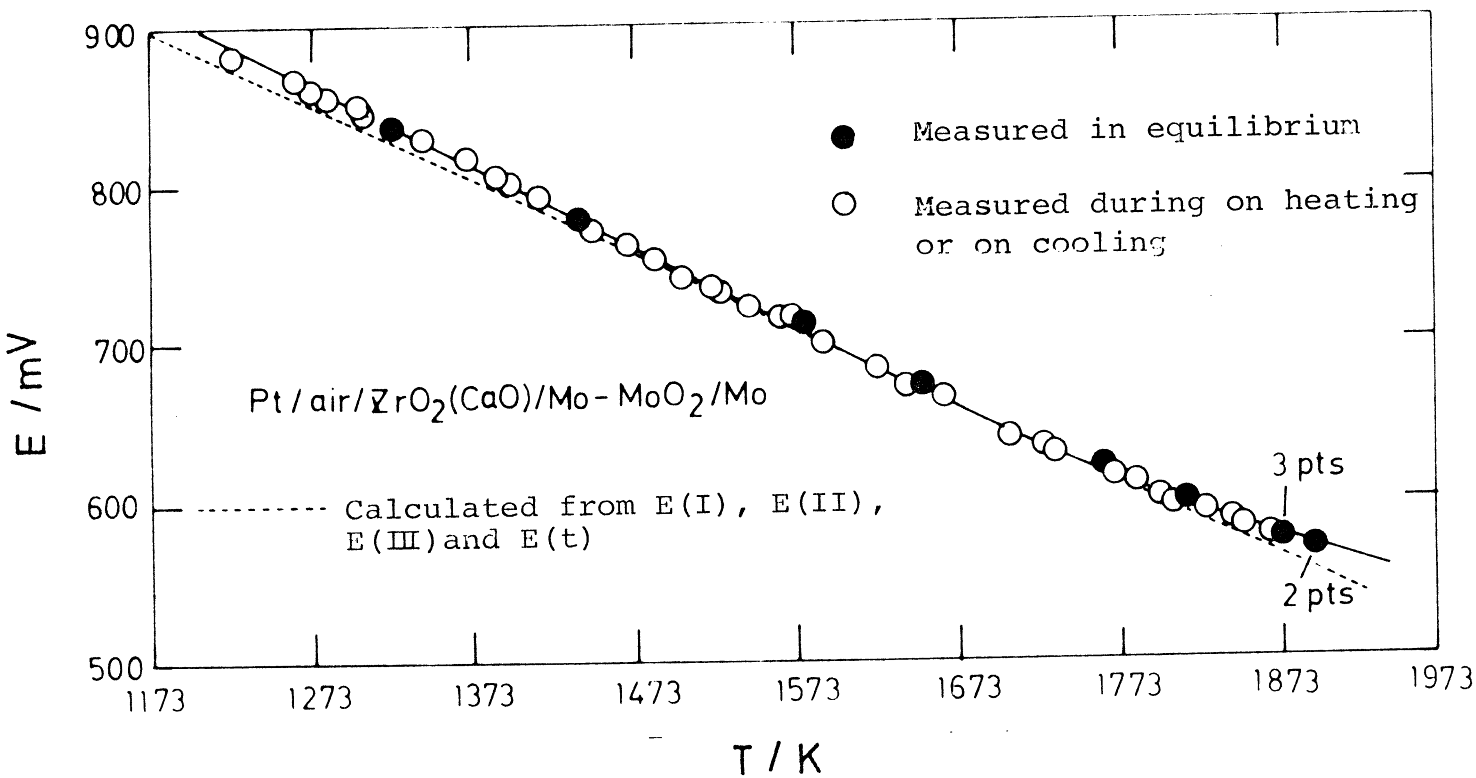

Fig.2.6 Relation between e.m.f. and temperature for cell(IV)

the blank circles indicate those obtained on heating or on cooling. Although the relationship between e.m.f. and temperature can be shown as slightly curved line in the range of temperature from 1213 to 1823 K, the e.m.f.'s obtained in thermodynamic equilibrium will be represented as a straight line in the limited range of temperature by using the least squares method;

$$E(IV)/mV = 1515 - 0.512\ (T/K) \pm 0.8 \qquad [10]$$
from 1273 to 1723 K

$$E(IV)/mV = 1342 - 0.410\ (T/K) \pm 0.4 \qquad [11]$$
from 1723 to 1923 K.

The standard deviations of these coefficients in eqs. [10] and [11] are $\pm$ 3 mV and $\pm$ 0.004 mV K^{-1} for eq. [10], and $\pm$ 0.3 mV and $\pm$ 0.04 mV K^{-1} for eq. [11], respectively. The broken line in Fig. 2.6 shows the e.m.f. calculated from E(I), E(II), E(III) and E(t). At the investigated range of temperature for cells(I), (II) and (III), this line show good agreement with the line for E(IV). This agreement would give a proof of experimental accuarcy. The thermoelectromotive force between Pt and Mo was measured in the range of temperature from 1273 to 1873 K. The results are shown in Fig. 2.7. By the least squares method, the line in Fig. 2.7 was represented as

$$E(t)/mV = -22.1 + 0.040\,(T/K) \pm 0.03. \qquad [12]$$

Introduction of eqs.[10], [11] and [12] into eq.[4] yields

$$\Delta G^\circ(MoO_2)/kJ\,mol\text{-}MoO_2^{-1} = -576.1 + 0.1693\,(T/K) \pm 0.30 \qquad [13]$$

from 1223 to 1723 K,

$$\Delta G^\circ(MoO_2)/kJ\,mol\text{-}MoO_2^{-1} = -509.6 + 0.1297\,(T/K) \pm 0.15 \qquad [14]$$

from 1723 to 1923 K.

The free energy data of MoO_2 obtained from E(IV) would be more reliable than those obtained from E(I), E(II) and E(III) because of small uncertainty.

The uncertainties of calculations of $\Delta G^\circ(NiO)$, $\Delta G^\circ(CoO)$ and $\Delta G^\circ(MoO_2)$ were estimated by eqs.[15], [16], [17] and [18]

$$[\sigma \Delta G^\circ(NiO)]^2 = (2F)^2\,[\sigma E(I)]^2 \qquad [15]$$

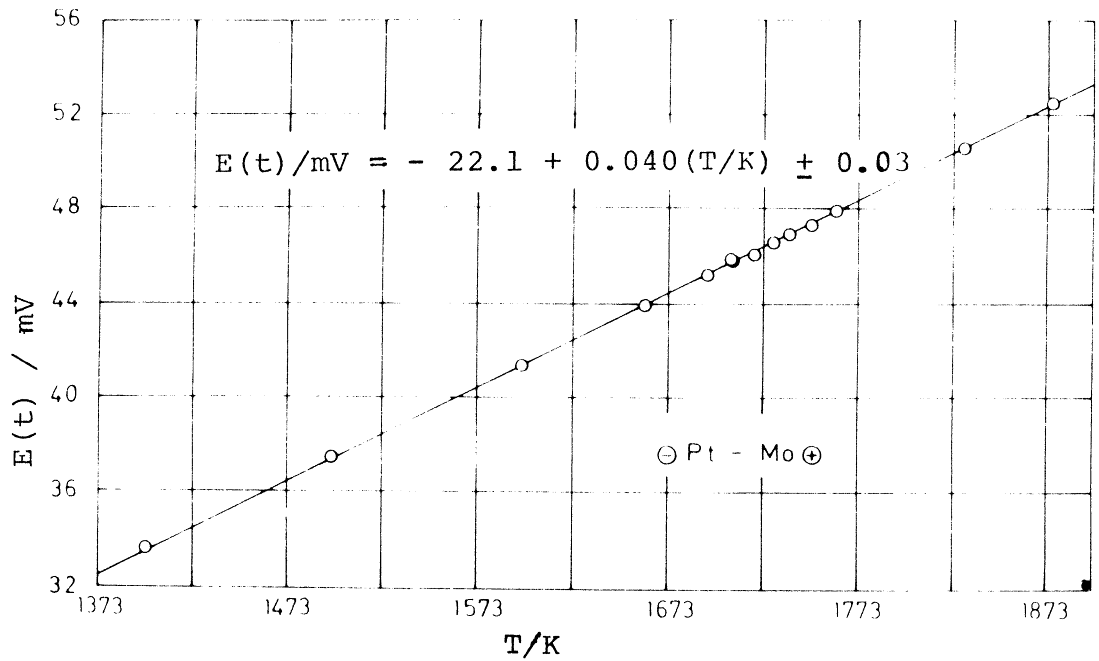

Fig.2.7 Thermoelectromotive force between Pt and Mo.

$$[\sigma\Delta G^\circ(CoO)]^2 = [\sigma\Delta G^\circ(NiO)]^2 + (2F)^2[\sigma E(II)]^2 \quad [16]$$

$$[\sigma\Delta G^\circ(MoO_2)]^2 = [\sigma\Delta G^\circ(CoO)]^2 + (4F)^2[\sigma E(III)]^2 \quad [17]$$

$$[\sigma\Delta G^\circ(MoO_2)]^2 = [\sigma E(IV)]^2 + [\sigma E(t)]^2, \quad [18]$$

where $\sigma(i)$ indicates the standard deviation of i, i.e. E(I), E(II), E(III) and E(t). The uncertainties of $\Delta G^\circ(NiO)$, $\Delta G^\circ(CoO)$ and $\Delta G^\circ(MoO_2)$ thus calculated are given in eqs.[5], [7], [9], [13] and [14].

2.3.4 Comparison With Other Data

The present results for the standard free energy of formation of CoO are compared with those reported by other workers (1,2 4,5) in Fig.2.8. The present results show a good agreement with those obtained by means of solid-oxide galvanic cell (1,4,5), but a fair disagreement with those obtained by gas-metal equilibrium method (2). Generally an experimental error in gas-metal equilibrium method can arise from thermal diffusion in gas phase.

The results for CoO are compared with those reported in the lietrature in Fig.2.9. The present results are shown in good agreement with values reported by Fischer and Pateisky (6). No obvious reasons can

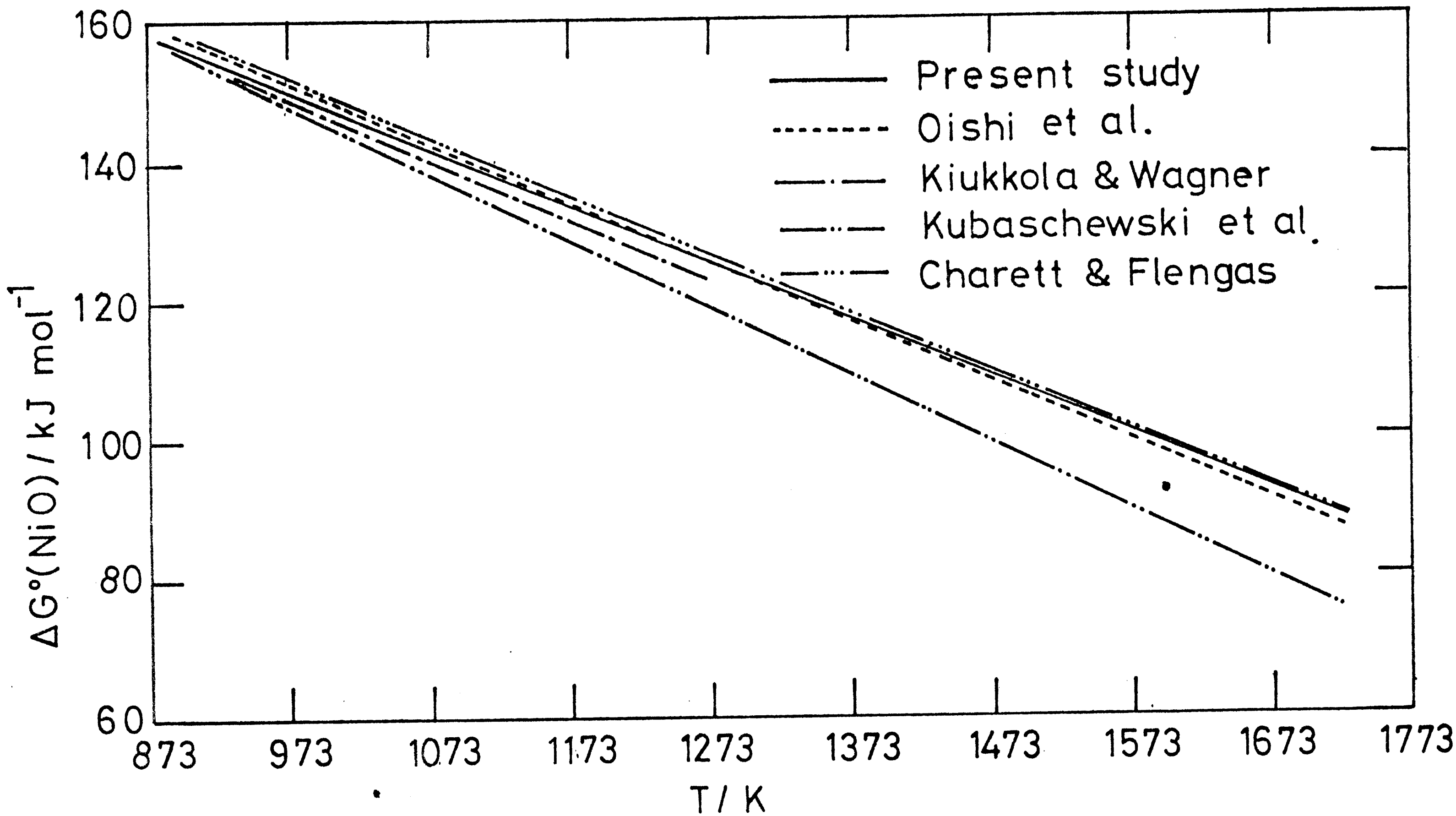

Fig. 2.8 Comparison of the values for standard free nergy of formation of nickel oxide.

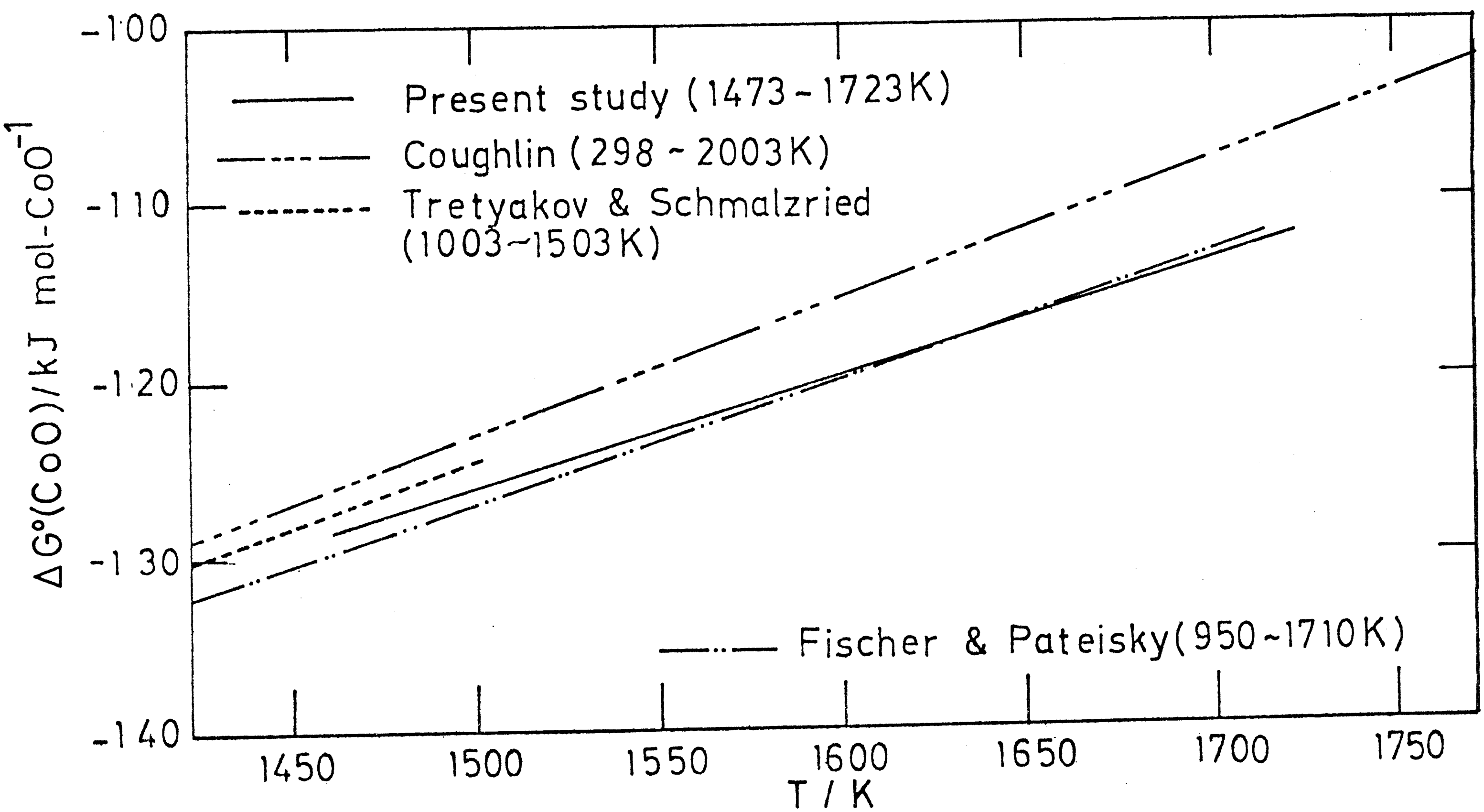

Fig.2.9 Comparison of the values for standard free energy of formation of cobalt oxide.

be found for the discrepancy between the present data and the compilation of Coughlin[7]. Data obtained at lower temperature by Moriyama et al.[8], Tretyakov and Schmalzried[9], and Bugden and Pratt[10] were extrapolated to 1723 K, and the present results were in good agreement with them within $\pm$ 1 kJ.

The results obtained for MoO_2 are compared with those by other investigators as shown in Fig. 2.10. At 1800 to 1900 K, the present results obtained from E(III) are in good agreement with the values reported by Alcock and Chan[11] and J.A.N.A.F.[12]. Alcock and Chan[11], and Chastant et al.[13] utilized a calcia-stabilized zirconia and CO/CO_2 gas mixture as the reference electrode. The relationship between e.m.f. and temperature obtained by Chastant et al.[13] and Fischer and Pateisky[6] would be shown as slightly curved line. Their data were represented by two equations in the separated range of temperature as listed in TABLE 2. Fischer and Pateisky[6] utilized the following cell;

$$Pt/O_2(1\ atm)/ZrO_2(CaO)/Mo\text{-}MoO_2/Mo.$$

The powder mixture of Mo and MoO_3 was initially packed

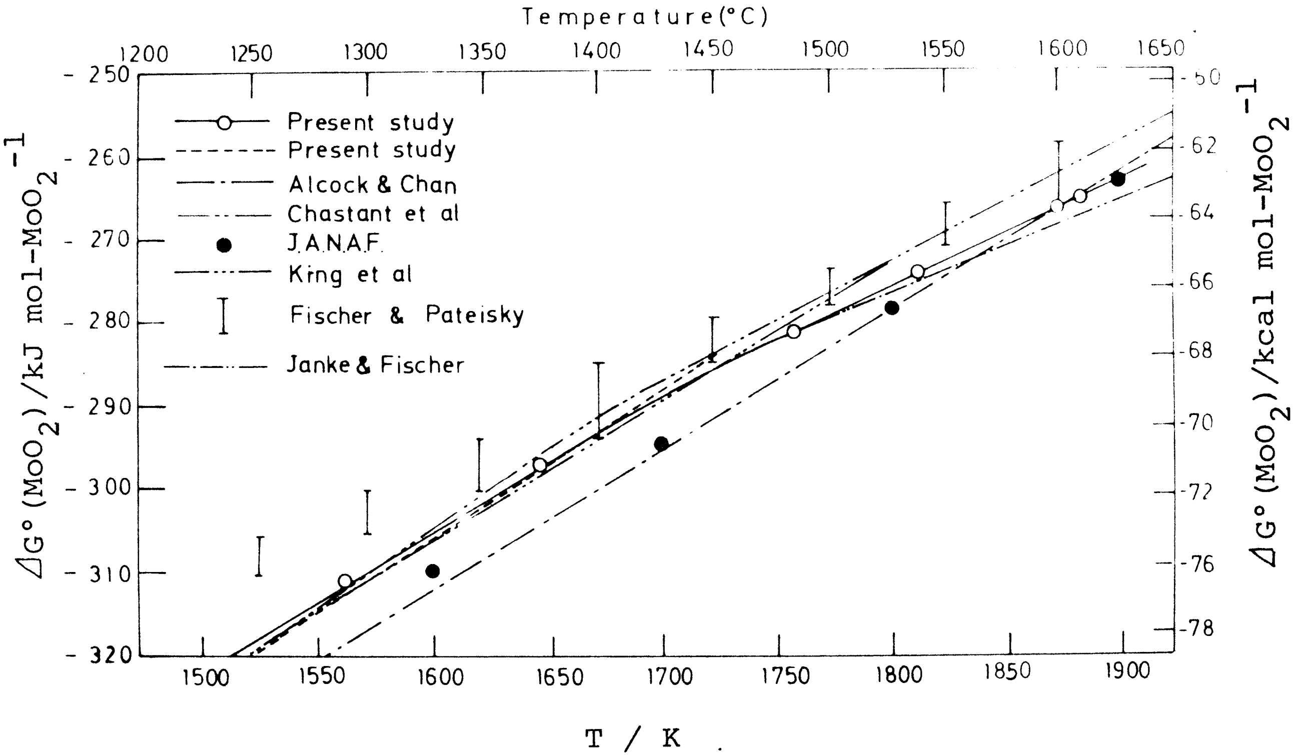

Fig.2.10 Comparison of the values for standard free energy of formation of molybdenum dioxide.

TABLE 2 Standard free energy of formation of molybdenum dioxide in literature

Year	Authors	Exp. Method	Temp. Range (K)	$\Delta G^o(MoO_2)$ (kJ mol-MoO_2^{-1})	Ref.
1940	Tonosaki	H_2/H_2O	918 - 1096	- 562.7 + 0.155 T	19
1953	Goksen	H_2/H_2O	950 - 1350	- 553.5 + 0.147 T	22
1960	King, Weller and Christensen	Carolimetry	400 - 1800	- 578.3 + 0.1699T	15
1962	Gleiser and Chipman	CO/CO_2	1200 - 1350	- 576.9 + 0.1681T	21
1963	Rapp	e.m.f.	1023 - 1323	- 575.3 + 0.167 T	17
1964	Barbi	e.m.f.	873 - 1073	- 578.86 + 0.178 T	24
1965	McIver and Teale	e.m.f.	1115 - 1280	- 530.5 + 0.174 T	18
1965	Drobyshev, Rezukina and Tarasov	e.m.f.	1280 - 1360	- 575.63 + 0.1694T	16
1968	Jordanov, Nikolov and Cimbulev	e.m.f.	973 - 1123	- 540.24 + 0.1337T	20
1969	Beglund and Kierkegaard	e.m.f.	1150 - 1450	- 564.80 + 0.1345T	23
1970	Fischer and Pateisky	e.m.f.	1673 - 1973 973 - 1673	- 508.65 + 0.1312T ----------------	6
1972	Alcock and Chan	e.m.f.	1273 - 1873	- 587.56 + 0.1773T	11
1973	Chastant, Gatellier Jon and Ollette	e.m.f.	1673 - 1973 1073 - 1673	- 579.9 + 0.167 T - 530.07 + 0.1430T	13
1975	Janke and Fischer	e.m.f.	1733 - 1933	- 490.70 + 0.1183T	14

in zirconia tube. Their data show a fairly large uncertainty as shown in Fig.2.10. Below 1673 K, values obtained in this study show a good agreement with those reported by Chastant et al.[13], Janke and Fischer[14], and King et al[15]. If the data obatined at lower temperature[16-24] are extrapolated to 1873 K these values show a spread of 107 kJ at 1873 K.

2.4 Summary

The standard free energies of formation of NiO, CoO and MoO_2 were determined by means of solid-oxide galvanic cell;

cell(I) Pt/air/ZrO_2(CaO)/Ni-NiO/Pt,

cell(II) Pt/Ni-NiO/ZrO_2(CaO)/ZrO_2(CaO)powder/Co-CoO/Pt,

cell(III) Pt/Co-CoO/ZrO_2(CaO)powder/ZrO_2(CaO)/Mo-MoO_2/Pt,

cell(IV) Pt/air/ZrO_2(CaO)/Mo-MoO_2/Mo.

The results obtained from cells(I), (II), and (III) are as follows

$$\Delta G°(\mathrm{NiO})/\mathrm{kJ\ mol\text{-}NiO}^{-1} = -\ 230.7 + 0.08489\ (T/K) \pm 0.4$$

from 973 to 1723 K,

$$\Delta G°(CoO)/kJ\ mol\text{-}CoO^{-1} = -229.0 + 0.06832\ (T/K) \pm 0.4$$

from 1473 to 1723 K,

$$\Delta G°(MoO_2)/kJ\ mol\text{-}MoO_2^{-1} = -549.9 + 0.1538\ (T/K) \pm 0.9$$

from 1523 to 1723 K.

The consistent data of free energy of formation of MoO_2 were also obtained from cell(IV);

$$\Delta G°(MoO_2)/kJ\ mol\text{-}MoO_2^{-1} = -576.1 + 0.1692\ (T/K) \pm 0.15$$

from 1273 to 1723 K,

$$\Delta G°(MoO_2)/kJ\ mol\text{-}MoO_2^{-1} = -509.6 + 0.1297\ (T/K) \pm 0.3$$

from 1723 to 1923 K.

Penetration of Co and/or CoO into solid electrolyte at high temperature was overcome by sandwitching a layer of calcia-stabilized zirconia powder between Co-CoO electrode and solid electrolyte.

2.5 References

1. O. Kubaschewski, E. Ll. Evans and C. B. Alcock; " Metallurgical Thermochemistry " 4 th Edition, Pergamon Press, London, (1967), p.426.
2. K. Kiukkola and C. Wagner : J. Electrochem. Soc., 104(1957), 379.
3. J. W. Patterosn ; J. Electrochem. Soc., 118(1971), 1033.
4. T. Oihsi, T. Hiruma and J. Moriyama ; J. Japan Inst. Metals, 36(1972), 487.
5. G. Charette and S. N. Flengas ; J. Electrochem. Soc., 115(1968), 796.
6. W. A. Fischer and G. Pateisky; Arch. Eisenhüttenw. 41(1970), 661.
7. J. P. Coughlin ; U. S. Bur. Mines, Bull., 542 (1954), 69.
8. J. Moriyama, N. Sato , H. Asao and Z. Kozuka ; Memoirs of the Faculty of Engineering, Kyoto University, 31(1969), 253.
9. J. D. Tretyakov and H. Schmalzried ; Ber. Bunsenges. Phys. Chem., 19(1965), 396.
10. W. C. Bugden and J. N. Pratt : Trans. Inst. Min. Met., C221(1970), 80.
11 C. B. Alcock and J. C. Chan ; Can. Met. Quart.

11(1972), 559.

12. JANAF Thermochemical Table, 2nd edition.

13. M. Chastant, C. Gatelier, M. M. Jon and M. Ollette ; Raport IRSID 138(1973), 951.

14. D. Janke and W. A. Fischer ; Arch. Eisenhüttenw., 46(1975), 755.

15. G. King, W. W. Weller and A. U. Christensen ; U. S. Bur. Min. Report Invest. No.5664, (1960), p.29.

16. V. N. Drobyshev, T. N. Rezukhina and L. A. Tarasova ; Russian J. Phys. Chem., 39(1965), 70.

17. R. A. Rapp ; Trans. Met. Soc. AIME., 227(1963), 37.

18. E. C. McIver and S. S. Teale ; U. K. Atomic Energy Authority Res. Group Atomic Energy Estab., Report. AERE-R. No. 4992, (1965), p.17.

19. K. Tonosaki ; Bull. Inst. Phys. Chem. Res., 19 (1940), 126.

20. C. V. Jordanov, T. G. Nikolov and M. T. Chimbilev, ; Neue Hütte., 13(1968), 215.

21. M. Gleiser and J. Chipman ; J. Phys. Chem., 66 (1962), 1539.

22. N. A. Gokcen ; Trans. AIME., 197(1953), 1019.

23. S. Bergulund and P. Kierkegaard ; Acta. Chem. Scandinavia, 23(1969), 329.

24. G. Barbi ; J. Phys. Chem., 68(1964), 1025.

CHAPTER 3

ELECTROCHEMICAL MEASUREMENT OF OXYGEN IN LIQUID IRON, NICKEL AND IRON-NICKEL ALLOYS

3.1 Intorduction

Oxygen in liquid iron, nickel and iron-nickel alloys has an important role on the refining of iron and ferro-nickel alloys. Measurements based on H_2/H_2O-metal equilibrium had been chiefly utilized to determin the oxygen activity in liquid iron, nickel and iron-nickel alloys;

$$H_2(g) \quad + \quad \underline{O}\ (\%\ \text{in liquid metal}) \quad = \quad H_2O(g), \qquad [1]$$

$$K' = \frac{P_{H_2O}}{P_{H_2}\ [\%O]}, \qquad [2]$$

$$K = \frac{P_{H_2O}}{P_{H_2}\ a_O(\%)}, \qquad [3]$$

$$\Delta G^\circ(O) = -\ RT\ \ln K, \qquad [4]$$

where K' is the apparent equilibrium constant for the reaction [1], K is the true equilibrium constant for the reaction [1], $\Delta G°(O)$ is the standard free energy change for the reaction [1], and $a_O(\%)$ is the Henrian activity of oxygen in liquid metal referred to dissolved oxygen in hypothetical 1 wt% solution.

Experimental data of oxygen activity in liquid iron based on H_2/H_2O-metal equilibrium study were inevitably affected by thermal segregation in the gas phase and temperature difference between the metal and the gas phases, and many investigators tried to overcome the errors caused by these effects. Since the pioneering work of Kiukkola and Wagner(1) on ZrO_2-based solid electrolyte, the solid-oxide galvanic cell has been extensively studied by a number of investigators. In 1965, Fischer and Ackermann(2) reported encouraging results on electrochemical measurements of oxygen in liquid iron, and had demonstrated the usefulness of the solid-oxide galvanic cell as a device for monitoring oxygen activity in liquid iron. Their results at 1873 K showed that the calcia-stabilized zirconia is predominantly anionic conductor above 200 ppm of oxygen in liquid iron. By electrochemical method with solid-oxide electrolyte, the undesirable effect of thermal segregation or cooling effect by hydrogen can be eliminated.

However, the full capability of this method has not been well established yet even in the case of laboratory use because of insufficient information concerning the undesirable electronic conduction, permeability of oxygen due to small electronic conduction and gas leakage through micropores in ceramic electrolyte.

The cells used in the present study are

Cell(I) $Mo/Mo\text{-}MoO_2/ZrO_2(CaO)/\underline{O}(\text{in Fe})/Mo$,

Cell(II) $Mo/Mo\text{-}MoO_2/ZrO_2(CaO)/\underline{O}(\text{in Ni})/LaCrO_3/Pt$,

Cell(III) $Mo/Mo\text{-}MoO_2/ZrO_2(CaO)/\underline{O}(\text{in Fe-Ni alloy})/Mo$.

If the transference number of ions in solid electrolyte is unity, the e.m.f.'s of cells(I),(II) and (III) are given by

$$E(I) = \frac{RT}{4F} \ln \frac{P_{O_2}(Fe)}{P_{O_2}(Mo\text{-}MoO_2)} , \qquad [5]$$

$$E(II) = \frac{RT}{4F} \ln \frac{P_{O_2}(Ni)}{P_{O_2}(Mo\text{-}MoO_2)} , \qquad [6]$$

$$E(III) = \frac{RT}{4F} \ln \frac{P_{O_2}(Fe\text{-}Ni)}{P_{O_2}(Mo\text{-}MoO_2)} . \qquad [7]$$

3.2 Experimental

3.2.1 Materials

Pure iron and electrolytic nickel were used as raw materials. The major impurities in these metals are shown in TABLE 1.

3.2.2 Experimental Apparatus And Procedure

a. Cells (I) and (III)

Experimental apparatus for cells (I) and (III) is shown in Fig. 3.1. An alumina crucible was charged with pure iron, or a mixture of iron and nickel. A $ZrO_2(CaO)$ solid electrolyte tube, closed at one end, 9 mm ID, 13 mm OD and 100 mm long, was cemented to an

TABLE 1 The chemical composition of pure iron and electrolytic nickel.

Pure Iron	%C	%Si	%Mn	%P	%S	%Al
	0.003 ~ 0.005	0.004 ~ 0.003	0.004 ~ 0.003	0.002 ~ 0.003	0.003	0.001
	%N	%O				
	0.0011 ~ 0.0018	0.011				
Electrolytic Nickel	%Co	%Cu	%Fe	%Mn	%Si	
	0.15	0.0015	0.0016	0.0001	0.0005	
	%Pb	%S	%O			
	0.0008	0.0005	0.005			

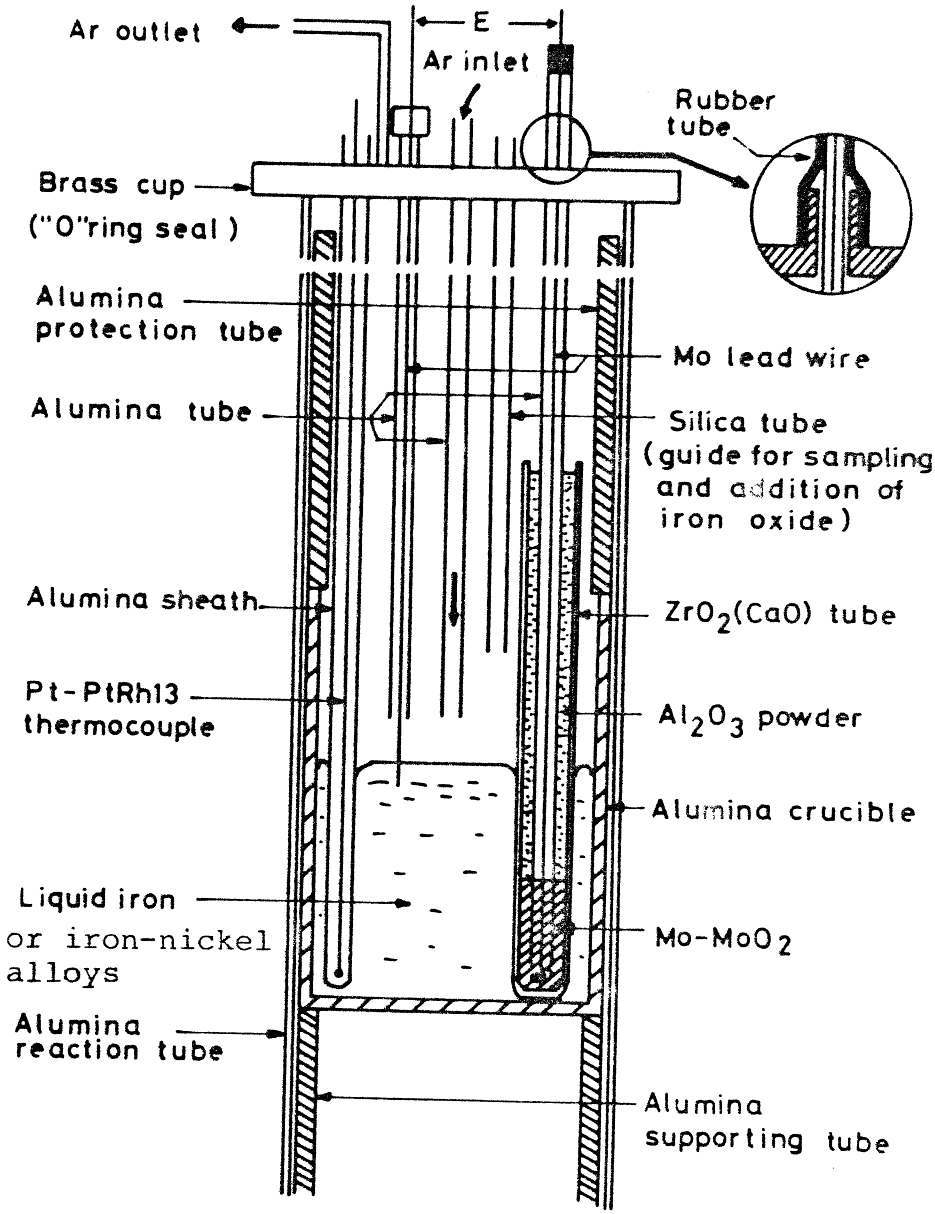

Fig.3.1 Experimental apparatus for cells (I) and (III).

alumina tube by means of alumina cement. A 4/1 volume ratio of Mo-MoO_2 powder mixture was packed in the zirocnia tube and used as reference electrode. Electrical contacts to Mo-MoO_2 reference electrode and to the melt were accomplished by Mo wires of 0.5 mm dia. and 2 mm dia., respectively.

Assembled cell was put on the solid metal sample in a SiC resistance furnace, heated in vacuum to 700 K in order to remove methyl alcohol and water used as binder for Mo-MoO_2 powder mixture, and then the furnace tube was filled with purified argon. During the slow heating of the cell to the experimental temperature, the alumina cement was sintered, and when the sample was melted, the "half cell" Mo-MoO_2/ZrO_2(CaO) tube with Mo wire was kept just above the melt. The half cell and Mo wire of 2 mm dia. was intermittently dipped into the melt for a few seconds by sliding through a rubber tube at intervals of about 1 to 2 min, and e.m.f.'s were measured by digital voltmeter with an internal impedance of 10^8 ohm. To avoid induction noise, the electric current for the furnace was instantaneously disconnected during each e.m.f. readings without any change of temperature. In all cases, the e.m.f.'s were confirmed to be unaffected by induction noise.

Temperature of the melt was measured by Pt-PtRh13 thermocouple placed at the bottom of the melt and controled within ± 1 K by using temperature regulator. The couple had been checked for the melting points of palladium and gold by the wire method. The overall error in temperature measurement and control was estimated to be within ± 2 to 4 K. Since the resistance furnace had a long homogeneous temperature zone of 80 mm long within ± 1 K, there would be no measurable temperature gradient across the cell.

After confirming steady e.m.f. values, the change of which was less than ± 1 to 2 mV for several e.m.f. readings, sampling was made by a silica tube of 3 mm ID by suction and the smaples were quenched in water. In order to increase the oxygen content in the melt, iron oxide packed by pure iron foil for cell(I), or oxide pellet containing Fe, Fe_2O_3, Ni and NiO, in which the atomic ratio of Fe/Ni was the same as that in the melt, for cell(III), was added to the melt. The e.m.f. measurements were thus repeated for 4 to 7 hrs. The e.m.f. measurements were performed at 1823 and 1873 K for cell(I) and 1873 K for cell(III), respectively.

The melt was thoroughly stirred with an alumina rod to minimize the change of oxygen concentration at the melt/solid electrolyte interface due to the oxygen transfer through micropores in ceramic electrolyte as discussed in a latter section. The e.m.f. was found to be independent of the flow rate of argon. The phases present in the reference electrode were determined before and after experiments by X-ray diffraction technique, and the results indicated only Mo + MoO_2. The reversibility of the cell potential was checked by passing a small external current in either direction for a few seconds. In each case , the e.m.f. was found to return to original value .

Oxygen content in the quenched sample was analysed by inert gas fusion coulometric titration. In this technique a sample is fused in a graphite crucible at a temperature higher than 2273 K. The CO evolved is swept by purified argon and is converted to CO_2 by I_2O_5 at 433K. The CO_2 is dissolved in H_2O + 50 kg m^{-3} $Ba(ClO_4)_2$ solution. The amount of CO_2 dissolved in the solution was determined by coulometric titration. Gravimetric method as nickel-dimethyl-glyoxime was adopted for the chemical analysis of nickel in alloys. The maximum content of molybdenum in liquid iron and iron-nickel alloys after experiments was 1.66 wt%, which would give negligible effect on the activity of oxygen[3].

b. Cell(II)

Fig.3.2 illustrates the experimental apparatus for cell(II), which is similar to that used for cell (I) or (III) with a slight modification in electrical lead to liquid nickel. In the case of cell(II), by using $LaCrO_3$ rod sintered to a Pt wire, e.m.f. of the cell was continuously measured. To increase the oxygen content in liquid nickel, following forms of nickel oxide were added to the melt;

1) nickel wire oxidized in air at 1273 K for low oxygen content,
2) mixed pellet of NiO and Ni for intermediate oxygen content,
3) NiO powder packed in pure nickel foil for high oxygen content.

Other details in experiments for cell(II) are the same as those for cells(I) and (III).

3.2.3 Electrical Lead Materials

At the initial experimental runs for cell(I),

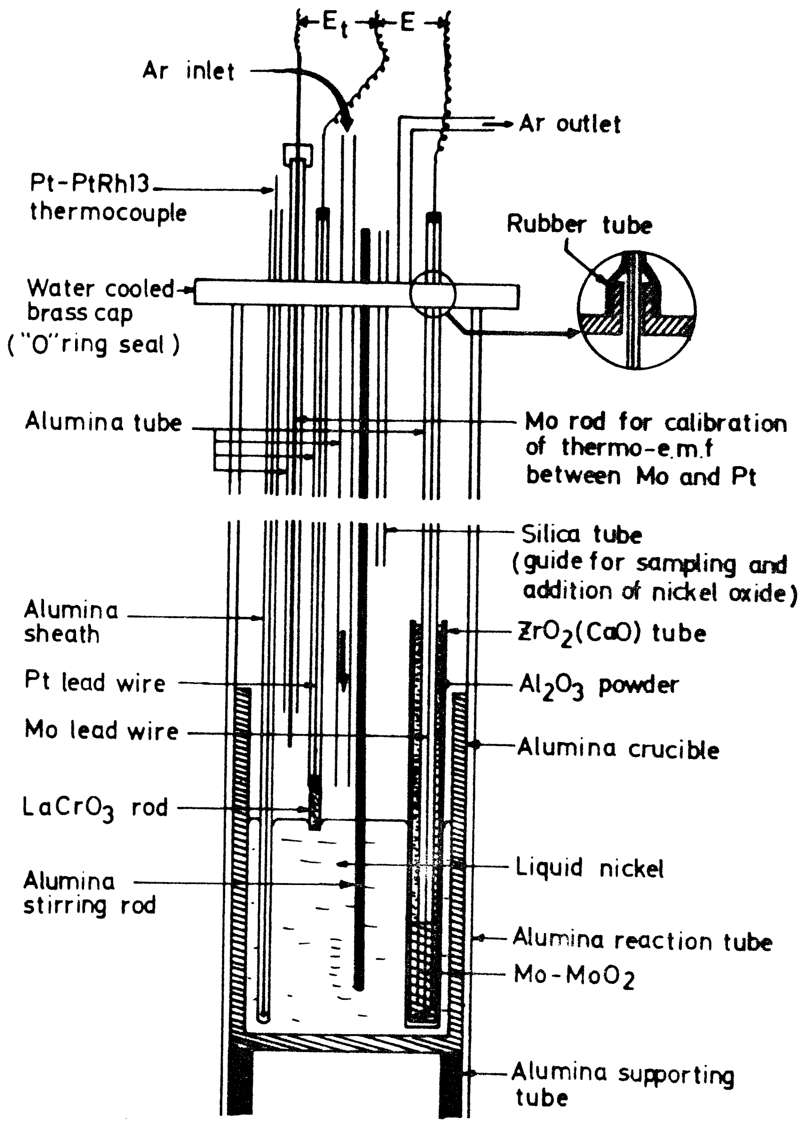

Fig.3.2 Experimental apparatus for cell(II).

Mo wire, V_2O_3 rod[4] sintered with ZrO_2 powder at 1273 K for 48 hrs, Mo-Al_2O_3 cermet, and $LaCrO_3$ rod were tested for their applicability as electrical lead material to liquid iron.

Mo wire was more convenient than the others because of its small heat capacity and suitable mechanical strength at the experimental temperature.

Though Kawakami and Goto[4] reported that the V_2O_3 rod was suitable as electrical lead wire to liquid iron and stable e.m.f.'s were obtained for 30 min with the cell, Mo-MoO_2/ZrO_2(CaO)/$\underline{O}$(in Fe), the author's results for V_2O_3 rod sintered with ZrO_2 powder showed that this material is easily dissolved in liquid iron, and stable e.m.f.'s were not obtained.

Mo-Al_2O_3 cermet was also easily dissolved into liquid iron. Furthermore, in this case, fine alumina particles, which would be arised from the dissolution of Mo-Al_2O_3 cermet, would cause an undesirable error in chemical analysis of oxygen in quenched sample.

Though $LaCrO_3$ was not suitable as electrical lead material to liquid iron and iron-nickel alloys, it was found that this material is very stable in liquid nickel, and by using the $LaCrO_3$, stable e.m.f.'s of cell(II) were continuously measured over 5 hrs.

3.3 Results and Discussion

3.3.1 Cell(I)

In the case of cell(I), two kinds of zirconia tubes were used for the e.m.f. measurements. One was made by slipcasting and the other was made by rubber-pressing. An experimental difficulties were experienced for the case of rubber-pressed tube. The experimental results obtained by these two kinds of tubes are shown in Fig.3.3 and 3.4. A fairly good linear relationship between e.m.f. and log [%O] were obtained by slipcast zirconia tube, while in the case of rubber-pressed tube the relationship was not linear. The difference in e.m.f.'s obtained by two kinds of tubes were increased with a decrease in oxygen concentration in liquid iron. Above 0.06 wt% oxygen the e.m.f. values obtained by two different tubes are shown in good agreement.

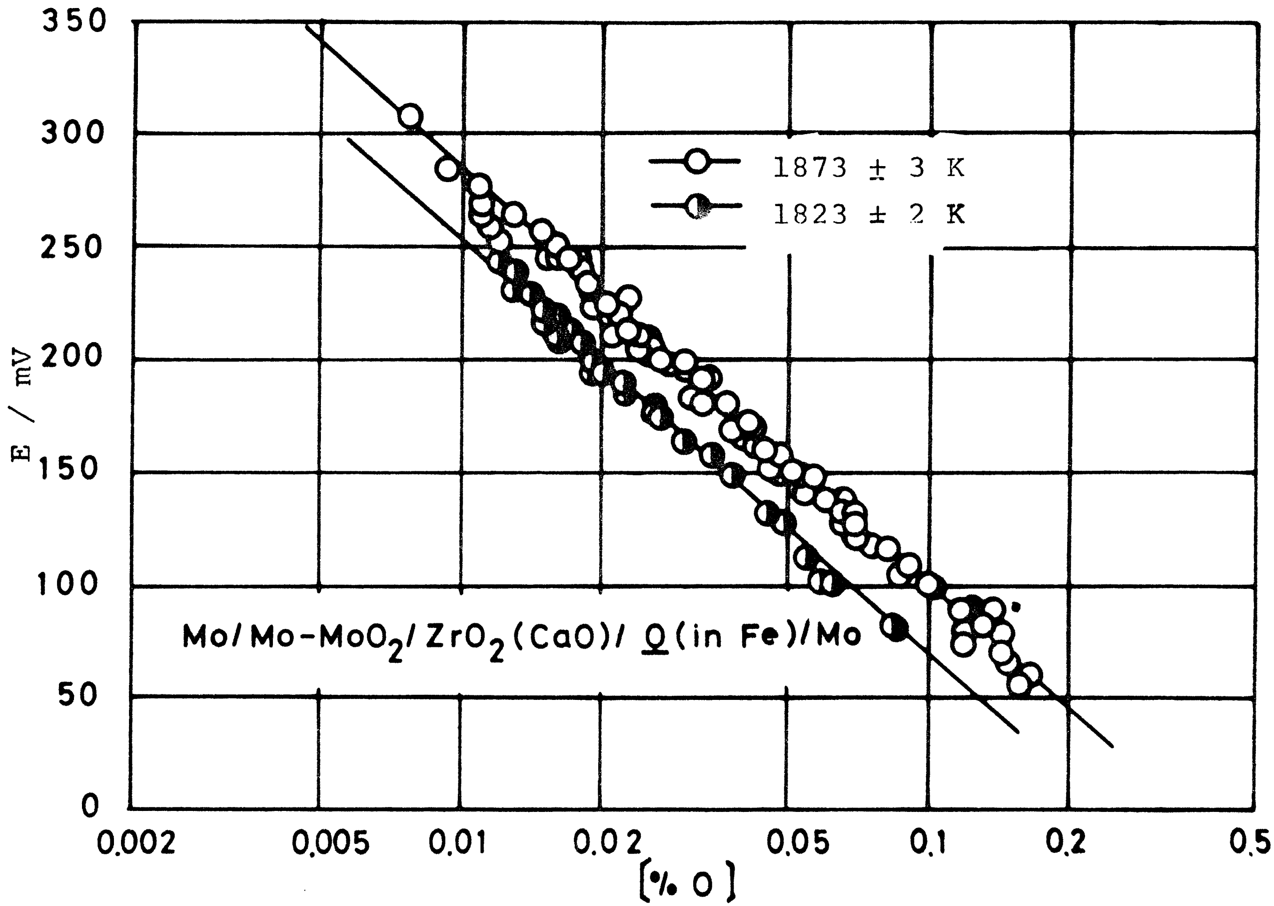

Fig.3.3 Relation between e.m.f. and log[%O] obtained by impervious slipcast zirconia tube for cell(I).

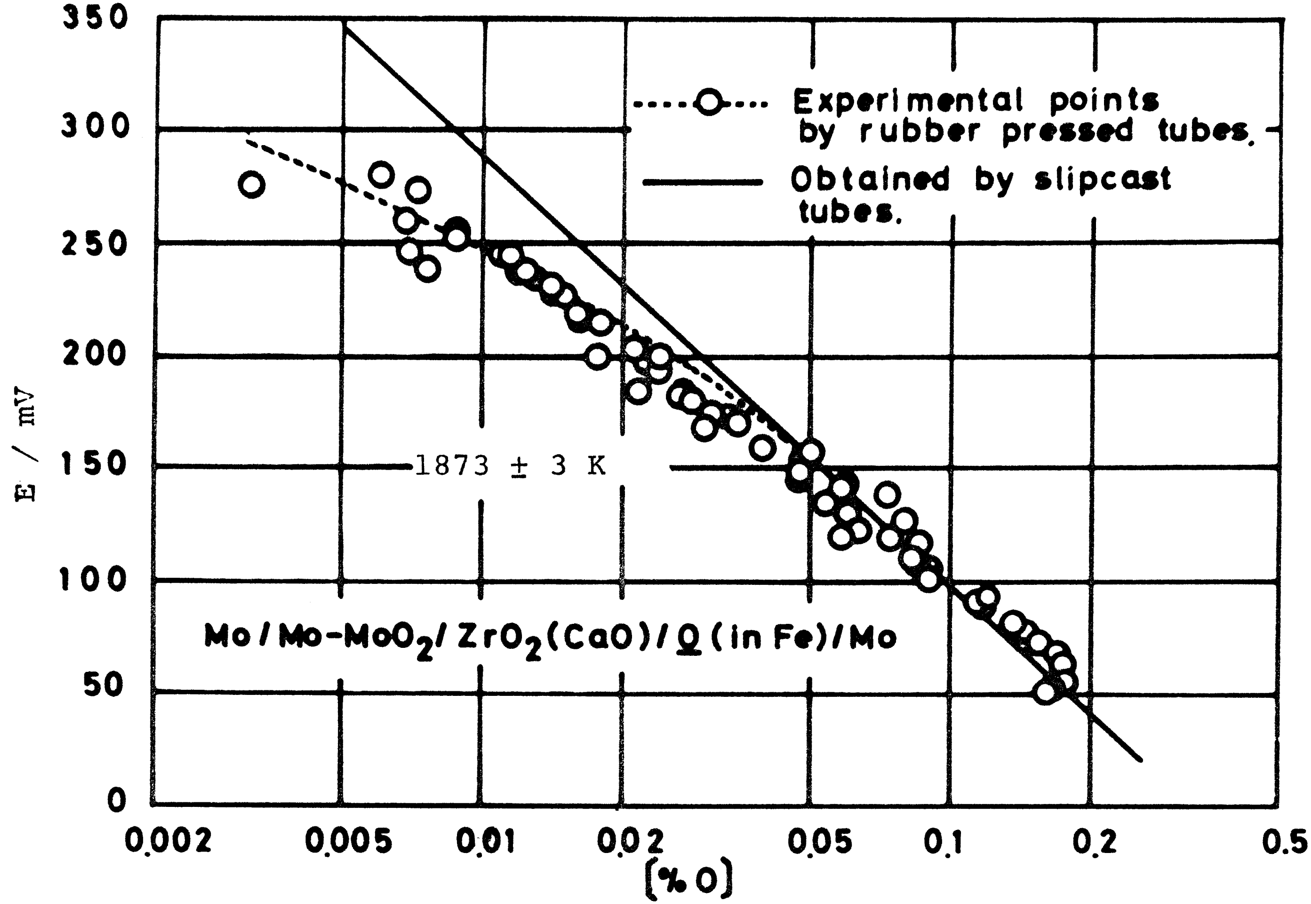

Fig.3.4 Relation between e.m.f. and log[%O] obtained by porous rubber-pressed tube for cell(I).

The color of the zirconia tube after experiment was changed to dark grey. The microstructure of the surface of the tubes are shown in Photo.3.1 for slipcast tube, and in Photo 3.2 for rubber-pressed tube, respectively. These photographs show that the microstructure of the surface are nearly the same with each other. The microstructure of the cross sections are shown in photos.3.3 and 3.5 for slipcast tube, and in photos. 3.4 and 3.6 for rubber-pressed tube, respectively. As shown in these photographs, the rubber-pressed tube was generally more porous than the slipcast tube. These photographs would give the most plausible explanation for the experimental difficulties appeared in the case of rubber-pressed tube. The micropores would permit oxygen to transfer from the $Mo-MoO_2$ electrode(high P_{O_2}) to liquid iron (low P_{O_2}). Since the difference in oxygen potential between $Mo-MoO_2$ reference electrode and liquid iron increases with decreasing oxygen concnetration in liquid iron, the "micropore effect" would cause a severe effect on measured e.m.f. at low oxygen concnetration as discussed in a later section.

TABLE 2 summarizes the values of critical oxygen activities in liquid iron at 1873 K below which the

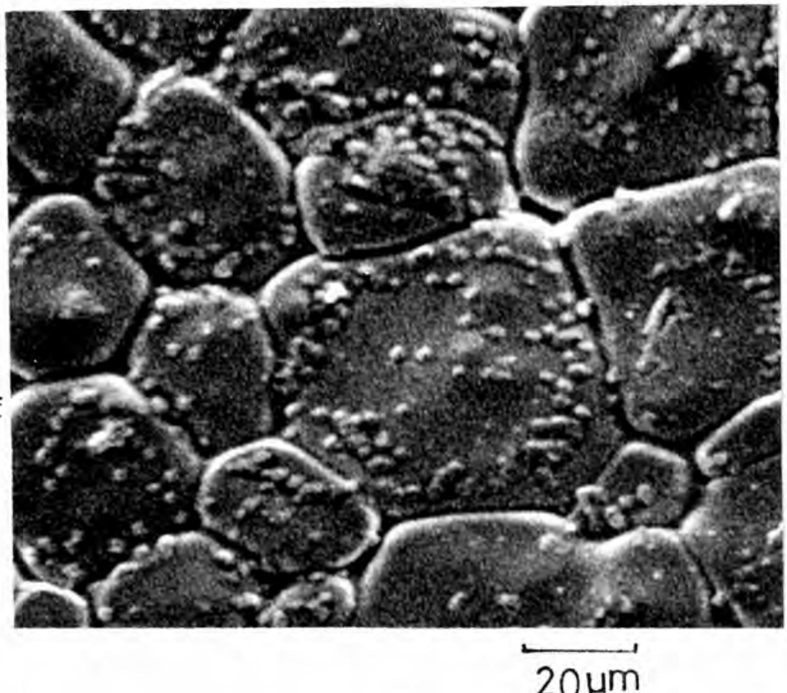

Photo.3.1

The surface of the zirconia tube made by slipcasting.

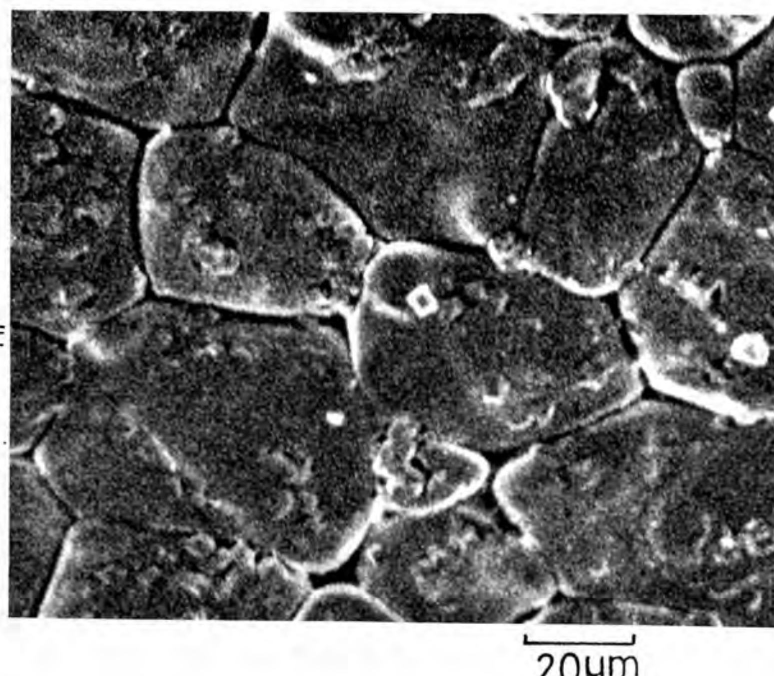

Photo.3.2

The surface of the zirconia tube made by rubber pressing.

Photo 3.3

The cross section of the zirconia tube made by slip-casting.

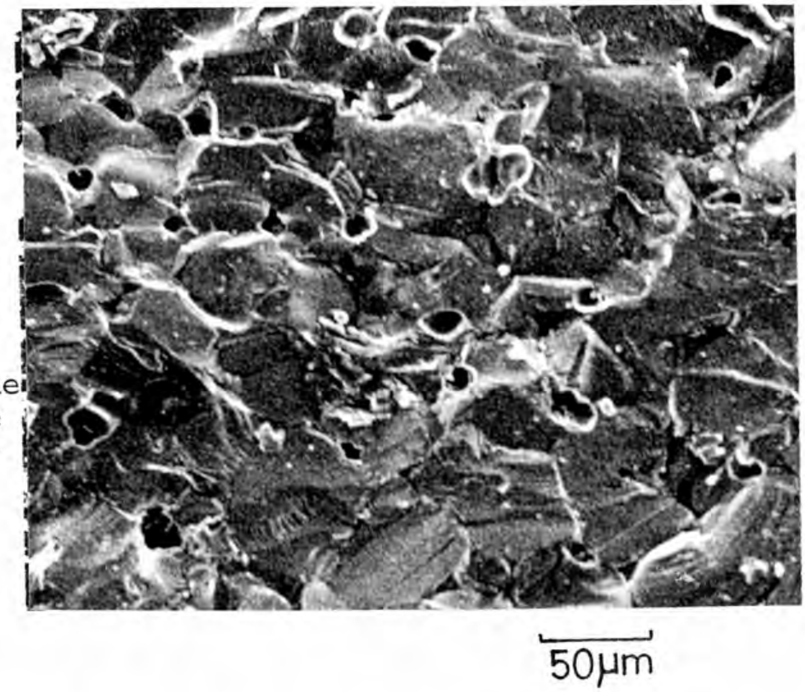

Photo.3.4

The cross section of the zirconia tube made by rubber-pressing.

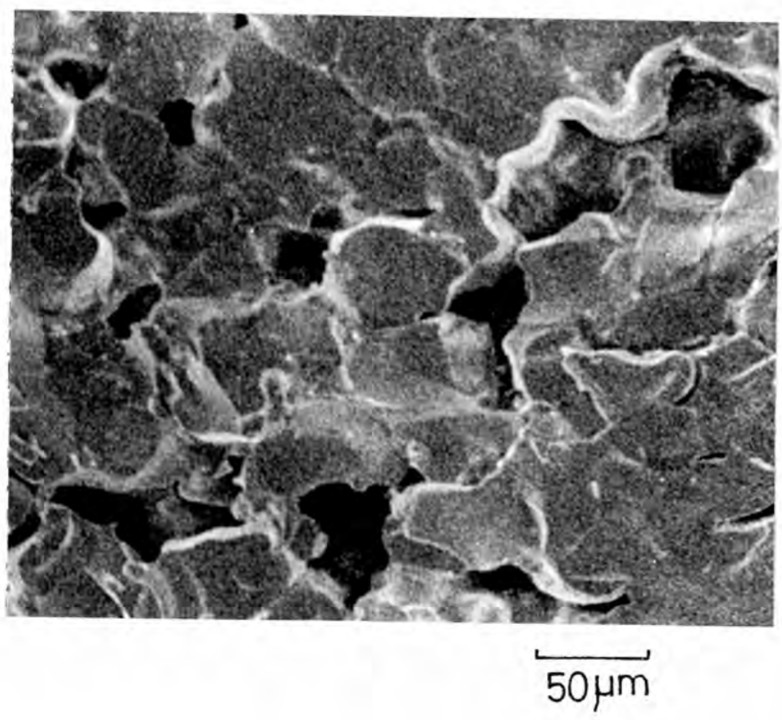

Photo.3.5

The cross section of the zirconia tube made by slipcasting.

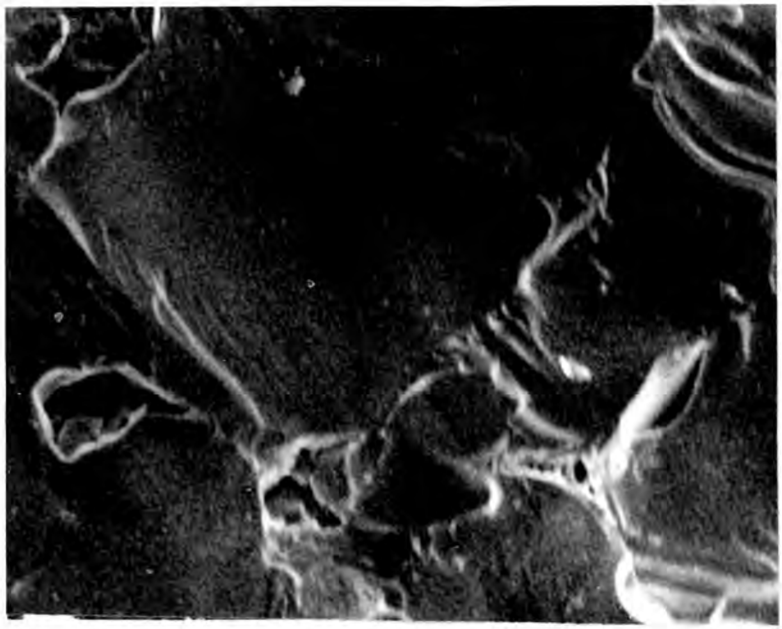

20um

Photo.3.6

The cross section of the zirconia tube made by rubber-pressing.

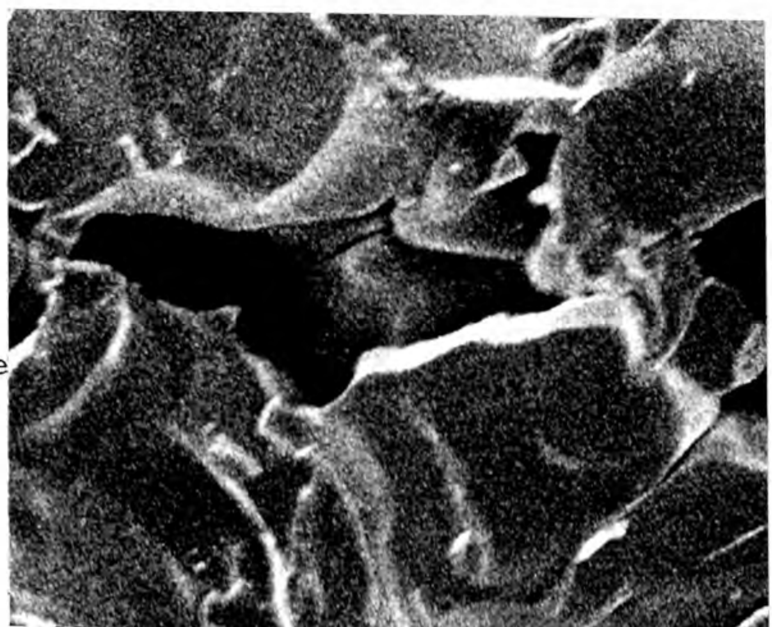

20um

TABLE 2 Critical oxygen activity with calcia-stabilized zirconia solid electrolyte in liquid iron at 1873 K.

Authors and ref.	Year	Reference electrode	Critical oxygen activity
Fischer and Ackerman (2)	1965	Air	0.02 %
Fischer and Pateisky (7)	1970	$Mo-MoO_2$	0.03 %
Fischer and Janke (5)	1970	Air	0.004 % *
Fruehan, Martonik and Turkdogan (8)	1969	$Cr-Cr_2O_3$	0.017 % **
Present Author	1975	$Mo-MoO_2$	0.008 %

* Melts were stirred.
** Value for Fe-Al-O melt is 0.001 %

n-type electronic conduction is significant. Generally the critical oxygen activity is evaluated from the linear dependence of measured e.m.f.'s on log [%O]. Therefore, in order to evaluate the critical oxygen activity, the " micropore effect" should be taken into account. In the absence of this undesirable effect, the critical oxygen activity should be equal to the critical oxygen concentration below which the relationship between e.m.f. and log [%O] is not linear.

Fischer and Ackermann(2) reported that below 0.02 wt% oxygen, the calcia-stabilized zirconia would show significantly electronic conduction since below 0.02 wt % the e.m.f.'s of their cell, Pt/air/ZrO_2(CaO)/$\underline{O}$(in Fe), did not show a liner dependence on log [%O]. However in their experiments, the micropore effect may cause a severe error on measured e.m.f. because of the large difference in oxygen potential between the air reference electrode and liquid iron.

Fischer and Janke(5) reported that when the melt was thoroughly stirred, the measured e.m.f.'s of their cell, Pt/air/ZrO_2(CaO)/$\underline{O}$(in Fe), show a linear dependence on log [%O] above 0.004 wt%.

Fischer and Pateisky[6] reported that the range of oxygen concentration in which the e.m.f.'s of their cell, $Mo/Mo\text{-}MoO_2/ZrO_2(CaO)/\underline{O}$(in Fe), show a linear dependence on log [%O] is restricted above 0.03 wt%. They utilized a small zirconia pellet fixed to the end of silica tube with $Mo\text{-}MoO_2$ reference electrode which is initially packed in the silica tube as $Mo\text{-}MoO_3$. The crevice between the zirconia pellet and the silica tube may be a source of oxygen transfer from $Mo\text{-}MoO_2$ reference electrode to liquid iron.

In the present study, the linear relationship between e.m.f. and log [%O] was obatined in the range of oxygen concentration from 0.0077 to 0.165 wt% at 1873 K. The e.m.f. measurements below 0.0077 wt% were impossible because the melt containing such a low oxygen content without any deoxidizer can not be obtained. In summary, the calcia -stabilized zirconia used in the present study would be predominantly ionic conductor above 0.0077 wt% oxygen, and in the absence of the "micropore effect", the relationship between e.m.f. and log[%O] would be linear.

The experimental results obtained by cell(I) with slipcast zirconia tubes are summarized in TABLE 3a and b.

TABLE 3a Experimental results for cell(I) with slipcast zirconia tube at 1873 K.

No.	e.m.f. (mV)	[%O]	$\frac{1}{2}$ log P_{O_2} (atm)	log K'(Fe)
32-01	224.0	0.015	- 5.15	3.33
-02	216.0	0.015	- 5.11	3.28
-03	215.5	0.015	- 5.11	3.28
-04	211.0	0.016	- 5.08	3.29
-05	208.5	0.016	- 5.07	3.27
-06	199.0	0.019	- 5.02	3.30
-07	194.5	0.019	- 4.99	3.27
-08	182.5	0.023	- 4.93	3.29
-09	174.0	0.027	- 4.88	3.31
-10	166.0	0.030	- 4.83	3.31
-11	157.5	0.034	- 4.79	3.32
-12	137.0	0.045	- 4.67	3.33
-13	129.5	0.049	- 4.63	3.32
-14	111.5	0.056	- 4.53	3.28
-16	84.5	0.084	- 4.38	3.31
34-01	230.0	0.014	- 5.19	3.333
-02	218.0	0.016	- 5.12	3.33
-03	213.0	0.017	- 5.09	3.32
-04	210.0	0.016	- 5.08	3.28
-05	191.0	0.022	- 4.97	3.31
-06	176.5	0.026	- 4.89	3.31
-07	177.0	0.026	- 4.89	3.31
-08	149.0	0.038	- 4.74	3.32

TABLE 3a Experimental results for cell(I) with slipcast zirconia tube at 1823 K(Continued)

No.	e.m.f. (mV)	[%O]	$\frac{1}{2}\log P_{O_2}$ (atm)	log K'(Fe)
35-01	245.0	0.012	- 5.27	3.35
-02	240.5	0.013	- 5.25	3.32
-03	233.5	0.013	- 5.21	3.32
-04	220.5	0.015	- 5.14	3.31
-05	214.0	0.015	- 5.10	3.28
-06	212.0	0.016	- 5.09	3.29
-07	208.0	0.018	- 5.07	3.32
-08	200.5	0.019	- 5.02	3.30
-09	194.5	0.021	- 4.99	3.31
-10	187.5	0.022	- 4.95	3.30
-11	181.0	0.023	- 4.92	3.28
-12	175.5	0.026	- 4.89	3.30
-15	103.5	0.062	- 4.49	3.28
-16	82.5	0.087	- 4.37	3.31

TABLE 3b Experimental results for cell(I) with slipcast zirconia tube at 1873 K.

No.	e.m.f. (mV)	[%O]	$\frac{1}{2}\log P_{O_2}$ (atm)	log K'(Fe)
25-01	245.5	0.018	- 5.04	3.30
-02	224.5	0.023	- 4.93	3.29
-03	218.0	0.023	- 4.90	3.26
-04	218.0	0.022	- 4.89	3.23
-05	213.0	0.024	- 4.87	3.25
-06	199.0	0.029	- 4.79	3.25
-07	197.0	0.027	- 4.78	3.21
-08	194.0	0.030	- 4.76	3.24
-09	181.5	0.037	- 4.70	3.26
-10	170.5	0.043	- 4.64	3.27
-11	161.5	0.048	- 4.59	3.27
-12	148.0	0.057	- 4.52	3.27
-13	139.0	0.066	- 4.47	3.29
-14	122.0	0.076	- 4.38	3.26
-15	93.0	0.126	- 4.22	3.32
-16	82.0	0.140	- 4.16	3.31
27-01	246.5	0.016	- 5.05	3.25
-02	229.0	0.023	- 4.95	3.31
-03	224.5	0.019	- 4.93	3.21
-04	211.0	0.021	- 4.85	3.18
-05	202.0	0.024	- 4.81	3.19
-06	198.5	0.026	- 4.79	3.20
-07	180.0	0.033	- 4.69	3.21

TABLE 3b Experimental results for cell(I) with slipcast zirconia tube at 1873 K(Continued).

No.	e.m.f. (mV)	[%O]	$\frac{1}{2}\log P_{O_2}$ (atm)	log K'(Fe)
27-08	166.6	0.038	- 4.62	3.19
-09	153.5	0.046	- 4.55	3.21
-10	148.0	0.048	- 4.52	3.20
-11	137.5	0.054	- 4.46	3.19
-12	121.0	0.072	- 4.37	3.23
-13	106.5	0.087	- 4.29	3.23
-14	98.5	0.100	- 4.25	3.25
-15	90.0	0.119	- 4.20	3.28
-16	81.5	0.119	- 4.16	3.23
-17	74.5	0.118	- 4.12	3.19
-18	66.0	0.148	- 4.07	3.24
-19	61.0	0.165	- 4.05	3.26
28-01	269.0	0.011	- 5.17	3.21
-02	264.0	0.011	- 5.14	3.18
-03	260.5	0.012	- 5.12	3.20
-04	254.0	0.012	- 5.09	3.17
-05	245.5	0.015	- 5.04	3.22
-06	240.5	0.015	- 5.01	3.19
-07	226.0	0.019	- 4.94	3.21
-08	219.0	0.020	- 4.90	3.20
-09	210.0	0.021	- 4.85	3.17
-10	187.5	0.032	- 4.73	3.23

TABLE 3b Experimental results for cell(I) with slipcast zirconia tube at 1873 K(Continued)

No.	e.m.f. (mV)	[%O]	$\frac{1}{2}\log P_{O_2}$ (atm)	log K'(Fe)
29-01	314.0	0.0077	- 5.41	3.30
-02	285.5	0.0092	- 5.26	3.22
-03	278.0	0.011	- 5.22	3.26
-04	264.5	0.013	- 5.14	3.26
-05	257.0	0.015	- 5.10	3.28
-06	245.0	0.017	- 5.04	3.27
-07	235.0	0.019	- 4.98	3.26
-08	225.0	0.020	- 4.93	3.23
-09	213.5	0.022	- 4.87	3.21
-10	181.5	0.031	- 4.70	3.19
-11	159.5	0.044	- 4.58	3.22
-12	153.5	0.047	- 4.55	3.22
-13	137.5	0.059	- 4.46	3.23
-14	128.5	0.064	- 4.41	3.22
-15	115.0	0.081	- 4.34	3.25
-16	101.5	0.102	- 4.27	3.27
-17	89.5	0.117	- 4.20	3.27
-18	84.5	0.131	- 4.17	3.29
-19	72.5	0.145	- 4.11	3.27
-20	55.5	0.157	- 4.02	3.21
30-01	251.0	0.016	- 5.07	3.27
-02	241.0	0.018	- 5.02	3.27
-03	228.5	0.019	- 4.95	3.23

TABLE 3b Experimental results for cell(I) with slipcast zirconia tube zt 1873 K(Continued).

No.	e.m.f. (mV)	[%O]	$\frac{1}{2}$ log P_{O_2} (atm)	log K'(Fe)
30-04	221.0	0.021	- 4.91	3.23
-05	211.5	0.024	- 4.86	3.24
-06	208.5	0.025	- 4.81	3.21
-07	203.5	0.025	- 4.81	3.21
-08	196.0	0.028	- 4.77	3.22
-09	184.5	0.031	- 4.71	3.20
-10	171.0	0.040	- 4.64	3.24
-11	163.0	0.043	- 4.60	3.23
-12	155.5	0.048	- 4.56	3.24
-13	137.5	0.060	- 4.43	3.25
-14	133.0	0.066	- 4.43	3.25
-15	128.5	0.069	- 4.41	3.25
-16	110.0	0.089	- 4.31	3.26
-17	89.0	0.137	- 4.20	3.33
31-01	246.0	0.016	- 5.04	3.25
-02	225.5	0.020	- 4.93	3.23
-03	214.5	0.022	- 4.87	3.22
-04	206.5	0.025	- 4.83	3.23
-05	198.5	0.028	- 4.79	3.23
-06	192.5	0.030	- 4.76	3.23
-07	184.5	0.034	- 4.71	3.24
-08	172.0	0.041	- 4.64	3.26
-09	170.5	0.041	- 4.64	3.25

TABLE 3b Experimental results for cell(I) with slipcast zirconia tube at 1873 K(continued)

No.	e.m.f. (mV)	[%O]	$\frac{1}{2}$ log P_{O_2} (atm)	log K'(Fe)
31-10	156.5	0.054	- 4.56	3.29
-11	151.5	0.052	- 4.53	3.25
-12	133.0	0.070	- 4.43	3.28

3.3.2 Cell(II)

The experimental results for cell(II) are shown in Fig.3.5. In the case of cell(II), the slipcast zirconia tube was used for the experiments. It was found by X-ray diffraction technique that the liquid nickel with high-oxygen content significantly reacts with the calcia-stabilized zirconia tube. Fig.3.6 shows the X-ray patterns for the zirconia tubes on the sections of both sides before and after the experiments. As shown in Fig.3.6(a), the solid electrolyte tube used in the present study was the "fully" stabilized zirconia. The crystal structure of the outer side of the wall of the zirconia tube which was continuously dipped into liquid nickel with 0.25 wt% of oxygen at 1873 K for over 7 hrs was converted into monoclinic structure as shown in Fig.3.6(c). The inner side of the wall of the tube after the experiments also containes a small amount of monoclinic ZrO_2 which should be transformed from tetragonal ZrO_2 at high temperature(Fig.3.6(b)). Liquid nickel and dissolved oxygen would react with the zirconia tube, and tetragonal ZrO_2-NiO-CaO solid solution was probably formed.

$$ZrO_2(CaO) \quad + \quad Ni(liquid) + \underline{O}(in\ Ni)$$
$$= \quad ZrO_2\text{-}NiO\text{-}CaO \text{ solid solution.}$$

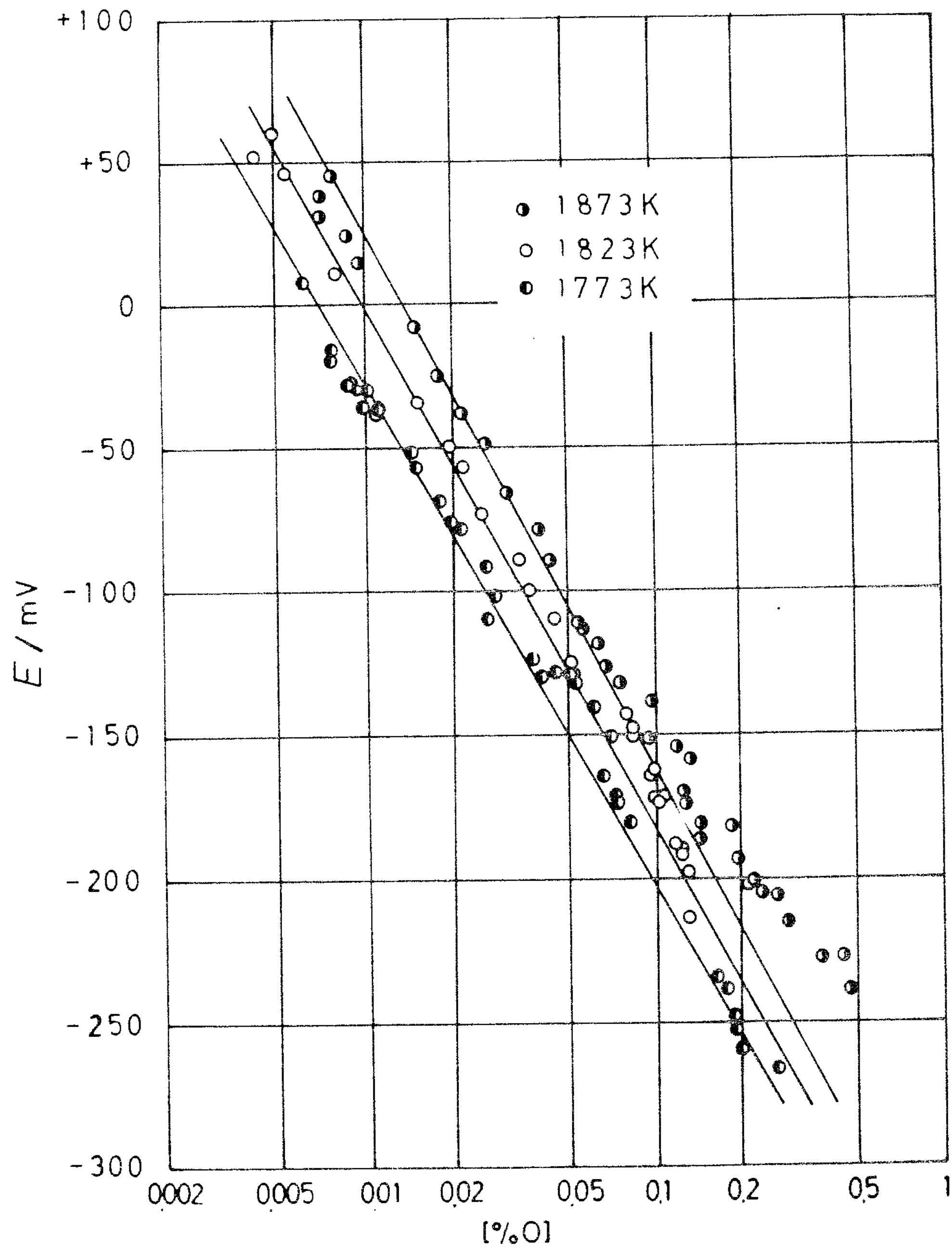

Fig.3.5 Relation between e.m.f. and log[%O] for cell(II).

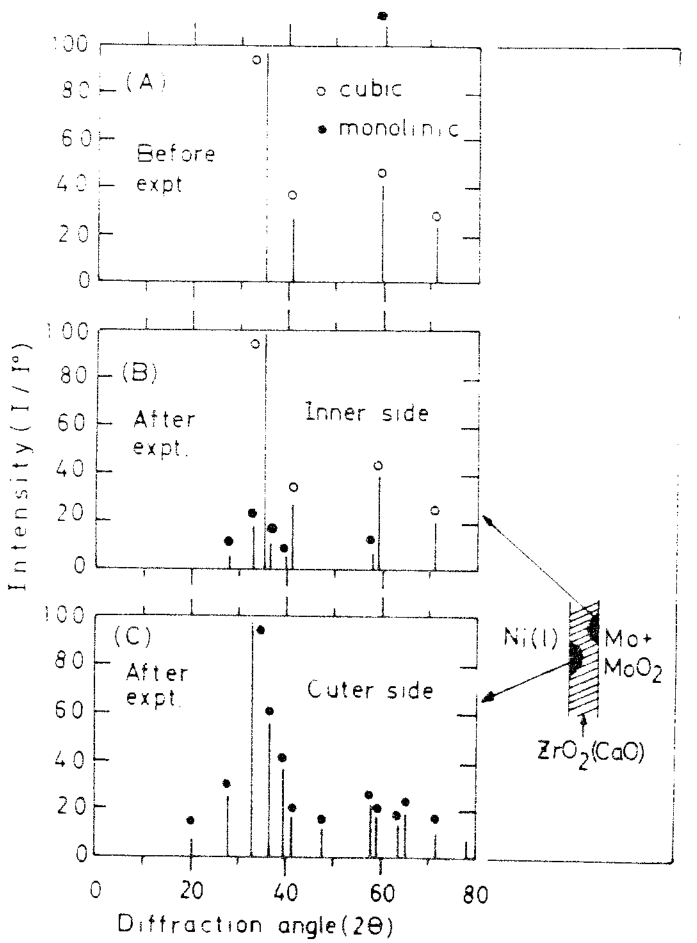

Fig.3.6 X-ray patterns for zirconia tube (a) before experiments, (b) inner side of the cross section of zirconia tube after dipped into liquid nickel containing 0.25 wt % oxygen at 1873 K over 7 hrs,(c) outer side of the cross section of zirconia tube after dipped into liquid nickel containing 0.25 wt% of oxygen at 1873K over 7 hrs.

The rate of reaction between the zirconia tube and liquid nickel increased with increasing oxygen concnetration, but did not show a clear dependence on temperature .

According to Kumar et al.[7], the monoclinic ZrO_2 would show predominantly electronic conduction even below 1273 K. The tetragonal ZrO_2 would show entirely electronic conduction because of its very small concentration of oxygen-ion vacancy and because of the very high temperature in the present study. Indeed, the e.m.f. obtained by the zirconia tube with only monoclinic ZrO_2(tetragonal at the experimental temperature) was unstable and very much lower than the theoretical value. If the experimental data concerning the ionic conductivity of tetragonal zirconia at the experimental temperature and the phase diagram of the system ZrO_2-NiO-CaO were available, one may have further discussion on the mechanism of de-stabilization of the zirconia tube.

The e.m.f. of cell(II) was continuously measured for over 4 to 7 hrs, but e.m.f. readings beyond 7 hrs were impossible because of the reaction between the zirconia tube and liquid nickel. The e.m.f. measurements were performed at 1773, 1823 and 1873 K. The experimental results for cell(II) are summarized in TABLE 4a to c.

3.3.3 Cell(III)

The e.m.f. measurements for cell(III) were performed at 1873 K. The slipcast zirocnia tube was used for this cell. Stable e.m.f.'s were obtained for 4 to 7 hrs, but prolonged e.m.f. measurements beyond 7 hrs were impossible because of the reaction between zirconia tube and the melt. The experimental results are summarized in TABLE 5 and are shown in Fig. 3.7.

TABLE 4a Experimental results for cell(II) at 1773 K

No.	e.m.f. (mV)	[%O]	$\frac{1}{2}\log P_{O_2}$ (atm)	log K'(Ni)
3-01	+ 8.5	0.0062	- 4.17	1.96
-02	- 109.5	0.027	- 3.50	1.92
-03	- 123.0	0.038	- 3.42	2.00
-04	- 129.0	0.046	- 3.39	2.05
-05	- 142.5	0.053	- 3.31	2.03
-06	- 140.0	0.054	- 3.32	2.05
-07	- 142.5	0.053	- 3.31	2.04
-08	- 164.5	0.067	- 3.18	2.00
-09	- 174.0	0.074	- 3.13	2.00
-10	- 180.5	0.082	- 3.09	2.00
4-01	- 19.5	0.0078	- 4.01	1.90
-02	- 37.0	0.011	- 3.91	1.96
-03	- 52.0	0.015	- 3.82	1.98
-04	- 69.0	0.018	- 3.73	1.99
-05	- 78.5	0.021	- 3.60	2.02
-06	- 91.0	0.027	- 3.60	2.02
-07	- 129.0	0.051	- 3.39	2.10
-08	- 140.5	0.061	- 3.32	2.11
-09	- 172.0	0.074	- 3.14	2.01
-10	- 180.5	0.081	- 3.09	2.00
-11	- 150.5	0.072	- 3.26	2.11
5-01	- 15.0	0.0077	- 4.04	1.93
-02	- 28.5	0.009	- 3.96	1.90

TABLE 4a Experimental results for cell(II) at 1773 K (Continued).

No.	e.m.f. (mV)	[%O]	$\frac{1}{2}\log P_{O_2}$ (atm)	log K'(Ni)
5-03	- 31.0	0.009	- 3.94	1.91
-04	- 29.0	0.009	- 3.96	1.92
-05	- 30.0	0.010	- 3.95	1.96
-06	- 36.0	0.010	- 3.92	1.92
-07	- 39.0	0.011	- 3.90	1.95
-08	- 57.0	0.015	- 3.80	1.98
-09	- 76.5	0.020	- 3.69	1.99
-10	- 102.0	0.028	- 3.54	1.99
-11	- 129.5	0.041	- 3.38	1.99
6-01	- 235.0	0.184	- 2.68	1.95
-02	- 238.5	0.173	- 2.76	2.00
-03	- 234.0	0.164	- 2.80	2.01
-04	- 247.5	0.180	- 2.71	1.97
-06	- 266.0	0.255	- 2.61	2.02

TABLE 4b Experimental results for cell(II) at 1823 K.

No.	e.m.f. (mV)	[%O]	$\frac{1}{2}$ log P_{O_2} (atm)	log K'(Ni)
1-01	+ 60.0	0.0049	- 4.25	1.94
-02	- 49.5	0.019	- 3.64	1.93
-03	- 73.5	0.025	- 3.51	1.91
-04	- 125.0	0.051	- 3.22	1.93
-05	- 162.5	0.098	- 3.01	2.00
-06	- 173.5	0.103	- 2.95	1.96
-07	- 192.0	0.122	- 2.85	1.94
-08	- 172.5	0.100	- 2.96	1.96
-09	- 172.5	0.106	- 2.96	1.99
-10	- 164.0	0.096	- 3.01	1.99
-11	- 188.0	0.118	- 2.87	1.95
-12	- 190.5	0.123	- 2.86	1.95
-13	- 214.5	0.128	- 2.73	1.84
2-01	+ 51.5	0.0042	- 4.20	1.82
-02	+ 45.5	0.005	- 4.17	1.90
-03	+ 10.5	0.008	- 3.97	1.87
-04	- 34.5	0.015	- 3.72	1.90
-05	- 57.0	0.0022	- 3.60	1.94
-06	- 89.5	0.034	- 3.42	1.95
-07	- 100.0	0.038	- 3.36	1.93
-08	- 110.0	0.045	- 3.31	1.96
-09	- 126.0	0.068	- 3.22	2.05
-10	- 143.0	0.080	- 3.12	2.02
-11	- 147.5	0.084	- 3.10	2.02

TABLE 4b Experimental results for cell(II) at 1823 K. (continued).

No.	e.m.f. (mV)	[%O]	$\frac{1}{2}\log P_{O_2}$ (atm)	log K'(Ni)
2-12	- 150.5	0.083	- 3.08	2.00
-13	- 197.5	0.129	- 2.82	1.93
-14	- 202.5	0.210	- 2.79	2.11

TABLE 4c Experimental results for cell(II) at 1873 K.

No.	e.m.f. (mV)	[%O]	$\frac{1}{2}\log P_{O_2}$ (atm)	log K'(Ni)
7-01	+ 45.0	0.0077	- 3.96	1.85
-02	+ 38.0	0.0070	- 3.92	1.77
-03	+ 30.5	0.0071	- 3.88	1.73
-04	+ 24.0	0.0088	- 3.85	1.79
-05	+ 14.0	0.0088	- 3.85	1.79
-06	- 8.0	0.015	- 3.68	1.85
-07	- 25.0	0.018	- 3.59	1.84
-08	- 39.0	0.021	- 3.51	1.84
-09	- 49.0	0.026	- 3.46	1.87
-10	- 66.0	0.031	- 3.36	1.85
-11	- 79.0	0.040	- 3.29	1.89
-12	- 89.5	0.044	- 3.24	1.88
-13	- 138.5	0.097	- 2.97	1.96
-14	- 154.5	0.119	- 2.89	1.96
-15	- 159.0	-.130	- 2.86	1.98
-16	- 182.0	0.181	- 2.74	2.00
8-01	- 111.0	0.054	- 3.12	1.85
-02	- 114.0	0.056	- 3.11	1.86
-03	- 119.0	0.063	- 3.08	1.88
-04	- 127.0	0.068	- 3.04	1.87
-05	- 132.0	0.075	- 3.01	1.89
-06	- 151.5	0.092	- 2.81	1.90
-07	- 169.5	0.123	- 2.81	1.90

TABLE 4c Experimental results for cell(II) at 1873 K. (Continued).

No.	e.m.f. (mV)	[%O]	$\frac{1}{2}$ log P_{O_2} (atm)	log K'(Ni)
8-08	- 174.0	0.127	- 2.78	1.88
-09	- 186.5	0.140	- 2.75	1.90
-10	- 180.5	0.1414	- 2.75	1.90
-11	- 193.0	0.189	- 2.68	1.96
-12	- 205.0	0.228	- 2.62	1.98
-13	- 200.5	0.218	- 2.64	1.98
-14	- 215.0	0.284	- 2.56	2.01
-15	- 206.0	0.260	- 2.61	2.03
-16	- 227.5	0.367	- 2.49	2.06
-17	- 239.0	0.466	- 2.43	2.10
-18	- 227.0	0.433	- 2.50	2.14

TABLE 5 Experimental results for cell(II) at 1873K.

No.	e.m.f. (mV)	[%O]	$\frac{1}{2}\log P_{O_2}$ (atm)	log K'(Fe-Ni)
		[%Ni] = 10.5		
15-01	+ 208.5	0.022	- 4.84	3.19
-02	+ 198.0	0.024	- 4.79	3.16
-03	+ 176.0	0.033	- 4.67	3.18
-04	+ 167.0	0.036	- 4.62	3.17
-05	+ 157.0	0.038	- 4.57	3.15
-06	+ 154.5	0.044	- 4.55	3.19
-07	+ 135.5	0.056	- 4.45	3.20
		[%Ni] = 20.8		
5-01	+ 206.5	0.014	- 4.83	2.99
-02	+ 175.5	0.020	- 4.67	2.96
-03	+ 158.5	0.023	- 4.57	2.92
-04	+ 136.0	0.029	- 4.45	2.91
-05	+ 118.5	0.038	- 4.36	2.93
-06	+ 106.0	0.047	- 4.29	2.96
-07	+ 89.0	0.060	- 4.20	2.98
-08	+ 77.0	0.076	- 4.13	3.01
-09	+ 64.5	0.098	- 4.07	3.06
-10	+ 59.5	0.109	- 4.04	3.08
-11	+ 53.0	0.118	- 4.00	3.07
-12	+ 33.0	0.122	- 3.90	2.99

TABLE 5 Experimental results for cell(III) at 1873 K (Continued).

No.	e.m.f (mV)	[%O]	$\frac{1}{2}\log P_{O_2}$ (atm)	log K'(Fe-Ni)
		[%Ni] = 31.1		
4-01	+ 193.0	0.016	- 4.76	2.97
-02	+ 176.0	0.018	- 4.67	2.93
-03	+ 169.0	0.019	- 4.63	2.91
-04	+ 148.5	0.025	- 4.52	2.91
-05	+ 135.5	0.029	- 4.45	2.91
-06	+ 118.0	0.041	- 4.36	2.97
-07	+ 103.0	0.055	- 4.27	3.01
-08	+ 58.0	0.078	- 4.03	2.92
-09	+ 64.5	0.098	- 4.07	3.06
-10	+ 59.5	0.109	- 4.04	3.08
-11	+ 53.0	0.118	- 4.00	3.07
-12	+ 33.0	0.122	- 3.90	2.99
		[%Ni] = 38.4		
6-03	+ 150.0	0.020	- 4.53	2.82
-04	+ 136.0	0.025	- 4.46	2.85
-05	+ 126.5	0.027	- 4.40	2.83
-06	+ 110.0	0.032	- 4.31	2.81
-07	+ 105.0	0.038	- 4.29	2.87
-08	+ 86.0	0.054	- 4.18	2.91
-09	+ 83.0	0.056	- 4.17	2.92
-10	+ 77.0	0.061	- 4.13	2.92
-11	+ 67.5	0.074	- 4.08	2.95

TABLE 5 Experimental results for cell(III) at 1873 K (Continued).

No.	e.m.f. (mV)	[%O]	$\frac{1}{2}\log P_{O_2}$ (atm)	log K'(Fe-Ni
		[%Ni] = 51.2		
7-01	+ 176.5	0.014	- 4.67	2.80
-02	+ 164.5	0.014	- 4.61	2.75
-03	+ 141.5	0.017	- 4.48	2.72
-04	+ 127.0	0.020	- 4.40	2.69
-05	+ 112.0	0.023	- 4.32	2.68
-06	+ 100.0	0.029	- 4.26	2.71
-07	+ 92.5	0.035	- 4.22	2.77
-08	+ 75.0	0.046	- 4.12	2.79
-09	+ 58.5	0.057	- 4.04	2.79
-10	+ 58.0	0.063	- 4.03	2.83
-11	+ 45.5	0.079	- 3.96	2.86
-12	+ 31.5	0.095	- 3.89	2.87
-13	+ 25.0	0.097	- 3.85	2.84
		[%Ni] = 61.2		
11-01	+ 128.0	0.013	- 4.41	2.52
-02	+ 123.0	0.016	- 4.38	2.58
-03	+ 110.5	0.016	- 4.32	2.52
-04	+ 98.5	0.018	- 4.25	2.50
-05	+ 84.5	0.022	- 4.18	2.53
-06	+ 75.5	0.025	- 4.13	2.53
-07	+ 70.0	0.027	- 4.10	2.53

TABLE 5 Experimental results for cell(III) at 1873 K (Continued).

No.	e.m.f. (mV)	[%O]	$\frac{1}{2}$ log P_{O_2} (atm)	log K'(Fe-Ni)
		[%Ni] = 61.2		
9-10	+ 40.0	0.053	- 3.94	2.65
-11	+ 33.0	0.057	- 3.90	2.66
-12	+ 16.0	0.072	- 3.81	2.66
-13	+ 8.5	0.083	- 3.77	2.69
-14	+ 14.0	0.074	- 3.80	2.67
		[%Ni] = 71.0		
11-01	+ 128.5	0.013	- 4.41	2.52
-02	+ 123.0	0.016	- 4.38	2.58
-03	+ 110.5	0.016	- 4.32	2.52
-04	+ 98.5	0.018	- 4.25	2.50
-05	+ 84.5	0.022	- 4.18	2.53
-06	+ 75.5	0.025	- 4.13	2.53
-07	+ 70.0	0.027	- 4.10	2.53
-08	+ 50.0	0.036	- 3.99	2.54
-09	+ 31.5	0.043	- 3.89	2.53
-10	+ 14.5	0.052	- 3.80	2.52
-11	+ 3.5	0.063	- 3.67	2.54
-12	- 10.0	0.066	- 3.67	2.54
-13	- 22.0	0.090	- 3.60	2.56

TABLE 5 Experimental results for cell(III) at 1873 K (continued).

No.	e.m.f. (mV)	[%O]	$\frac{1}{2}$ log P_{O_2} (atm)	log K'(Fe-Ni
		[%Ni] = 80.8		
14-01	+ 129.0	0.0086	- 4.42	2.35
-02	+ 124.5	0.0093	- 4.39	2.36
-03	+ 111.5	0.010	- 4.32	2.33
-04	+ 95.0	0.012	- 4.23	2.31
-05	+ 80.0	0.015	- 4.15	2.31
-06	+ 63.0	0.018	- 4.06	2.32
-07	+ 53.5	0.023	- 4.01	2.36
-08	+ 32.0	0.028	- 3.89	2.34
-09	+ 14.0	0.036	- 3.80	2.36
-10	- 3.0	0.046	- 3.70	2.36
-11	- 19.5	0.054	- 3.61	2.34
-12	- 35.5	0.068	- 3.53	2.36
-13	- 46.5	0.078	- 3.47	2.36
-14	- 57.5	0.097	- 3.41	2.39
-15	- 50.5	0.087	- 3.45	2.39
-16	- 68.0	0.105	- 3.36	2.38

TABLE 5 Experimental results for cell(III) at 1873 K (Continued).

No.	e.m.f. (mV)	[%O]	$\frac{1}{2}\log P_{O_2}$ (atm)	log K'(Fe-Ni)
		[%Ni] = 90.4		
10-01	- 51.0	0.012	- 3.39	2.07
-02	- 46.5	0.012	- 3.97	2.04
-03	- 6.5	0.021	- 3.75	2.07
-04	- 3.0	0.022	- 3.74	2.07
-05	- 8.5	0.027	- 3.67	2.10
-06	- 15.5	0.029	- 3.64	2.10
-07	- 51.0	0.047	- 3.44	2.12
-08	- 45.0	0.043	- 3.48	2.12
-09	- 55.5	0.051	- 3.42	2.13
-10	- 79.5	0.069	- 3.29	2.13
-11	- 87.0	0.079	- 3.25	2.15
-12	- 79.0	0.068	- 3.29	2.13
-13	- 107.0	0.107	- 3.14	2.17
-14	- 100.5	0.097	- 3.18	2.17
-15	- 115.0	0.157	- 3.10	2.30

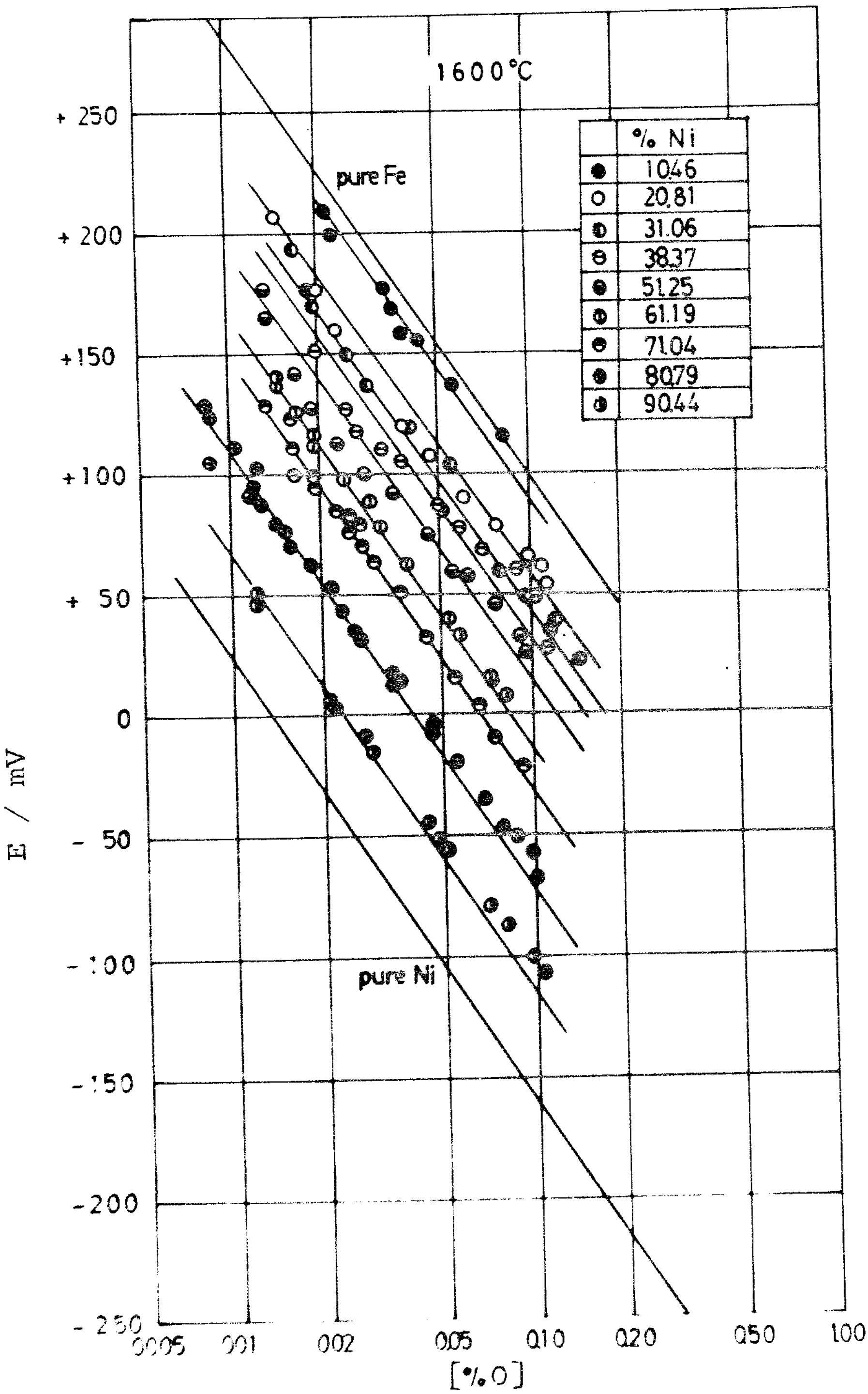

Fig.3.7 Relation between e.m.f. and log[%O] for cell(Ⅲ).

3.4 Thermodynamics Of Oxygen In Liquid Iron, Nickel And Iron-Nickel Alloys

3.4.1 Iron-Oxygen System

The apparent equilibrium constant, K'(Fe), and the true equilibrium constant, K(Fe), for the following reaction [8] are given by eqs.[9] and [10], respectively.

$$1/2\ O_2(g) = \underline{O}(\%\ \text{in Fe}), \qquad [8]$$

$$K'(Fe) = \frac{[\%O]}{P_{O_2}(Fe)^{1/2}}, \qquad [9]$$

$$K(Fe) = \frac{a(O\text{-}Fe)}{P_{O_2}(Fe)^{1/2}}. \qquad [10]$$

The Henrian activity of oxygen in liquid iron, a(O-Fe), is defined by

$$RT \ln a(O\text{-}Fe) = \mu(O\ \text{in Fe}) - \mu^\circ(O\text{-}Fe), \qquad [11]$$

where $\mu°(O\text{-}Fe)$ is the chemical potential of oxygen dissolved in hypothetical (Fe + 1 wt pct O) alloy, and $\mu(O \text{ in } Fe)$ is the chemical potential of oxygen dissolved in lqiuid iron.

The Henrian activity coefficient of oxygen, $f_O(Fe)$, is defined by

$$f_O(Fe) = a(O\text{-}Fe)/\,[\%O]. \qquad [12]$$

It follows from these definitions

$$\lim_{[\%O] \longrightarrow 0} a(O\text{-}Fe) = [\%O] , \qquad [13]$$

$$\lim_{[\%O] \longrightarrow 0} f_O(Fe) = 1 \quad . \qquad [14]$$

As mentioned in the foregoing section, the standard free energy of formation of MoO_2 is given by

$$\Delta G°(MoO_2)/kJ\ mol\text{-}MoO_2^{-1} = RT \ln P_{O_2}(Mo\text{-}MoO_2)$$
$$= -\ 509.6 + 0.1297\ (T/K) \pm 0.3 \qquad [15]$$

from 1723 to 1923 K.

The oxygen partial pressure in equilibrium with oxygen dissolved in liquid iron, P_{O_2}(Fe), can be calculated by combining eqs.[5] and [15], and the results are summarized in TABLE 3.

The effect of oxygen concentration on log K'(Fe) is shown in Fig.3.8. The relationship between log K'(Fe) and [%O] were represented as

$$\log K'(Fe) = 3.30 + 0.2\,[\%O] \quad \text{at } 1823\text{ K}, \qquad [16]$$

$$\log K'(Fe) = 3.23 + 0.2\,[\%O] \quad \text{at } 1873\text{ K}. \qquad [17]$$

The interaction parameter, e_O^O(Fe), is defined by

$$e_O^O(Fe) = \frac{\partial \log f_O(Fe)}{\partial\,[\%O]} . \qquad [18]$$

Therefore,

$$e_O^O(Fe) = \frac{\partial\,[\log K(Fe) - \log K'(Fe)]}{\partial\,[\%O]} \qquad [19]$$

$$= -\frac{\partial \log K'(Fe)}{\partial\,[\%O]} . \qquad [20]$$

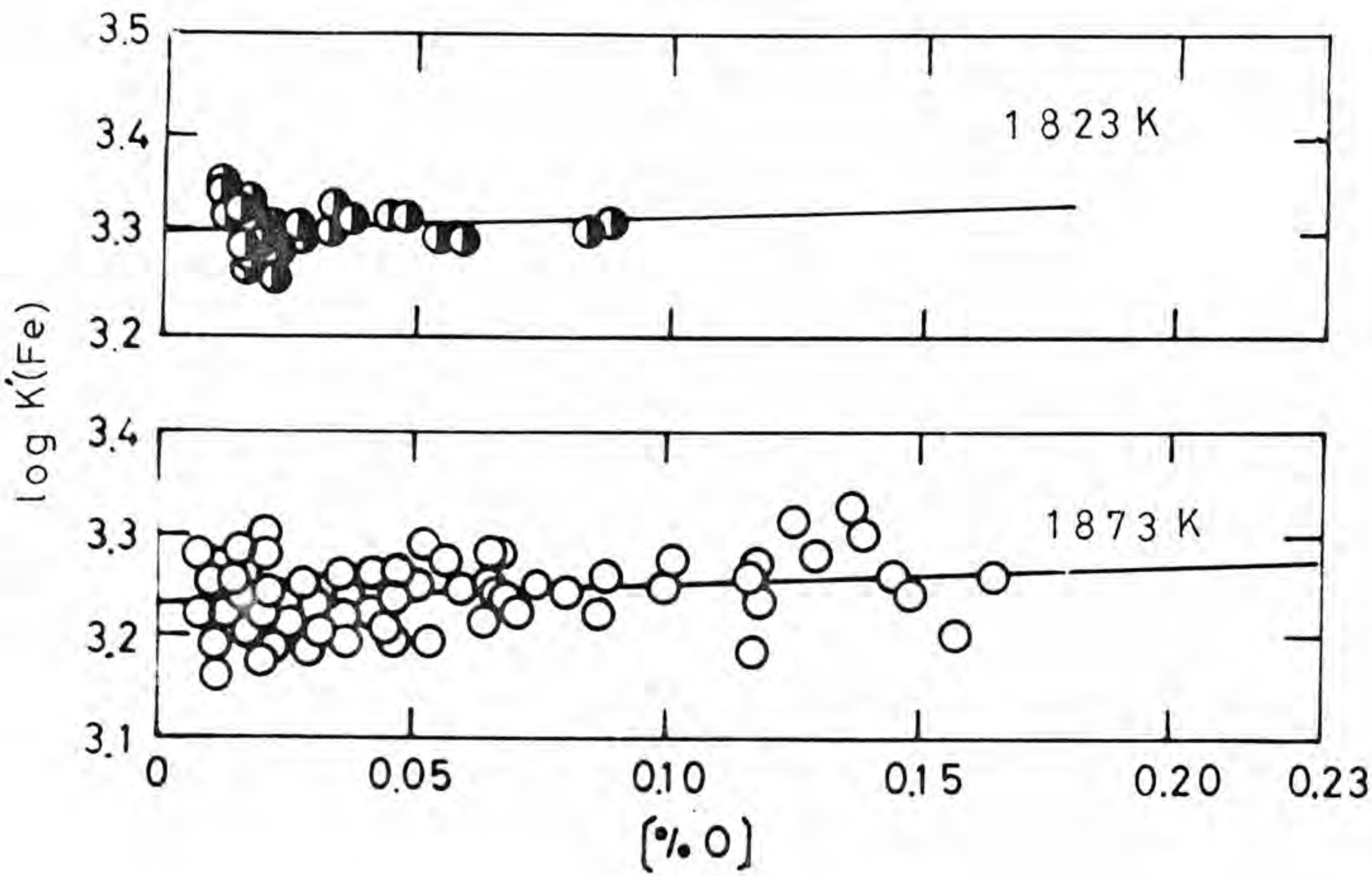

Fig. 3.8 The effect of oxygen concentration on the apparent equilibrium constant, log K'(Fe).

Combination of eqs.[16], [17] and [19] yields

$$e_O^O(Fe) = -0.2 \qquad \text{at 1823 to 1873 K .} \qquad [20]$$

The free energy change for the reaction [8] is given by

$$\Delta G°(O\text{-}Fe) = - RT \ln K(Fe). \qquad [21]$$

The true equilibrium constant, K(Fe), is independent of oxygen concentration, [%O]. Therefore, one can obtain

$$\log K(Fe) = 3.30 \qquad \text{at 1823 K ,} \qquad [22]$$

$$\log K(Fe) = 3.23 \qquad \text{at 1873 K .} \qquad [23]$$

Therefore,

$$\Delta G°(O\text{-}Fe)/kJ\ mol^{-1} = -(115.2 \pm 1.2) \qquad [24]$$

at 1823 K

$$\Delta G°(O\text{-}Fe)/kJ\ mol^{-1} = -(115.8 \pm 1.2) \qquad [25]$$

at 1873 K .

Combination of eq.[24] and [25] yields

$$\Delta G°(\text{O-Fe})/\text{kJ mol}^{-1} = -93.3 - 0.012\,(T/K) \pm 1.2\,. \quad [26]$$

From the standard deviations of E(I), T, and [%O], the uncertainty of $\Delta G°$(O-Fe) was estimated to be $\pm$ 1.2 kJ.

The present results for $\Delta G°$(O-Fe) are shown in Fig.3.9 for the sake of comparison with those reported in earlier literature. Values reported by Sakao and Sano (8), and Floridis and Chipman (9) were based on H_2/H_2O-metal equilibrium, and about 8.4 kJ lower than the present values. In general, errors in the H_2/H_2O-metal equilibrium method can arise from thermal diffusion in gas phase and hydrogen dissolved in liquid metal.

By using solid-oxide galvanic cell technique, Fischer and Janke(5), Fischer and Pateisky(6) and Mathew et al.(10) reported the same value of - 119.7 kJ at 1873 K, which is about 3.7 kJ lower than the present values. This disagreement would be attributed to the difference in reference electrode and the experimental difficulties of e.m.f. measurements at steelamking temperature.

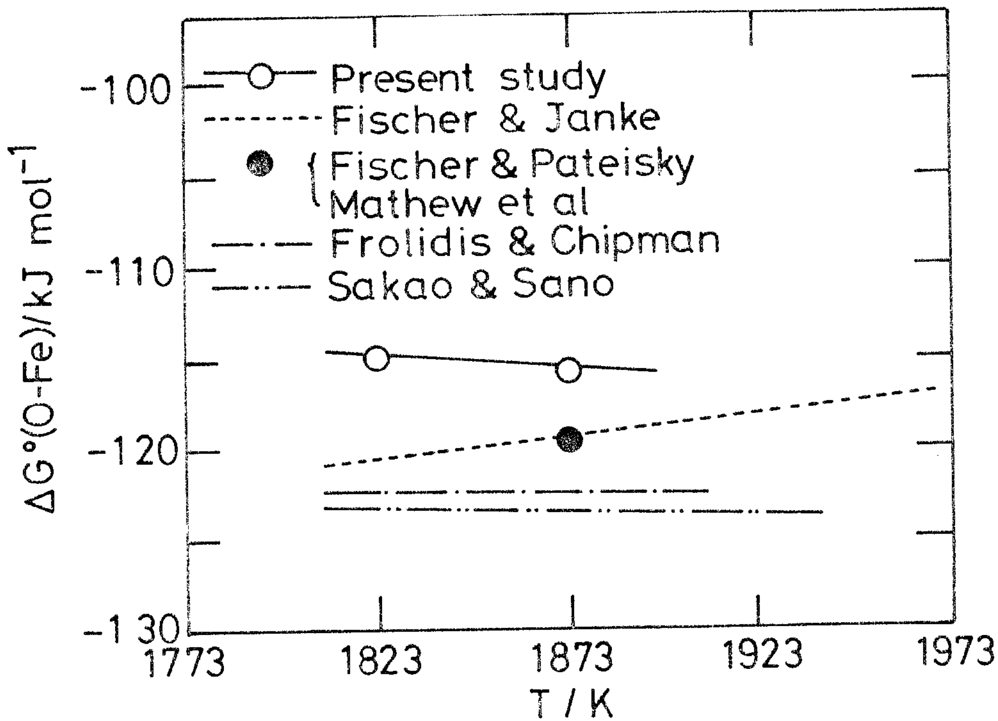

Fig.3.9 Temperature dependence of the standard free energy change for the reaction $1/2\ O_2(g) = \underline{O}(\text{in Fe}), \Delta G^\circ(\text{O-Fe})$.

3.4.2. Nickel-Oxygen-System

One can obtain the following equations for the reaction [27]

$$1/2\ O_2(g) \quad = \quad \underline{O}(\%\ \text{in Ni}), \tag{27}$$

$$K'(\text{Ni}) \quad = \quad \frac{[\%O]}{P_{O_2}(\text{Ni})^{1/2}} \quad , \tag{28}$$

$$K(\text{Ni}) \quad = \quad \frac{a(\text{O-Ni})}{P_{O_2}(\text{Ni})^{1/2}} \quad , \tag{29}$$

where K'(Ni) and K(Ni) are the apparent and true equilibrium constants for the reaction [27], respectively.

The definitions of several thermodynamic quantities for oxygen in liquid nickel are as follows,

$$RT \ln a(\text{O-Ni}) = \mu(\text{O in Ni}) - \mu^\circ(\text{O-Ni}), \tag{30}$$

$$f_O(\text{Ni}) \quad = \quad a(\text{O-Ni}) \ / \ [\%O] \ , \tag{31}$$

$$\lim_{[\%O] \to 0} a(O\text{-}Ni) = [\%O] , \qquad [32]$$

$$\lim_{[\%O] \to 0} f_O(Ni) = 1 , \qquad [33]$$

$$e_O^O(Ni) = \frac{\partial \log f_O(Ni)}{\partial [\%O]}$$

$$= \frac{\partial [\log K(Ni) - \log K'(Ni)]}{\partial [\%O]}$$

$$= - \frac{\partial \log K'(Ni)}{\partial [\%O]} , \qquad [34]$$

where a(O-Ni) is the Henrian activity of oxygen in liquid nickel, $\mu°$(O-Ni) is the chemical potential of oxygen dissolved in hypothetical (Ni + 1 wt pct O) solution, μ(O in Ni) is the chemical potential of oxygen in liquid nickel, f_O(Ni) is the Henrian activity coefficient of oxygen in liquid nickel, and e_O^O(Ni) is the interaction parameter for oxygen in liquid nickel, respectively.

The effect of oxygen concentration, [%O], on log K'(Ni) is shown in Fig.3.10. The least squares method was applied to determine the relationship betweeen log K'(Ni) and [%O] at 1873 K

$$\log K'(Ni) = 1.84 + 0.6\,[\%O] . \qquad [35]$$

Therefore,

$$e_O^O(Ni) = -0.6 \quad \text{at } 1873 \text{ K} . \qquad [36]$$

The interaction parameters, $e_O^O(Ni)$, at 1773 and 1823 K were assumed to be the same as that at 1873 K, because the experimental accuracy of the data obtained at 1773 and 1823 K can not allow their calculation. With this assumption, one can obtain

$$\log K'(Ni) = 1.97 + 0.6\,[\%O] \quad \text{at } 1773 \text{ K}, \qquad [37]$$

$$\log K'(Ni) = 1.90 + 0.6\,[\%O] \quad \text{at } 1823 \text{ K}, \qquad [38]$$

The standard free energy change for the reaction [27] can be calculated as

$$\Delta G^\circ(O\text{-}Ni)\,/\text{kJ mol}^{-1} = -(66.9 \pm 1.2) \qquad [39]$$

at 1773 K

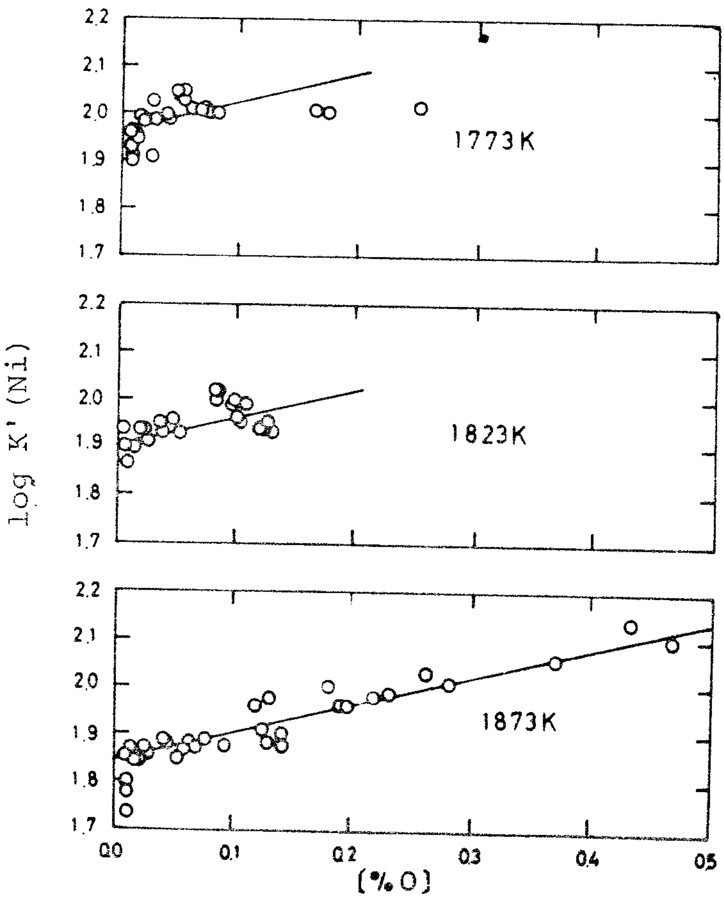

Fig.3.10 The effect of oxygen concentration on the apparent equilibrium constant, log K'(Ni).

$$\Delta G°(O\text{-}Ni)/kJ\ mol^{-1} = -\ (66.3 \pm 1.2) \quad \text{at } 1823\ K, \qquad [40]$$

$$\Delta G°(O\text{-}Ni)/kJ\ mol^{-1} = -\ (66.0 \pm 1.2) \quad \text{at } 1873\ K, \qquad [41]$$

and $\Delta G°(O\text{-}Ni)/kJ\ mol^{-1} = -\ 82.8 + 0.009(T/K) \pm 1.2$ [42]

as temperature function at steelamking temperatures. The assigned uncertainties in these equations were calculated from the standard deviations of E(II), [%O] and T, and the uncertainty of $\Delta G°(MoO_2)$.

Figure 3.11 shows the temperature dependence of $\Delta G°(O\text{-}Ni)$ for the comparison of the present results with those by other investigators. The experimental results by H_2/H_2O-metal equilibrium by Wriedt and Chipman(11), Tankins et al.(12), Belev et al.(13), and Sakao and Sano(14) show a spread of 10.6 kJ at 1873 K. On the contrary, values obtained by means of solid-oxide galavnic cell by Fischer and Ackerman(2), Kemori et al.(15) and the present author show a good agreement with each other. Values reported by Bowers(16) by means of CO/CO_2-metal equilibrium are shown in good agreement with the present results. On the other hand, values reported by Schenk et al.(17) by means of the

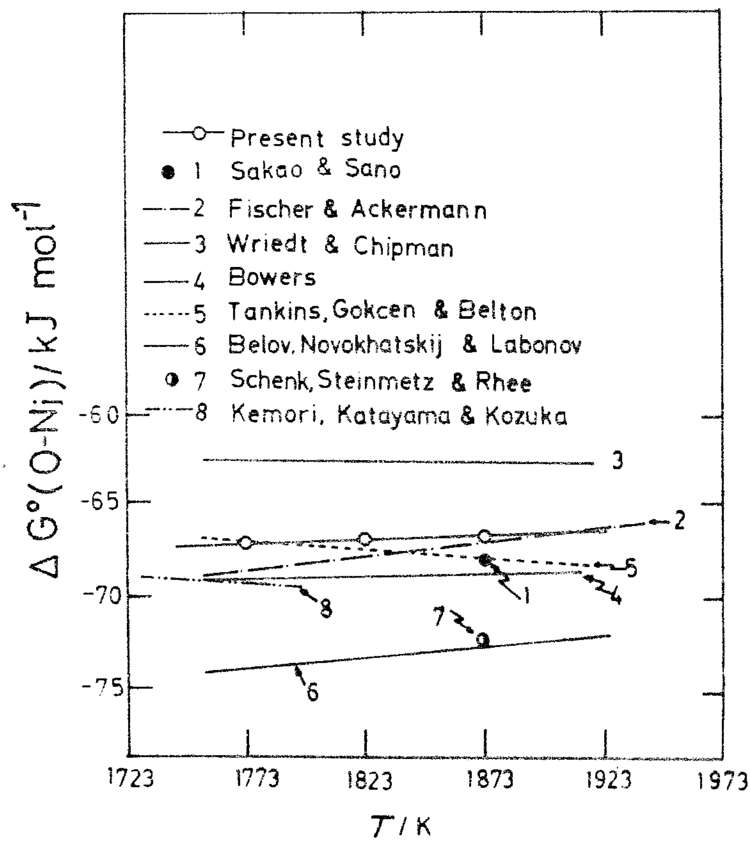

Fig.3.11 The temperature dependence of the standard free energy change for the reaction 1/2 $O_2(g)=\underline{O}(\text{in Ni})$, $\Delta G°$(O-Ni).

same method as that used by Bowers[15] are about 6 kJ lower than the present values..

It is well known that oxygen in liquid iron does not obey Henry's law. The interaction parameter for oxygen in liquid iron, $e_O^O(Fe)$, was reported to be - 0.2[3], and the present author reported the same value at 1873 K as mentioned in the foregoing section 3.4.1. For oxygen in liquid nickel, experimental values of $e_O^O(Ni)$ are not available except for thoese reported by Kemori et al.[14] It had been assumed that oxygen in liquid nickel showed an ideal behavior, i.e. $e_O^O(Ni) = 0$. In order to obtain the interaction parameter, $e_O^O(Ni)$, with a good accuracy, it is desirable to measure the e.m.f. values in a wide range of oxygen concentration because the values of $e_O^O(Ni)$ are determined by the slope of log K'(Ni) against [%O]. In reality, the values of log K'(Ni) at 1773 and 1823 K did not show a clear dependence on [%O], probably because of the narrow range of oxygen concnetration investigated.
Kemori et al.[14], by using the cell, $Pt/LaCrO_3/ZrO_2(CaO)/\underline{O}(\text{in Ni})/LaCrO_3/Pt$, at 1733 and 1783 K, found that the interaction parameter, e_O^O, was zero.
Their investigated range of oxygen concnetration is

restricted below 0.22 wt% at 1733 K and 0.35 wt% at 1783 1783 K, respectively. If their e.m.f. measurements were performed in a wide range of oxygen concnetration, they may obtain a clear dependence of log K'(Ni) on [%O].

In the present study, the alumina crucible was significantly attacked by the melt and a bluish layer of $NiAl_2O_4$ was always found on the inside of crucible after experiments. Since the solubility of oxygen in liquid nickel in equilibrium with $NiAl_2O_4$ decreases with decreasing temperature, a large portion of nickel oxide added to the melt at lower temperature(1773 and 1823 K) would react with the alumina crucible and form $NiAl_2O_4$. It was found that when the oxygen content exceed 0.3 wt% at 1773 and 1823 K, and 0.5 wt% at 1873 K, the oxygen content decreased with time. Thus the e.m.f. measurements at oxygen content above the largest values investigated at each temperature were impossible since the content of oxygen can not be held constant above these largest values .

3.4.3. Iron-Nickel-Oxygen

Let us consider the following reaction;

$$1/2\ O_2(g) \quad = \quad \underline{O}(\text{in Fe-Ni}) . \qquad [43]$$

The apparent equilibrium constant, K'(Fe-Ni), is given by

$$K'(\text{Fe-Ni}) \quad = \quad \frac{[\%O]}{P_{O_2}(\text{Fe-Ni})^{1/2}} . \qquad [44]$$

The values of K'(Fe-Ni) for each alloy composition can be experimentally determined by the chemical analysis of oxygen and e.m.f. measurements. The true equilibrium constant, K(Fe) and K(Ni), for the reaction [43] are given by

$$K(\text{Fe}) \quad = \quad \frac{a(\text{O-Fe})}{P_{O_2}(\text{Fe-Ni})^{1/2}} , \qquad [45]$$

$$K(Ni) = \frac{a(O\text{-}Ni)}{P_{O_2}(Fe\text{-}Ni)^{1/2}} . \qquad [46]$$

Combination of eqs.[44] and [45] yields

$$\log f_o(Fe) = \log K(Fe) - \log K'(Fe\text{-}Ni) . \qquad [47]$$

Similarly,

$$\log f_o(Ni) = \log K(Ni) - \log K'(Fe\text{-}Ni) . \qquad [48]$$

Therefore,

$$\frac{\partial \log f_o(Fe)}{\partial [\%O]} = \frac{\partial \log f_o(Ni)}{\partial [\%O]}$$

$$= - \frac{\partial \log K'(Fe\text{-}Ni)}{\partial [\%O]} . \qquad [49]$$

Following to Lupis and Elliott(18), the activity coefficient can be expressed as a sereies expansion;

$$\log f_O(\mathrm{Fe}) = e_O^O(\mathrm{Fe})\,[\%O] + e_O^{Ni}(\mathrm{Fe})\,[\%Ni] + r_O^O(\mathrm{Fe})\,[\%O]^2 + r_O^{Ni}(\mathrm{Fe})\,[\%Ni]^2 + r_O^{ONi}(\mathrm{Fe})\,[\%Ni]\,[\%O] , \qquad [50]$$

or

$$\log f_O(\mathrm{Ni}) = e_O^O(\mathrm{Ni})\,[\%O] + e_O^{Fe}(\mathrm{Ni})\,[\%Fe] + r_O^O(\mathrm{Ni})\,[\%O]^2 + r_O^{Fe}(\mathrm{Ni})\,[\%Fe]^2 + r_O^{OFe}(\mathrm{Ni})\,[\%Fe]\,[\%O] . \qquad [51]$$

The first order interaction parameters, $e_O^O(\mathrm{Fe})$, $e_O^O(\mathrm{Ni})$, $e_O^{Ni}(\mathrm{Fe})$, and $e_O^{Fe}(\mathrm{Ni})$, are defined by

$$e_O^O(\mathrm{Fe}) = \left.\frac{\partial \log f_O(\mathrm{Fe})}{\partial [\%O]}\right|_{[\%O]=0,\ [\%Ni]=0} , \qquad [52]$$

$$e_O^{Ni}(\mathrm{Fe}) = \left.\frac{\partial \log f_O(\mathrm{Fe})}{\partial [\%Ni]}\right|_{[\%O]=0,\ [\%Ni]=0} , \qquad [53]$$

$$e_O^O(\mathrm{Ni}) = \left.\frac{\partial \log f_O(\mathrm{Ni})}{\partial [\%O]}\right|_{[\%O]=0,\ [\%Fe]=0} , \qquad [54]$$

$$e_O^{Fe}(\mathrm{Ni}) = \left.\frac{\partial \log f_O(\mathrm{Ni})}{\partial [\%Fe]}\right|_{[\%O]=0,\ [\%Fe]=0} . \qquad [55]$$

The second-order interaction parameters, $r_O^O(Fe)$, $r_O^{Ni}(Fe)$ $r_O^{ONi}(Fe)$, $r_O^O(Ni)$, $r_O^{Fe}(Ni)$ and $r_O^{OFe}(Ni)$, are defined as

$$r_O^O(Fe) = \frac{1}{2}\left.\frac{\partial^2 \log f_O(Fe)}{\partial [\%O]^2}\right|_{[\%O]=0,\ [\%Ni]=0}, \tag{56}$$

$$r_O^{Ni}(Fe) = \frac{1}{2}\left.\frac{\partial^2 \log f_O(Fe)}{\partial [\%Ni]^2}\right|_{[\%O]=0,\ [\%Ni]=0}, \tag{57}$$

$$r_O^{ONi}(Fe) = \frac{1}{2}\left.\frac{\partial^2 \log f_O(Fe)}{\partial [\%O]\,\partial [\%Ni]}\right|_{[\%O]=0,\ [\%Ni]=0}, \tag{58}$$

$$r_O^O(Ni) = \frac{1}{2}\left.\frac{\partial^2 \log f_O(Ni)}{\partial [\%O]^2}\right|_{[\%O]=0,\ [\%Fe]=0}, \tag{59}$$

$$r_O^{Fe}(Ni) = \frac{1}{2}\left.\frac{\partial^2 \log f_O(Ni)}{\partial [\%Fe]^2}\right|_{[\%O]=0,\ [\%Fe]=0}, \tag{60}$$

$$r_O^{OFe}(Ni) = \frac{1}{2}\left.\frac{\partial^2 \log f_O(Ni)}{\partial [\%O]\,\partial [\%Fe]}\right|_{[\%O]=0,\ [\%Fe]=0} \tag{61}$$

The third-order terms were assumed to be negligible, since the accuracy of the experimental data can not allow their calculations. Moreover, $r_O^O(Fe)$ and $r_O^O(Ni)$ were assumed to be zero. With these assumptions, one can obtain eq.[62] from eqs.[49], [50] and [51]

$$e_O^O(Fe) + r_O^{ONi}(Fe)[\%Ni] = e_O^O(Ni) + r_O^{OFe}(Ni)[\%Fe]. \qquad [62]$$

As mentioned in the foregoing sections of 3.4.1 and 3.4.2,

$$e_O^O(Fe) = -0.2 , \qquad [63]$$

$$e_O^O(Ni) = -0.6 . \qquad [64]$$

Therefore,

$$r_O^{ONi}(Fe) = -r_O^{OFe}(Ni) = -0.004 . \qquad [65]$$

Introduction of eqs.[62], [63], [64] and [65] in eq.[50] yields,

$$\begin{aligned} \log f_O(Fe) &= \log K(Fe) - \log K'(Fe\text{-}Ni) \\ &= -0.2\,[\%O] + e_O^{Ni}(Fe)\,[\%Ni] + r_O^{Ni}(Fe)\,[\%Ni]^2 \\ &\quad - 0.004\,[\%O]\,[\%Ni] . \end{aligned} \qquad [66]$$

Eq.[66] indicates that plots of log K'(Fe-Ni) against [%O] at fixed alloy composition should be straight lines with the slope of (-0.2 - 0.004[%Ni]) and the intercept of $\{\log K(Fe) + e_O^{Ni}(Fe)\ [\%Ni] + r_O^{Ni}(Fe)\ [Ni]^2\}$. Furthermore, one can obtain eq.[67] from eq.[66].

$$\log f_O(Fe) = e_O^{Ni}(Fe)\ [\%Ni] + r_O^{Ni}(Fe)\ [\%Ni]^2 \quad \text{at} \quad [\%O] = 0 \quad . \qquad [67]$$

Similarly,

$$\log f_O(Ni) = e_O^{Fe}(Ni)\ [\%Fe] + r_O^{Fe}(Ni)\ [\%Fe]^2 \quad \text{at} \quad [\%O] = 0. \qquad [68]$$

Figure 3.12 shows the relaiton between log K'(Fe-Ni) and [%O]. The values of log K'(Fe-Ni) were well represented as linear functions of [%O] as listed in TABLE 6, where the slope of log K'(Fe-Ni) at each alloy composition was assumed to be $-\{0.2 + 0.004[\%Ni]\}$.

The activity coefficients, $f_O(Fe)$ and $f_O(Ni)$, were calculated by eqs.[47] and [48], respectively, and are shown in Fig.3.13. The lines in this figure were obtained by the method of least squares as

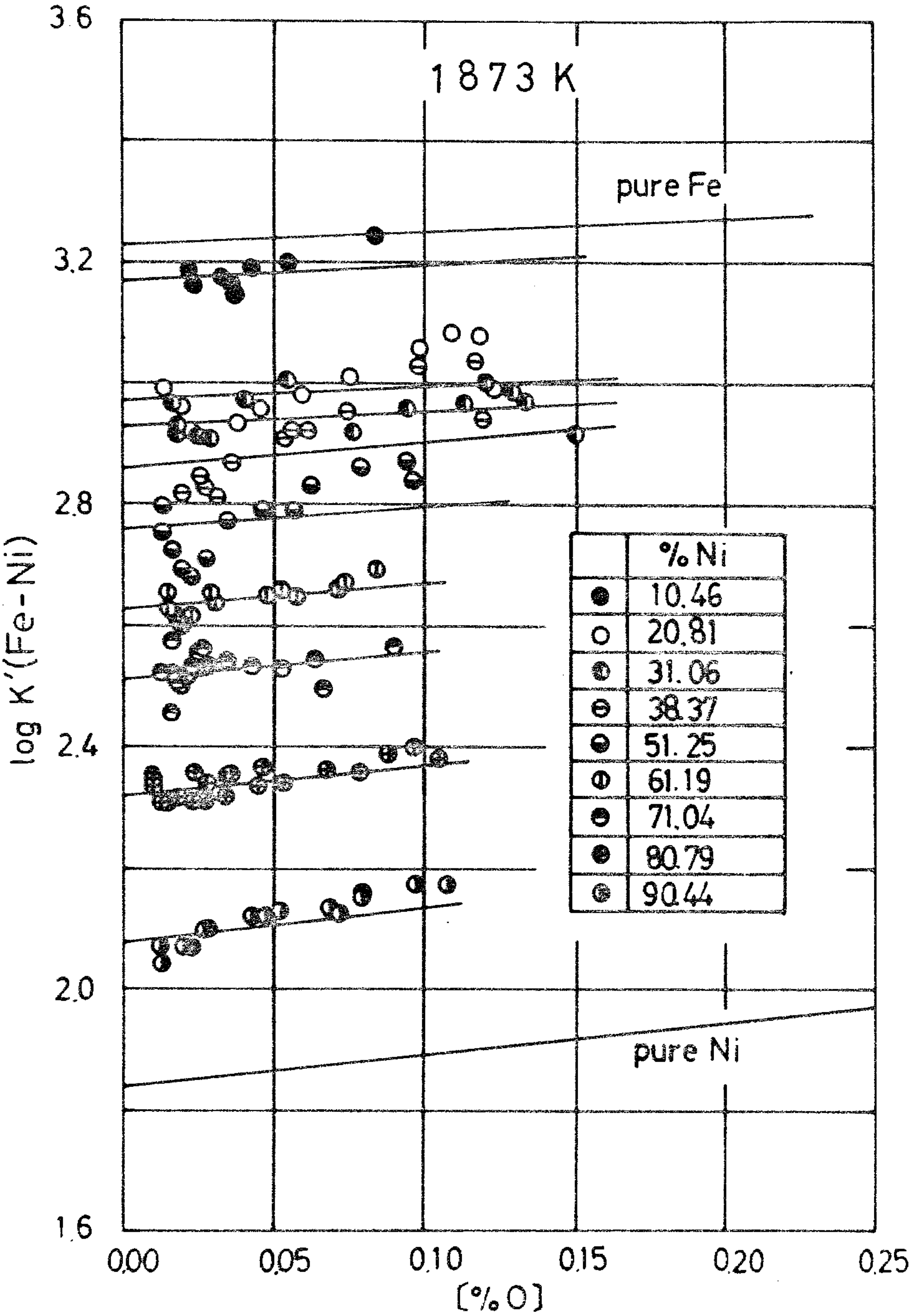

Fig.3.12 The effect of oxygen concentration on the apparent equilibrium constant, log K'(Fe-Ni).

TABLE 6 Variation of log K'(Fe-Ni) with the oxygen concentration in liquid iron-nickel alloys at 1873 K.

[%Ni]	log K'(Fe-Ni)
0	3.23 + 0.20 [%O]
10.5	3.17 + 0.24 [%O]
20.8	2.98 + 0.28 [%O]
31.1	2.93 + 0.32 [%O]
38.4	2.86 + 0.35 [%O]
51.2	2.76 + 0.40 [%O]
61.2	2.63 + 0.44 [%O]
71.0	2.51 + 0.48 [%O]
80.8	2.32 + 0.52 [%O]
90.4	2.08 + 0.56 [%O]
100	1.84 + 0.60 [%O]

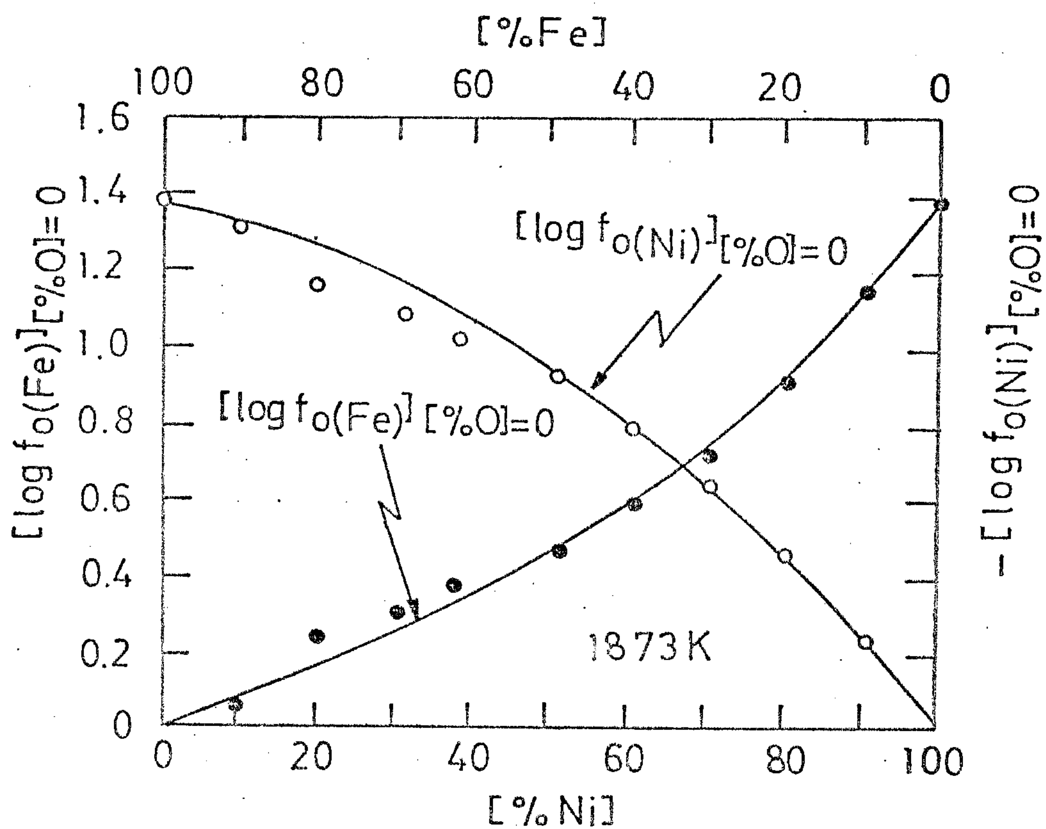

Fig.3.13 Relation between log f_O(FeO or log f_O(Ni), and [%Ni] or [%Fe].

$$\log f_O(\mathrm{Fe}) = (0.006 \pm 0.002)\ [\%\mathrm{Ni}] + (7 \pm 8) \times 10^{-5}\ [\%\mathrm{Ni}]^2 \quad \text{at } [\%\mathrm{O}]=0\ , \qquad [69]$$

$$\log f_O(\mathrm{Ni}) = -\ (0.024 \pm 0.002)\ [\%\mathrm{Fe}] + (1 \pm 0.8) \times 10^{-4}\ [\%\mathrm{Fe}]^2 \quad \text{at } [\%\mathrm{O}] = 0\ . \qquad [70]$$

As mentioned in the foregoing sections of 3.4.1 and 3.4.2,

$$\log K(\mathrm{Fe}) = 3.23 \qquad \text{at } 1873\ \mathrm{K}\ , \qquad [71]$$

and $$\log K(\mathrm{Ni}) = 1.84 \qquad \text{at } 1873\ \mathrm{K}\ . \qquad [72]$$

Therefore ,

$$\log K(\mathrm{Fe}) - \log K(\mathrm{Ni}) = 1.39\ . \qquad [73]$$

On the other hand, the difference of eqs.[69] and [70] yields,

$$\log f_O(\mathrm{Fe}) - \log f_O(\mathrm{Ni}) = = 1.40 + 0.002\ [\%\mathrm{Ni}] - 3 \times 10^{-5}\ [\%\mathrm{Ni}]^2\ . \qquad [74]$$

Therefore,

$$\left| \left\{ \log K(\mathrm{Fe}) - \log K(\mathrm{Ni}) \right\} - \left\{ \log f_O(\mathrm{Fe}) - \log f_O(\mathrm{Ni}) \right\} \right| = \left| 0.01 + 0.002\ [\%\mathrm{Ni}] - 3 \times 10^{-5}\ [\%\mathrm{Ni}]^2 \right|\ . \qquad [75]$$

Assuming that $r_o^o(Fe) = r_o^o(Ni) = 0$, and the third-order interaction parameters are negligible, the right hand of eq.[75] should be zero(eq.[47] and [48]). The maximum value of the terms on the right hand of eq.[75] is 0.11 at [%Ni]=100. This value may be regarded to be within experimental error.

Comparison with the results obtained by other investigators for log $f_o(Fe)$ at [%O]=0 are shown in Fig.3.14. The present results show a fairly good agreement with values reported by Sakao and Sano[14], Wriedt and Chipnam[11], Schenck et al.[17], and Matoba and Kuwana[19]. All of these authors used the gas-metal equilibrium method. Goto et al.[20], by using CO/CO_2-metal equilibruum method, reported the activities of carbon and oxygen in liquid iron-nickel alloys. The values reported by them are somewhat smaller than the others in the range of high nickel concnetration, and would be affected by the dissolved carbon in liquid iron-nickel alloy probably because of low oxygen pressure in their experiments.

The interaction parameters obtained in the present study are listed in TABLE 7. The first-order interaction parameter, $e_o^{Ni}(Fe)$, is in good agreement

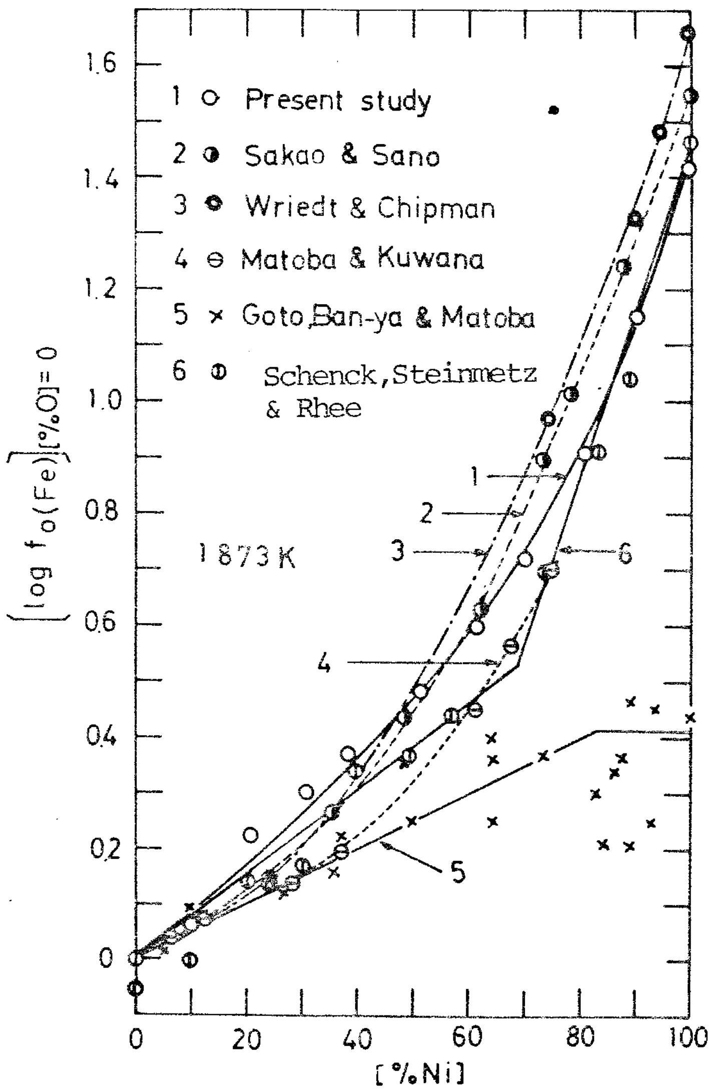

Fig.3.14 Comparison of the values for $\log f_O(Fe)$.

TABLE 7 The first and second order interaction parameters for oxygen dissloved in liquid iron-nickel alloys at 1873 K.

Authors	e_O^{Ni} (Fe)	e_O^{Fe} (Ni)	r_O^{Ni} (Fe)	r_O^{Fe} (Ni)
Present Study	0.006	- 0.024	$(7 \pm 8) \times 10^{-5}$	$(1 \pm 0.8) \times 10^{-4}$
Sakao and Sano (14)	0.005	- 0.026	1.25×10^{-4}	1.25×10^{-4}
Wriedt and Chipman (11)	0.006	-	-	-
Matoba and Kuwana (19)	0.0053	-	-	-
Goto et al. (21)	0.005	-	-	-
Schenk et al. (17)	0.006	-	-	-
Fischer and Ackermann (2)	0.006	- 0.025	-	-

with those by other investigators. No paper has been reported the second-order interaction parameter, $r_O^{Ni}(Fe)$ and $r_O^{Fe}(Ni)$. Calculation of these parameters was carried out by using the experimental data of Sakao an and Sano[14], and the results show a fairly good agreement with the present results.

3.5 Summary

An electrochemical method using solid-oxide electrolyte has been used to determine the thermodynamic properties of oxygen in liquid iron, nickel and iron-nickel alloys. The cells used are

Cell(I) $Mo/Mo\text{-}MoO_2/ZrO_2(CaO)/\underline{O}(\text{in Fe})/Mo$,

Cell(II) $Mo/Mo\text{-}MoO_2/ZrO_2(CaO)/\underline{O}(\text{in Ni})/LaCrO_3/Pt$,

Cell(III) $Mo/Mo\text{-}MoO_2/ZrO_2(CaO)/\underline{O}(\text{in Fe-Ni})/Mo$.

The free energy changes for the solution of gaseous oxygen in liquid iron and nickel are given by,

$$\Delta G°(O\text{-}Fe)/kJ\ mol^{-1} = -\ 93.3 - 0.012\ (T/K) \pm 1.2,$$

$$\Delta G^\circ(\text{O-Ni})/\text{kJ mol}^{-1} = -\ 82.8 + 0.009\ (T/K) \pm 1.2,$$

respectively.

The Henrian activity coefficients, $f_o(\text{Fe})$ and $f_o(\text{Ni})$, are given by

$$\log f_o(\text{Fe}) = -\ 0.2\ [\%\text{O}] + (0.006 \pm 0.002)\ [\%\text{Ni}] + (7 \pm 8) \times 10^{-5}\ [\%\text{Ni}]^2 + 0.004\ [\%\text{O}]\ [\%\text{Ni}],$$

$$\log f_o(\text{Ni}) = -\ 0.6\ [\%\text{O}] + (0.024 \pm 0.002)\ [\%\text{Fe}] + (1 \pm 0.8) \times 10^{-4}\ [\%\text{Fe}]^2 - 0.004\ [\%\text{O}]\ [\%\text{Fe}]$$

at 1873 K.

3.6 References

1. K. Kiukkola and C. Wagner ; J. Electrochem. Soc., 104(1957), 379.
2. W. A. Fisher and W. Ackerman ; Arch. Eisenhüttenw., 36(1965), 643.
3. J. F. Elliott, M. Gleiser and V. Ramakrischna ; "Thermochemistry for Steelmaking", vol.2, Addison-Wesley Reading, Mass., 1963.
4. M. Kawakami and K. S. Goto ; Met. Trans., 2(1971), 2965.
5. W. A. Fischer and W. Ackermann ; Arch. Eisenhüttenw., 41(1970), 1027.
6. W. A. Fischer and G. Pateisky ; ibid, 41(1970),661.
7. A. Kumar, D. Rajedev and D. L. Doughlass; J. Amer. Ceram. Soc., 55(1972), 439.
8. H. Sakao and K. Sano ; Trans. Japan Inst. Met., 1 (1960), 38.
9. T. P. Frolidis and J. Chipman ; Trans. Met. Soc. AIME., 212(1958), 549.
10. P. M. Mathew, M. L. Kapoor and M. G. Frohberg; Arch. Eisenhüttenw., 43(1973), 865.
11. H. A. Wriedt and J. Chipman ; Trans. AIME., 206 (1956), 1195.
12. E. S. Tankins, N. A. Gokcen and G. R. Belton ;

Trans. Met. Soc. AIME., 230(1960), 820.

13. B. F. Belov, J. A. Novakhatsky, and Y. A. Lavanov ; Izv. Akad. Nauk. SSSR. Metally, (1967), 53. Russian Metallurgy Metally, (1967), 19.

14. H. Sakao and K. Sano ; J. Japan Inst. Met., 40(196 (1962), 30.

15. N. Kemori, I. Katyama and Z. Kozuka ; J. Japan Inst. Met., 40(1976), 750.

16. J. E. Bowers ; J. Inst. Met., 90(1962),321.

17. H. Schenck, E. Steinmetz and P. C. Rhee ; Arch. Eisenhüttenw., 40(1969), 619.

18. C. H. P. Lupis and J. F. Elliott ; Acta. Met., 14(1966), 529.

19. S. Matoba and T. Kuwana ; Tetsu-to-Hagane, Overseas, 5(1965), 187.

20. K. S. Goto, S. Ban-ya and S. Matoba ; Tetsu-to-Hagane, 48(1963), 138.

CHAPTER 4

OXYGEN PERMEABILITY OF CALCIA-STABILIZED ZIRCONIA

4.1 Introduction

The usefulness of the calcia-stabilized zirconia as a solid electrolyte of galvanic cell has been experimentally demonstrated in the foregoing chapters. Oxygen, however, permeates through zirconia at high temperature, consequently oxygen permeability may be a main source of experimental error in the electrochemical measurement of oxygen in liquid iron as mentioned in the foregoing chapter(3.3.1).

In order to confirm the path of transfer that mainly contributes to oxygen permeability through zirconia, it is decided to measure the permeability of both oxygen and nitrogen. If the main causes of oxygen transfer were not due to the electronic conduction of the zirconia electrolyte, both oxygen and nitrogen would permeate through zirconia. Oxygen permeation due to Knudesn diffusion through pores, diffusion through grain boundaries and molecular diffusion through microcracks will be reduced by improving the physical properties of zirconia, i.e. by making dense ceramics. Therefore, in the absence of these other effects, oxygen transfer which may cause an experimental error during the e.m.f. measurement of oxygen concentration cell would be due to electronic conduction. The oxygen permability due to electronic conduction, and the relationship between permeability and partial electronic conductivity of commercial solid electrolyte were studied.

The permeability measurement cells in the present study are represented schematically as

Cell(I)

$$\begin{array}{c|c|c} O_2 & ZrO_2(CaO) & N_2 - O_2 \\ (P'_{O_2} = 1\ \mathrm{atm}) & & (P''_{O_2} = 10^{-3} \text{ to } 0.39\ \mathrm{atm}) \end{array}$$

Cell(II)

$$\begin{array}{c|c|c} O_2 & ZrO_2(CaO) & CO/CO_2 \\ (P'_{O_2} = 1\ \mathrm{atm}) & & (P''_{O_2} = 10^{-7} \text{ to } 10^{-12}\ \mathrm{atm}) \end{array}$$

4.2 Experimental

Experimental apparatus is shown in Fig.4.1 for cell(I) and in Fig.4.2 for cell(II), respectively. A zirconia solid electrolyte tube, about 13 mm OD, 9 mm ID and 500 mm long, stabilized by 11 mol % of CaO and closed at one end, was used for the experiments. The chemical composition and physical properties of the zirconia tube, supplied by Nippon Kagaku Togyo Co. Ltd., are given in TABLE 1 of Chapter 2.

The open end of the tube was connected to a mercury manometer through glass tubing. The zirconia tube was tested for its gas tightness at room temperature by evacuating the inside of the tube. These tubes which showed a pressure increase of less than 0.0026 to 0.0040 atm during 30 minutes after turning off the stopcock connceted to the vacuum system, were selected and used for these experiments. The tube was heated very slowly to avoid thermal cracking in a SiC resistance furnace from room temperature to experimental temperature.

Gas leakage resulting from open porosity or cracks was evaluated by determining the ratio of O_2 to N_2 which

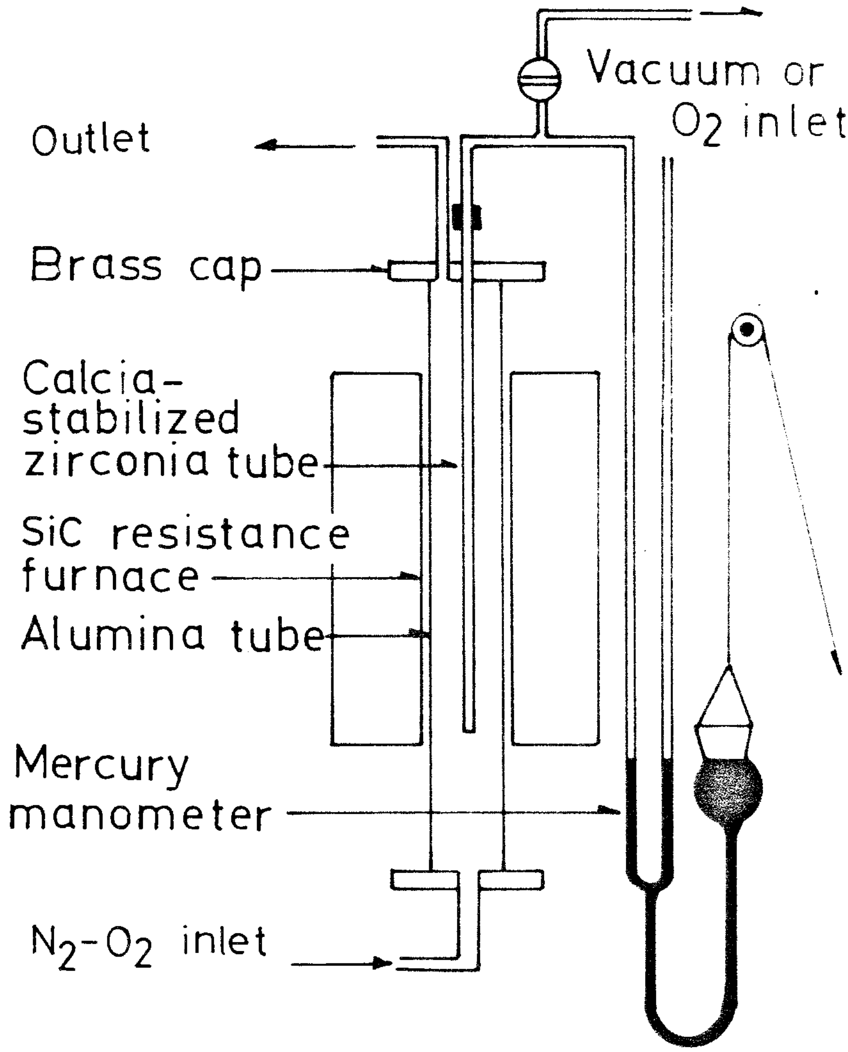

Fig.4.1 Experimental apparatus for cell(I).

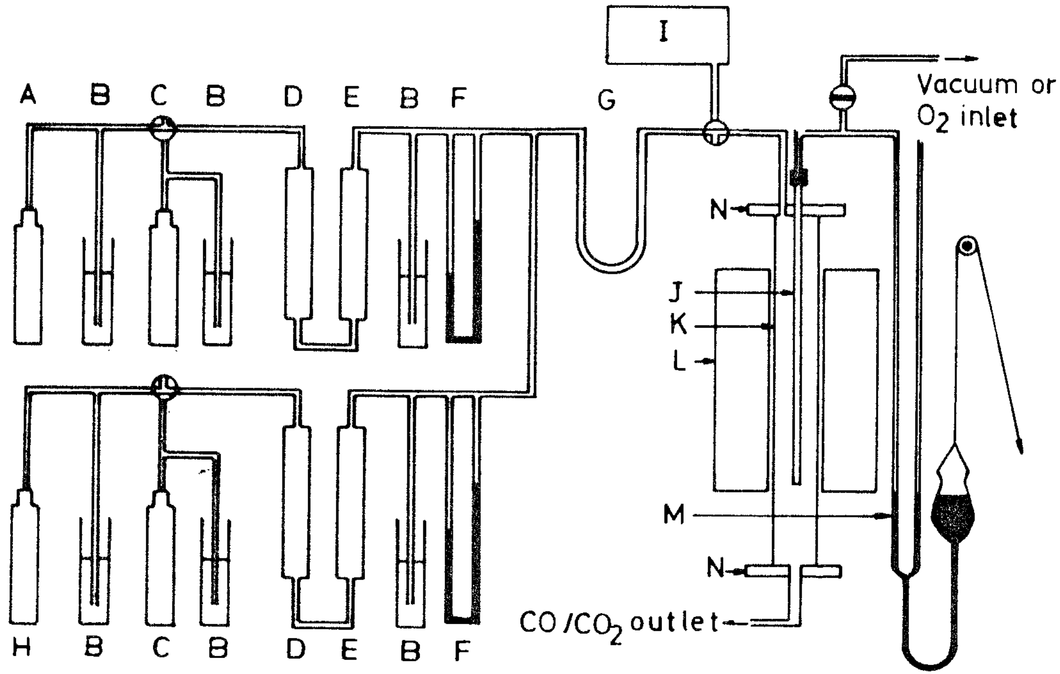

Fig.4.2   Experimental apparatus for cell(II)
A; CO_2 gas cylinder, B; oil bleeder, C; N_2 gas cylinder, D; silica gel, E; phosphorous pentoxide, F; flow meter, G; glass beeds mixer, H; CO gas cylinder, I; Orasat gas analysis apparatus, J; ZrO_2-CaO tube, K; alumina tube, L; SiC resistance furnace, M; mercury manometer, N; water cooled brass cap.

permeated through zirconia tube at 1704 to 1873 K.*
The observed ratio was > 500. The inside of the zirconia tube was filled with pure oxygen at atmospheric pressure, and the outside was flushed with a stream of N_2-O_2 gas mixture having the oxygen partial pressure of 0.39, 0.21, 0.056, 0.009 and 0.001 atm, for cell(I), or CO/CO_2 gas mixture for cell(II), respectively. The mass of pure oxygen inside the tube was gradually decreased due to the permeation of oxygen from inside but no permeation from outside. The mercury leveller was adjusted, therefore, to keep the pressure of pure oxygen at a constant atmospheric pressure, and the change of mercury level was measured for every one to three minutes ranging from 10 to 30 minutes. Since the oxygen pressure gradient across the tube was kept constant during these experiments, the oxygen permeability through zirconia tube can be calculated as a steady-state diffusion by eq.[1]

---

* The details of this preliminary experiments for determining the ratio of O_2 to N_2 at 1704 to 1873 K will be described in APPENDIX-A.

$$J \cdot A = \dot{n}_{O_2} = - \frac{\pi r^2 P}{R T_r} \frac{\Delta h}{\Delta t}, \qquad [1]$$

where J is oxygen flux (mol cm^{-2} sec^{-1}), $\dot{n}_{O_2}$ is the molecular number of oxygen diffused through zirconia per unit time (mol sec^{-1}), A is effective permeation area* = 39 cm^2, r is the inner radius of the mercury manometer (cm),

---

* The details of calibration of effective permeation area will be described in APPENDIX-B

P is the atmospheric pressure, (atm), R is the gas constant, T_r is the temperature of mercury manometer (K), and $\Delta h (< 0)$ is the change of mercury level (cm) during the time Δt (sec), respectively.

Temperature of the zirconia tube was measured by Pt-PtRh13 thermocouple, and the hot junction was placed at homogeneous temperature zone of the SiC resistance furnace, and controlled within $\pm$ 3 K. The flow rate of gase was measured by capilary-type flow meter which was previously calibrated by soap-film technique. The fraction of CO/CO_2 was determined by Orsat gas-analysis apparatus, and the results showed a fairly good agreement with those determined by flow meters.

4.3 Results and Discussion

4.3.1 Cell(I)

Representative results for cell(I) are shown in Fig.4.3. Quite linear relationship between Δh and Δt was obtained. Calculated values of oxygen permeability from eq.[1] are shown in TABLE 1. The effect of the difference in oxygen partial pressure on permeability is shown in Fig. 4.4. The oxygen permeability in zirconia is proportional to $(1 - P''^{1/4}_{O_2})$ in the range of oxygen pressure from 1 to 10^{-3} atm. The results would be due to p-type electronic conduction in the solid electrolyte. The oxygen pressure dependence is the same as those reported by Smith et al.[1], Fischer[2] and Palguev et al.[3], but not accord with that of Alcock and Chan[4], who reported a relation proportional to the 1/2 power of the pressure difference. Results obtained by Kitazawa and Coble[5] did not show a clear dependence of permeability on oxygen partial pressure.

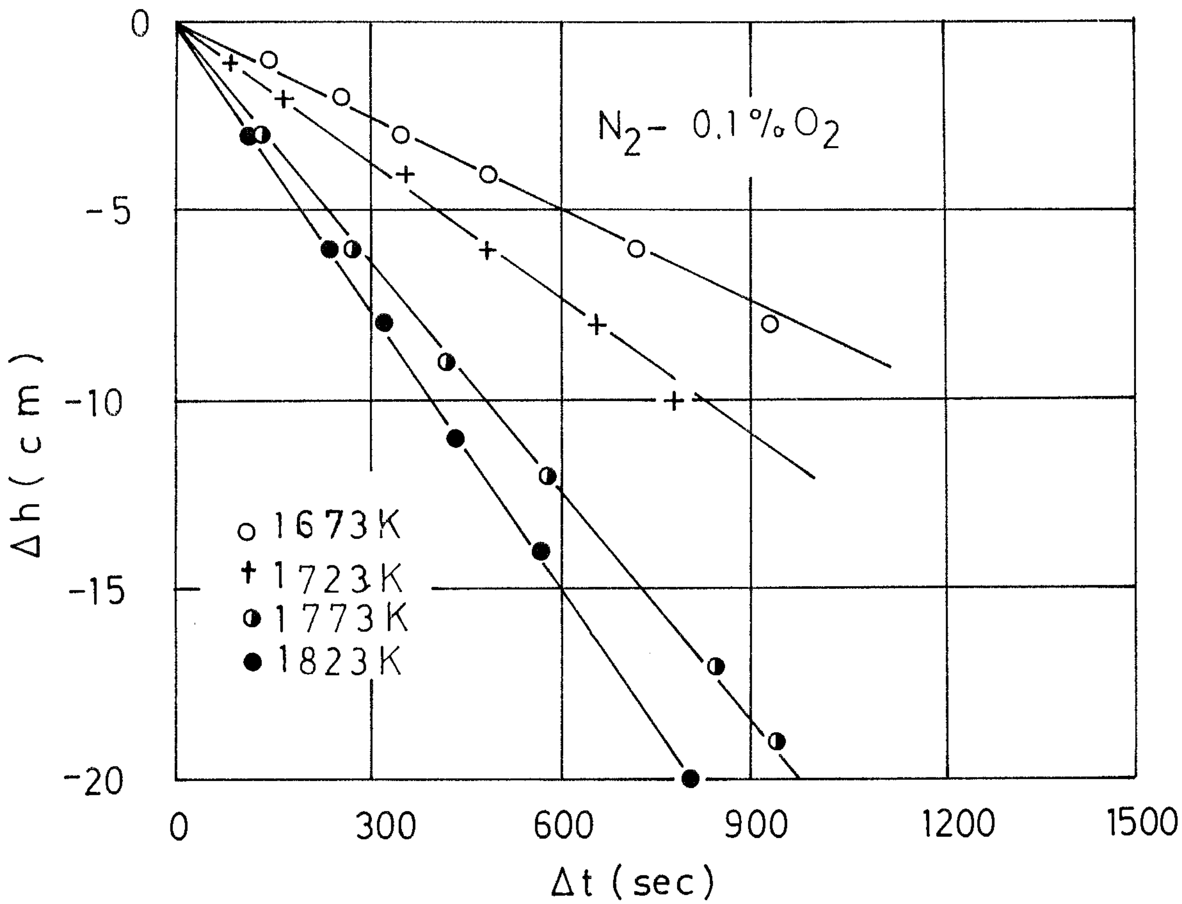

Fig.4.3 a   Experimental results for cell(I)

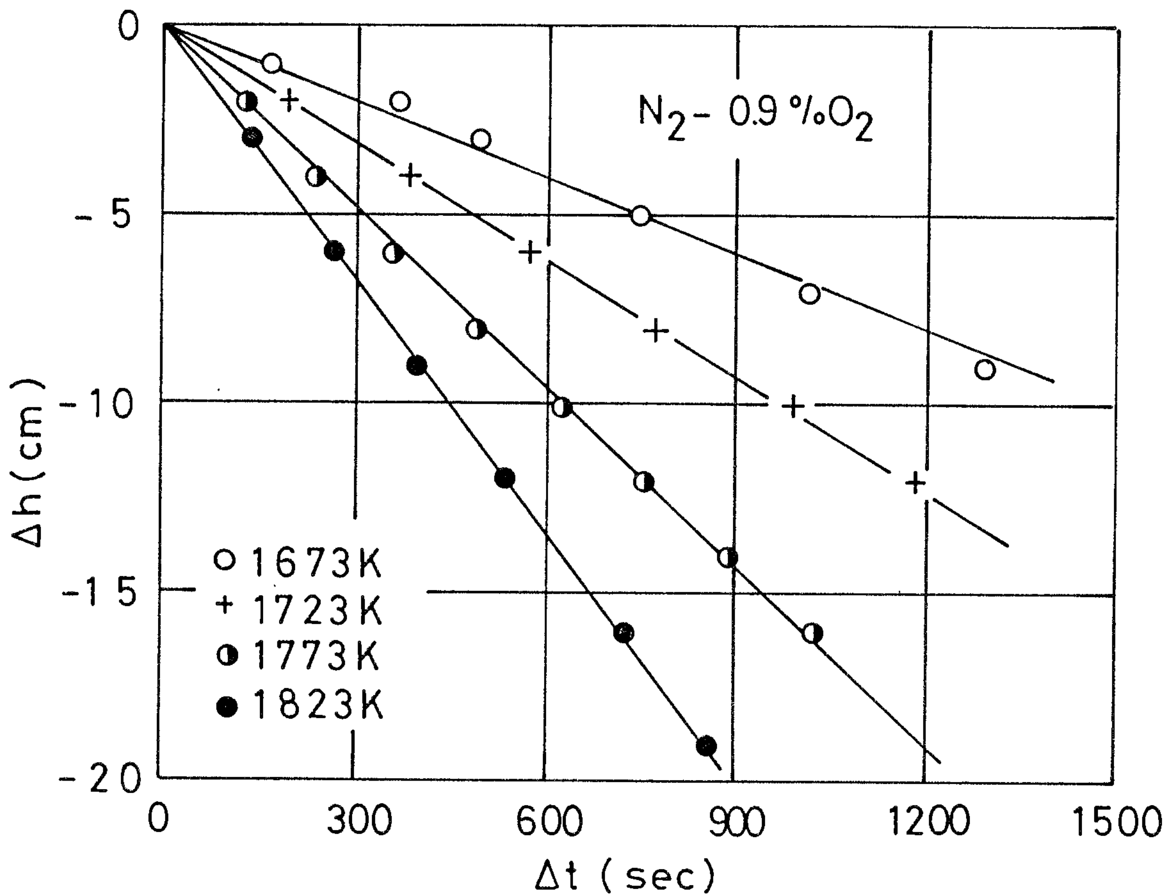

Fig.4.3 b Experimental results for cell(I)

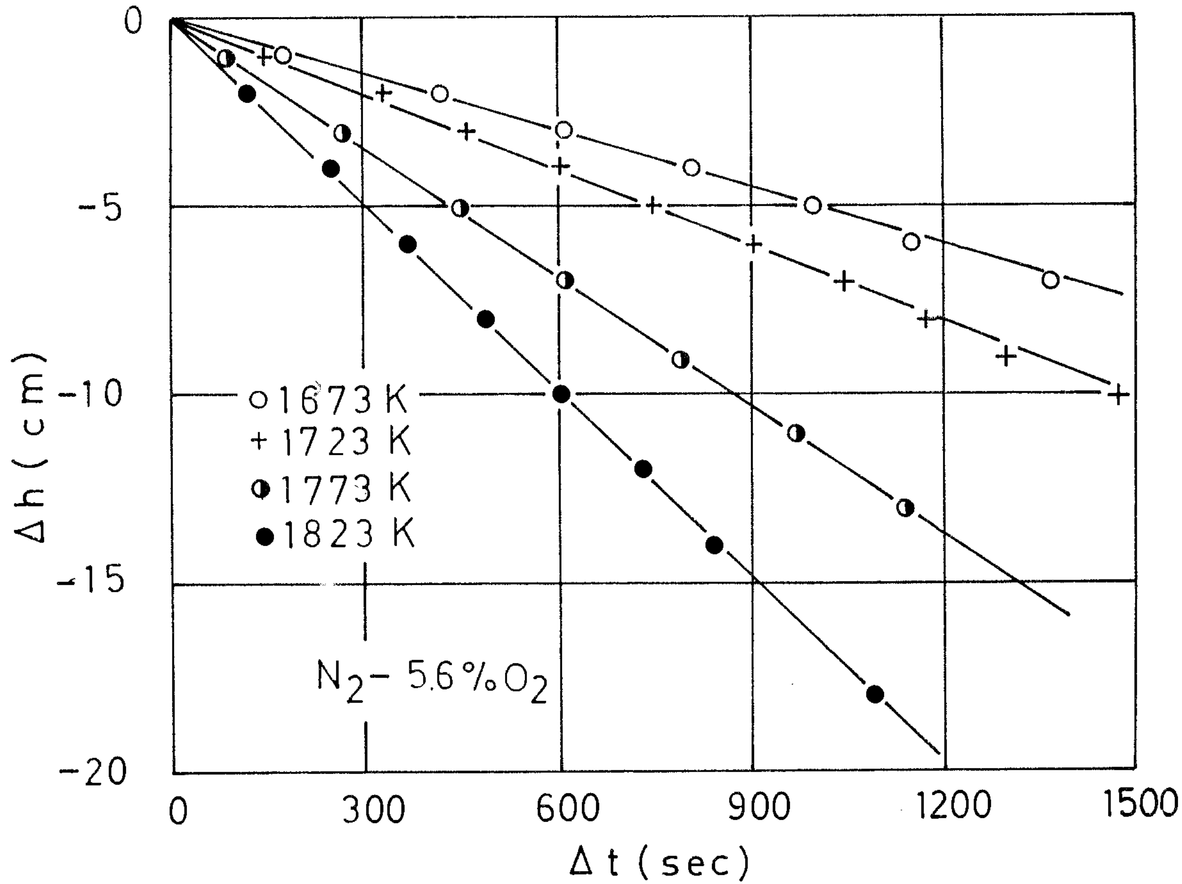

Fig.4.3 c Experimental results for cell(I)

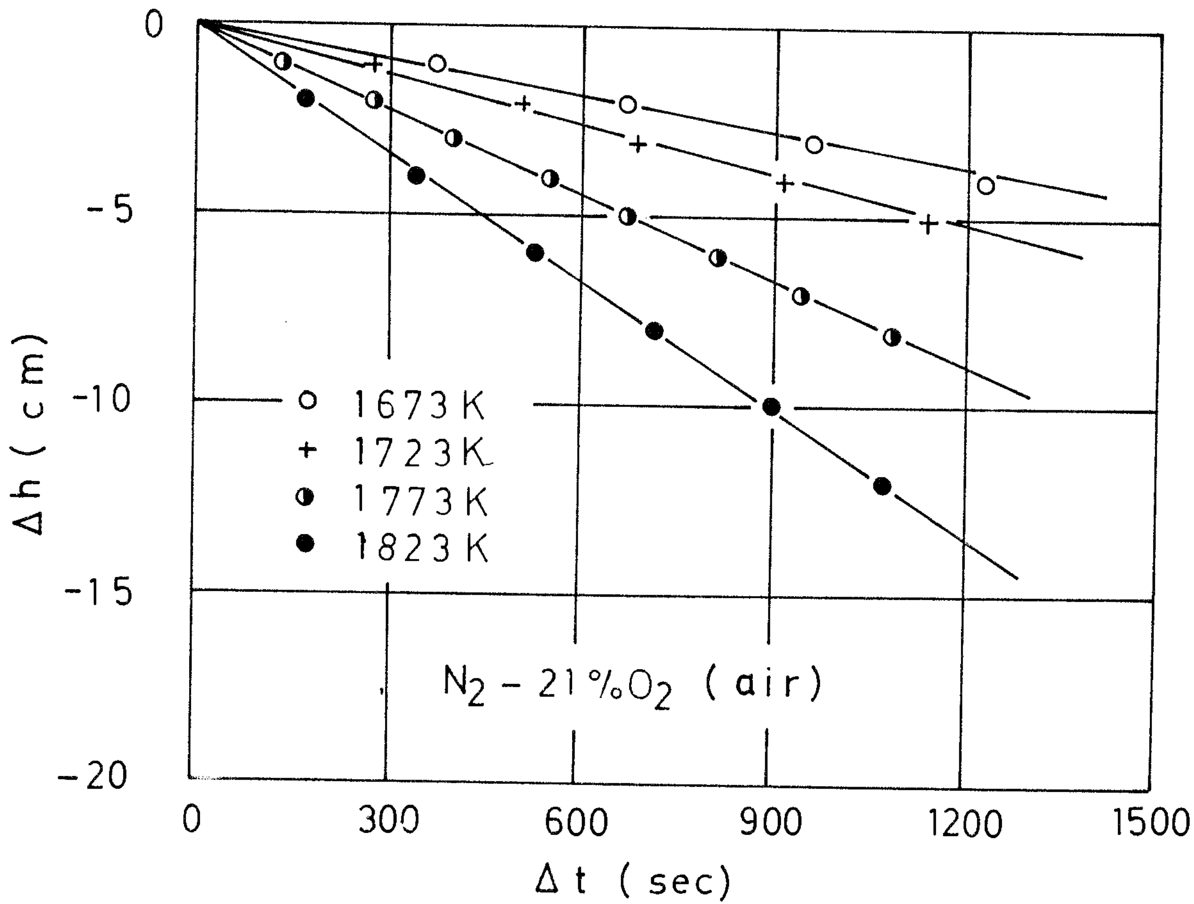

Fig.4.3 d Experimental results for cell(I)

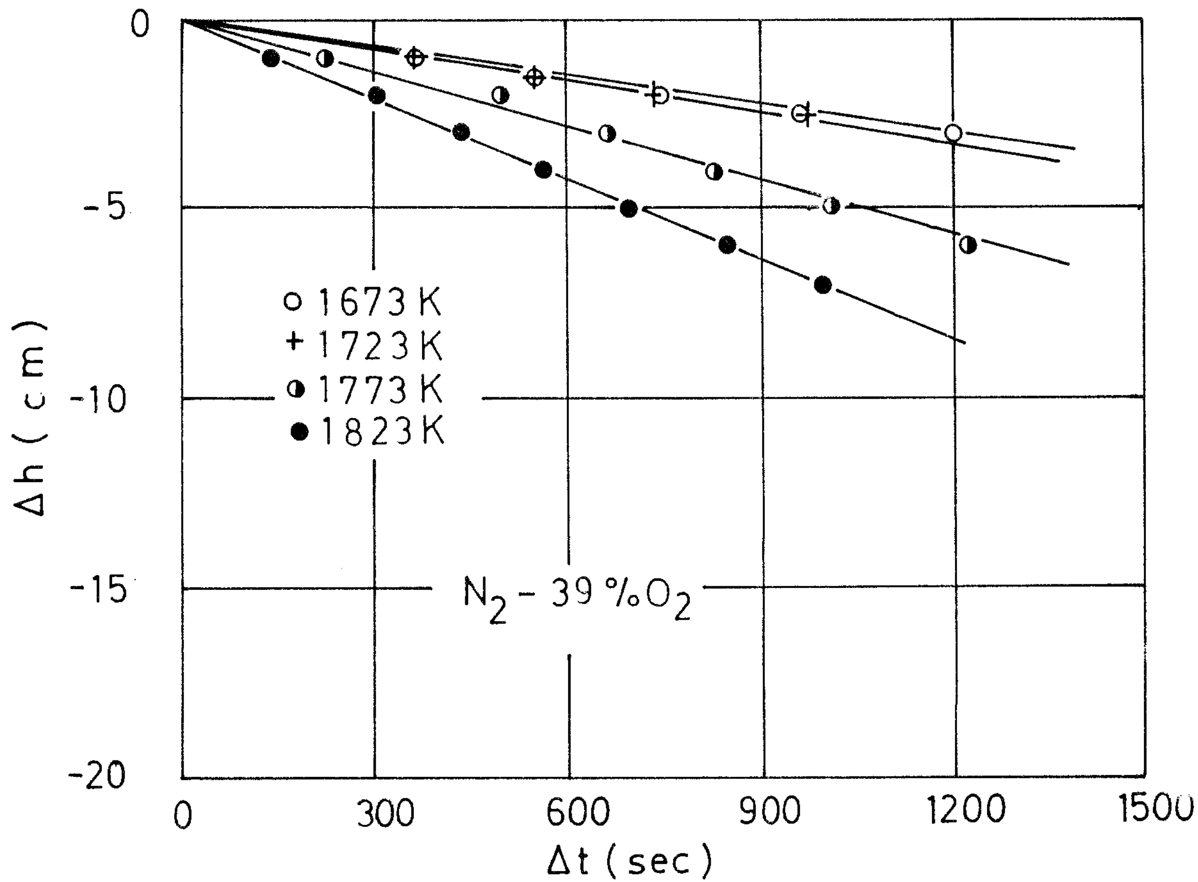

Fig.4.3 e   Experimental results for cell(I)

The apparent activation energy of oxygen permeability can be obtained by plotting log $\dot{n}_{O_2}$ against 1/T as seen in Fig.4.5. The slope in Fig.4.5 gives the apparent activiation energy as

$$\Delta Q = 220 \pm 16 \text{ kJ} .$$

This value is in good agreement with that reported by Smith et al[1] (ΔQ = 241 kJ).

The transport of oxygen from the inside of the zirconia tube(pure O_2) to the outside(N_2 - O_2) during these experiments involves a series of independent steps;

1) transport of molecular oxygen from the bulk of pure oxygen to gas/solid electrolyte interface,
2) absorption of molecular oxygen on the electrolyte surface,
3) transport of oxygen through the electrolyte,
4) desorption of oxygen on the electrolyte surface,
5) transfer of molecular oxygen from the gas/solid electrolyte interface to the bulk of N_2-O_2 gas mixture.

Since the purpose of the present study is to investigate the diffusion mechanism of oxygen through zirconia due to the electronic conduction, experimental

TABLE 1 Results of calculation for oxygen permeability at various temperature and various oxygen pressure difference with cell(I).

No.	O_2 (%)	Temp. (K)	P (atm)	$-\Delta h/\Delta t \times 10^3$ ($cm\ sec^{-1}$)	$\dot{n}_{O_2} \times 10^8$ ($mol\ sec^{-1}$)	$J_{O_2} \times 10^{10}$ ($mol\ cm^{-2}\ sec^{-1}$)
110.	39	1673	0.997	2.67	2.98	7.50
111	39	1723	0.997	2.75	3.07	7.72
112	39	1773	0.997	4.75	5.30	13.3
108	39	1823	1.004	7.00	7.86	19.8
103	21	1673	1.003	3.17	3.56	8.96
104	21	1723	1.003	4.42	4.96	12.5
99	21	1773	1.005	7.42	8.34	21.0
98	21	1823	1.005	11.2	12.6	31.7
94	5.6	1673	1.003	5.00	5.61	14.1
95	5.6	1723	1.003	6.75	7.57	19.1
96	5.6	1773	1.003	11.4	12.8	32.2
97	5.6	1823	1.004	16.6	18.6	46.9
109	0.9	1673	0.997	6.67	7.44	18.7
105	0.9	1723	1 004	10.3	11.6	29.2
106	0.9	1773	1.004	15.8	17.7	44.7
107	0.9	1823	1.004	22.0	24.7	62.2
116	0.1	1673	0.997	8.53	9.51	23.9
115	0.1	1723	0.997	12.1	13.6	34.0
113	0.1	1773	0.997	20.3	22.6	57.0
114	0.1	1823	0.997	24.7	27.5	69.3

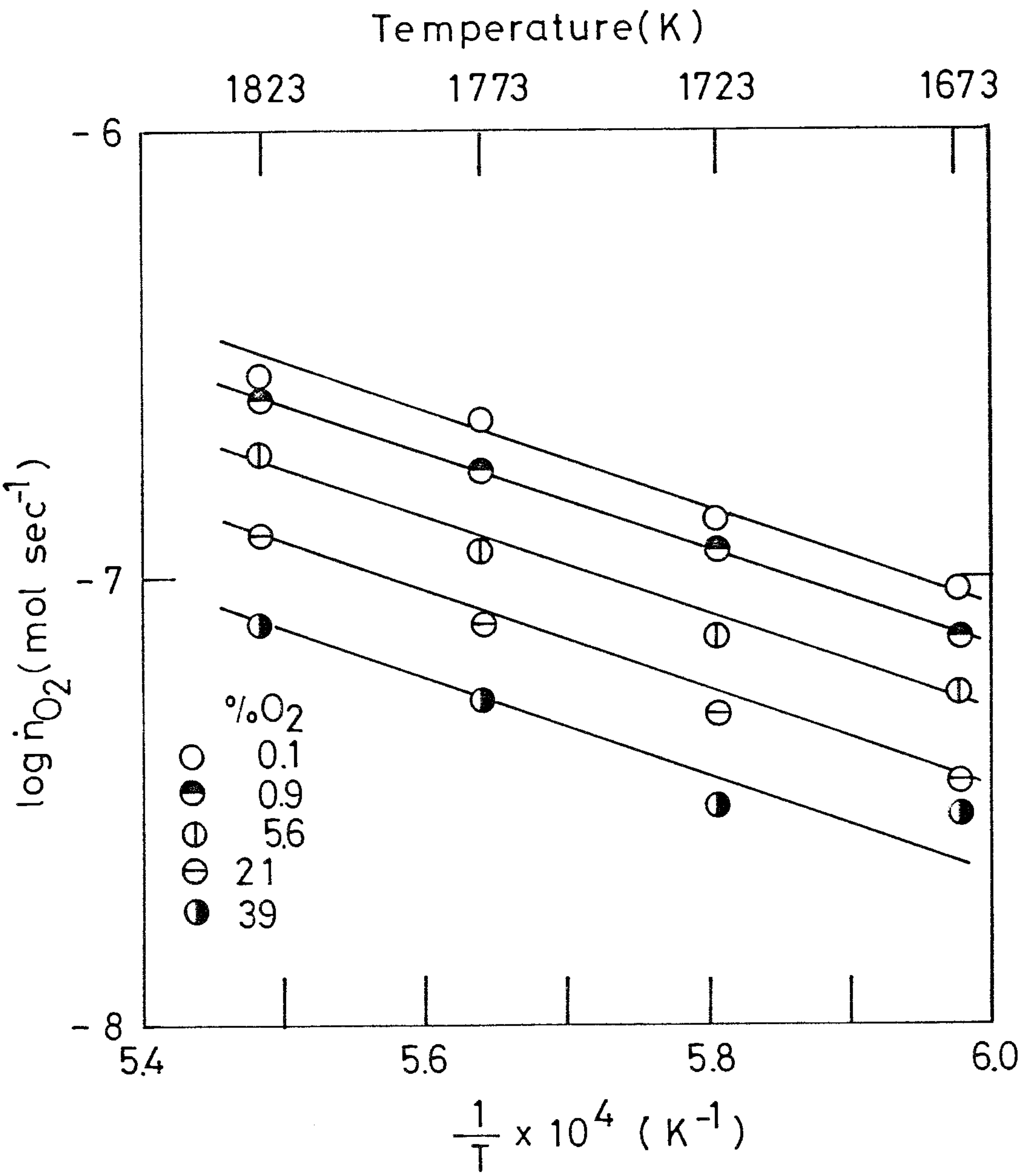

Fig.4.5 Temperature dependence of oxygen permeability with cell(II).

conditions should be arranged so as to make the transport of oxygen through zirconia the rate-controlling step. According to Takahashi et al.[6], the rate of chemical reaction between gaseous oxygen and ionic oxygen in the zirconia solid electrolyte at high temperature is very rapid. Furthermore, the oxygen pressure gradient in the laminar gas film of pure oxygen is negligible, so that the most likely rate-controlling step would be the mixed control of the transport of oxygen through electrolyte and gaseous diffusion through the boundary layer at the outer N_2-O_2 gas mixture. For the conditions of the present study, the resistance of molecular diffusion through the outer gas phase boundary was estimated to be negligibly small in comparison with the resistance of the oxygen transfer through electrolyte as discussed in the APPENDIX-E.

4.3.2. Theory of Oxygen Permeability

The reaction between lattice defects and electron defects in the solid electrolyte, and the gaseous oxygen may be formulated as

$$O_2(g) \quad + \quad 2\ V_o^{\bullet\bullet} \quad = \quad 2\ O_o \quad + \quad 4\ h^{\bullet}\ , \qquad [2]$$

$$2\ O_o \quad = \quad O_2(g) \quad + \quad 2\ V_o^{\bullet\bullet} \quad + \quad 4\ e'\ , \qquad [3]$$

where $V_o^{\bullet\bullet}$ is an oxygen ion vacancy in normal site occupation with "plus" two charge relative to the normal lattics site, O_o is an oxygen ion on an oxygen site, $h^{\bullet}$ is a positive hole, and e' is an excess electron(7).

The following discussion is based on the oxidation theory of Wagner(8). The transport rate of charge carrier i through electrolyte is given by

$$\frac{\dot{n}_i}{A} = - D_i \frac{d[i]}{dX} - B_i\ [i]\ Z_i\ e \frac{d\varphi}{dX}\ , \qquad [4]$$

where $\dot{n}_i$ is molecular number of i transported per unit time (mol sec^{-1}) expressed as vector, D_i is diffusion coefficient($cm^2\ sec^{-1}$), [i] is concentration(mol cm^{-3}),

B_i is absolute mobility(cm sec^{-1} dyne^{-1}), Z_i is electric valency, e is elementary electric charge(C), φ is electrical potential(dyne cm C^{-1}) and X is distance(cm), respectively.

The Nernst-Einstein equation interrelating diffusion coefficient and absolute mobility is given by

$$D_i = k\, T\, B_i\,, \qquad [5]$$

where K is Boltzman constant and T is temperature(K). Substituting eq.[5] for eq.[4] yields

$$\frac{\dot{n}_i}{A} = -\ D_i\ \left[\ \frac{d(i]}{d\ X} + \frac{[i]\ Z_i\ e}{k\ T}\ \frac{d\,\varphi}{d\ X}\ \right]. \qquad [6]$$

a. Oxygen Permeability Due To Positive Hole

Let us consider the specific case corresponding to the change in oxygen pressure. When the oxygen pressure surronuding the solid electrolyte is comparatively high, main charge carriers in zirconia electrolyte are oxygen ion and positive hole, i.e. oxygen permeability would be explained as fòllows

1) gaseous oxygen fills oxygen-ion vacancy, and oxygen ion and positive hole are created,

2) oxygen ion and positive hole migrate from the interface of high oxygen pressure to the another interface of low oxygen pressure,

3) reaction with oxygen ion and positive hole yields molecular oxygen and oxygen-ion vacancy on gas/ electrolyte interface of low oxygen pressure.

Eq.[6] can be rewritten for oxygen-ion vacancy and positive hole as follows;

$$\frac{\dot{n}_{V_O^{\cdot\cdot}}}{A} = - D_{V_O^{\cdot\cdot}} \left[\frac{d[V_O^{\cdot\cdot}]}{d X} + \frac{2[V_O^{\cdot\cdot}]\, e}{k T} \frac{d \varphi}{d X}\right], \qquad [7]$$

$$\frac{\dot{n}_{h^{\cdot}}}{A} = - D_{h^{\cdot}} \left[\frac{d[h^{\cdot}]}{dX} + \frac{[h^{\cdot}]e}{k T} \frac{d \varphi}{dX}\right]. \qquad [8]$$

Condition of electrical nuetrality in the zirconia, which is surrounded by considerablly high oxygen pressure, is described as

$$2[Ca_{Zr}''] = [h^{\cdot}] + 2 [V_O^{\cdot\cdot}] . \qquad [9]$$

Any volume element must remain electrically nuetral and only equivalent amounts of oxygen-ion vacancy and positive hole can migrate, because the cation diffusivity in the calcia-stabilized zirconia is negligiblly small, therefore,

$$\dot{n}_{h^{\cdot}} = - 2 \dot{n}_{V_o^{\cdot\cdot}} \quad . \qquad [10]$$

If there is no macro-segregation in its composition of zirconia; then

$$\frac{d\,[Ca''_{Zr}]}{d\,X} = 0 \ . \qquad [11]$$

Differentiation of eq.[9] by dX and combination of eq. [11] yield

$$\frac{d\,[h^{\cdot}]}{d\,X} = - 2 \frac{d[V_o^{\cdot\cdot}]}{d\,X} \ . \qquad [12]$$

From eqs.[9],[10] and [12], eq.[9] becomes

$$\frac{\dot{n}_{V_o^{\cdot\cdot}}}{A} = - \frac{\dot{n}_{h^{\cdot}}}{2\,A} \qquad [13]$$

$$= - D_{V_o^{\cdot\cdot}} [- \frac{1}{2} \frac{d[h^{\cdot}]}{d\,X} + \frac{\{2[Ca''_{Zr}] - [h^{\cdot}]\} e}{k\,T} \frac{d\varphi}{dX}] \ . \qquad [14]$$

Elimination of $(d\varphi/dX)$ from eq.[8] and eq.[14] yields

$$\left[\frac{D_{h^\cdot}\ [h^\cdot]}{2} - D_{V_o^{\cdot\cdot}}\left\{2[Ca_{Zr}''] - [h^\cdot]\right\}\right]\frac{\dot{n}_{h^\cdot}}{A}$$

$$= \left[\frac{1}{2} D_{h^\cdot} D_{V_o^{\cdot\cdot}} [h^\cdot] + D_{h^\cdot} D_{V_o^{\cdot\cdot}} \left\{2[Ca_{Zr}''] - [h^\cdot]\right\}\right]\frac{d[h^\cdot]}{dx}. \qquad [15]$$

Since, $[Ca_{Zr}''] \gg [h^\cdot]$, eq.[15] can be simplified to

$$\frac{\dot{n}_{h^\cdot}}{A} = - D_{h^\cdot} \frac{d[h^\cdot]}{dX} \qquad [16]$$

$$= (D_{h^\cdot}/L)\left\{[h^\cdot]_{(P'_{O_2})} - [h^\cdot]_{(P''_{O_2})}\right\}, \qquad [17]$$

where L is the thickness of electrolyte(cm), $[h^\cdot]_{(P'_{O_2})}$ and $[h^\cdot]_{(P''_{O_2})}$ are the concentration of positive hole at the designated oxygen partial pressures, P'_{O_2} and P''_{O_2}. Applying the law of mass action to reaction [2] yields

$$K_h = \frac{[O_o]^2 [h^\cdot]^4}{P_{O_2} [V_o^{\cdot\cdot}]^2}. \qquad [18]$$

Consequently,

$$J_{O_2(\oplus)} = \dot{n}_{O_2}/A = \dot{n}_{O_o}/2A = \dot{n}_{h^\cdot}/4A = - \dot{n}_{V_o^{\cdot\cdot}}/2A$$

$$= \frac{1}{4} D_{h^\cdot} K_h^{\frac{1}{4}} \left[\frac{[V_o^{\cdot\cdot}]}{[O_o]}\right]^{\frac{1}{2}} \frac{P'^{\,1/4}_{O_2} - P''^{\,1/4}_{O_2}}{L}, \qquad [19]$$

where $J_{O_2(\oplus)}$ is the flux of gaseous oxygen(mol cm^{-2} sec^{-1}) due to positive hole.

P-type electronic conductivity is defined by

$$\sigma_{\oplus} = [h^{\cdot}]\, N_{\circ}\, e\, \mu_{\oplus}\, , \qquad [20]$$

where $N_{\circ}$ and $\mu_{\oplus}$ are Avogadro's number and mobility($C^2 cm\ dyne^{-1}\ sec^{-1}$), respectively.

Introduction of eq.[18] into [20] gives

$$\sigma_{\oplus} = K_h^{\frac{1}{4}} \left[\frac{[V_O^{\cdot\cdot}]}{[O_O]}\right]^{\frac{1}{2}} P_{O_2}^{\frac{1}{4}}\, N_{\circ}\, e\, \mu_{\oplus}\, . \qquad [21]$$

Combination of the Nerst-Einstein equation and eq.[21] with eq.[19] yields

$$J_{O_2(\oplus)} = \frac{RT}{4F^2\, L}\left[\sigma_{\oplus(P'_{O_2})} - \sigma_{\oplus(P''_{O_2})}\right] \qquad [22]$$

$$= \frac{R\ T}{4F^2 L}\, \sigma^{\circ}_{\oplus}\, ({P'_{O_2}}^{1/4} - {P''_{O_2}}^{1/4})\, , \qquad [22]'$$

where $\sigma_{\oplus(P'_{O_2})}$ and $\sigma_{\oplus(P''_{O_2})}$ are the p-type electronic conductivities at the designated oxygen partial pressures, P'_{O_2} and P''_{O_2} , and $\sigma^{\circ}_{\oplus}$ is the p-type electronic conductivity at $P_{O_2} = 1$ atm. This is analogus to the Hartung-Möbius equation(9).

b. Oxygen Permeability Due To Excess Electron

When the oxygen pressure surrounding the solid electrolyte is very low, the oxygen permeability would be explained by using eq.[3] as follows;

1) gaseous oxygen and oxygen-ion vacancy react with excess electron, and oxygen ion on an oxygen site is created at the interface of higher oxygen pressure,
2) oxygen ion migrates from the interface of higher oxygen pressure to that of lower oxygen pressure, while excess electron migrates to the opposite direction,
3) reverse reaction described in 1) is occurred at the interface of lower oxygen pressure.

In this case, the equation corresponding to eq.[7] is given by

$$\frac{\dot{n}_{e'}}{A} = - D_{e'} \frac{d[e']}{dX} = D_{e'} \frac{[e']_{(P'_{O_2})} - [e']_{(P''_{O_2})}}{L} , \quad [23]$$

where $[e']_{(P'_{O_2})}$ and $[e']_{(P''_{O_2})}$ are the concentrations of excess electron at the designated oxygen partial pressures, P'_{O_2} and P''_{O_2}. The equilibrium constant K_e for the reaction [3] is

$$K_e = \frac{[V_o^{\cdot\cdot}]^2 \, [e']^4 \, P_{O_2}}{[O_o]^2} . \quad [24]$$

Substituting eq.[24] for eq.[23] yields

$$\frac{\dot{n}_{e'}}{A} = D_{e'} K_e^{\frac{1}{4}} \left[\frac{[O_o]}{[V_o^{\cdot\cdot}]}\right]^{\frac{1}{2}} \frac{P'^{-\frac{1}{4}}_{O_2} - P''^{-\frac{1}{4}}_{O_2}}{L} \quad . \qquad [25]$$

Condition of electrical nuetrality at any volume element of electrolyte is given by

$$\dot{n}_{e'} = 2 \dot{n}_{V_o^{\cdot\cdot}} \quad . \qquad [26]$$

Therefore,

$$J_{O_2(\theta)} = \dot{n}_{O_2}/A = \dot{n}_{O_o}/2A = - \dot{n}_{e'}/4A = - \dot{n}_{V_o^{\cdot\cdot}}/2A$$

$$= - \frac{1}{4} D_{e'} K_{e'}^{\frac{1}{4}} \left[\frac{[O_o]}{[V_o^{\cdot\cdot}]}\right]^{\frac{1}{2}} \frac{P'^{-\frac{1}{4}}_{O_2} - P''^{-\frac{1}{4}}_{O_2}}{L} \quad . \qquad [27]$$

The equation corresponding to eq.[22] is

$$J_{O_2(\theta)} = - \frac{R T}{4 F^2 L} [\sigma_{\theta(P'_{O_2})} - \sigma_{\theta(P''_{O_2})}] \quad . [28]$$

$$= - \frac{R\,T}{4\,F^2\,L}\ \sigma_{\ominus}^{\circ}\left(P'^{\,-1/4}_{O_2} - P''^{\,-1/4}_{O_2} \right), \qquad [28]'$$

where $\sigma_{\ominus(P'_{O_2})}$ and $\sigma_{\ominus(P''_{O_2})}$ are the n-type electronic conductivities at the designated oxygen partial pressures, P'_{O_2} and P''_{O_2}, and $\sigma_{\ominus}^{\circ}$ is the n-type electronic conductivity at $P_{O_2} = 1$ atm.

c. Oxygen Permeability Due To Positive Hole And Excess Electron

Summation of eqs.[22] and [23] gives a total oxygen permeability, if the reactions [2] and [3] coexist at equilibrium,

$$J_{total} = J_{O_2(\oplus)} + J_{O_2(\ominus)}$$

$$= \frac{R\ T}{4\ F^2\ L}\left\{\left[\sigma_{\oplus(P'_{O_2})} - \sigma_{\oplus(P''_{O_2})}\right] - \left[\sigma_{\ominus(P'_{O_2})} - \sigma_{\ominus(P''_{O_2})}\right]\right\} \qquad [29]$$

$$= \frac{R\ T}{4F^2L}\left[\sigma^{\circ}_{\oplus}\left(P'^{\frac{1}{4}}_{O_2} - P''^{\frac{1}{4}}_{O_2}\right) - \sigma^{\circ}_{\ominus}\left(P'^{-\frac{1}{4}}_{O_2} - P''^{-\frac{1}{4}}_{O_2}\right)\right]. \qquad [29]'$$

The eq.[29] is general equation interrelating oxygen permeability and partial conductivity of positive hole and excess electron.

A parameter of oxygen permeability, $P_{\oplus\ominus}$, would be convenient to discuss specific case which arise from eq.[29],

$$P_{\oplus\ominus} = (\sigma^{\circ}_{\oplus} / \sigma^{\circ}_{\ominus})^{-2}, \qquad [30]$$

where $\sigma^{\circ}_{\oplus}$ and $\sigma^{\circ}_{\ominus}$ are p-type and n-type electronic conductivities at P_{O_2}= 1 atm, respectively. This parameter shows the oxygen potential at which the p-type and n-type electronic conductivities are equal. Figure 4.6 shows the partial conductivities of stabilized zirconia as the functions of oxygen partial pressure.

(A) if the sequence of oxygen partial pressure is

$$P_{\oplus}{}^{*} \gg P'_{O_2} > P''_{O_2} \gg P_{\oplus\ominus} \qquad \text{(Fig.4.6(a))},$$

J_{total} is nearly equal to $J_{\oplus}$ which is given by eq.[22].

(B) The condition

$$P_{\oplus} \gg P'_{O_2} \gg P_{\oplus\ominus} \gg P''_{O_2} \gg P_{\ominus} \text{*} \qquad \text{(Fig.4.6(b))}$$

leads to

$$J_{total} \doteqdot \frac{RT}{4F^2L}\left(\sigma^{\circ}_{\oplus} P'^{\frac{1}{4}}_{O_2} + \sigma^{\circ}_{\ominus} P''^{-\frac{1}{4}}_{O_2}\right) . \qquad [31]$$

(C) In the case

$$P_{\oplus\ominus} \gg P'_{O_2} > P''_{O_2} \gg P_{\ominus} \qquad \text{(Fig.4.6(c))},$$

J_{total} is approximately given by eq.[28].

---

* According to Schmalzried(10,11), the parameters, $P_{\oplus}$ and $P_{\ominus}$, show the oxygen potentials at which the p-type and n-type electronic conductivities equal to the ionic conductivity.

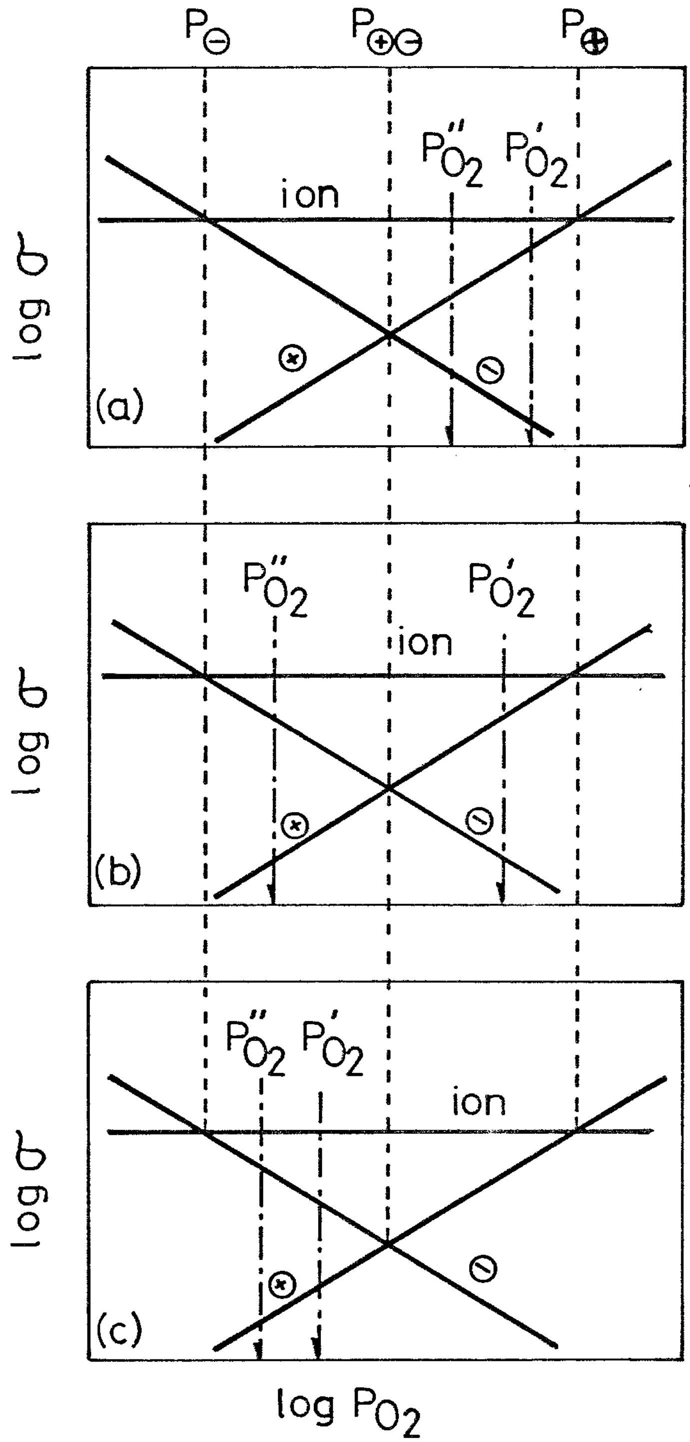

Fig.4.6 The partial conductivities of calcia-stabilized zirconia as the functions oxygen partial pressure

4.3.3 Comparison With Other Data

The cell used for permeability measurement by Smith et al[1] is represented schematically as

O_2 (P'_{O_2} = 3.9 x 10^{-3} to 1.3 x 10^{-1} atm)	ZrO_2(CaO) solid electrolyte tube	Ultrahigh vacuum with carbon susceptor (total pressure is 10^{-6} to 10^{-7} torr, P''_{O_2} = unknown)

The oxygen permeability was measured by omegatron mass spectrometer connected to the high vacuum side of the zirconia tube in the temperature range from 1373 to 2323 K. In this case the sequence of oxygen partial pressure may be

$$P_{\oplus} \gg P'_{O_2} \gg P_{\oplus\ominus} \gg P''_{O_2} \gg P_{\ominus}.$$

Consequently eq.[31] should be used for the analysis of their results.

One of the permeability measurement cell used by Fischer[2] at 1873 K is

$N_2 - O_2$ (P'_{O_2} = 0.1 to 1 atm)	$ZrO_2(CaO)$ solid electrolyte tube	Liquid Iron (constant oxygen content = 1000 ppm) ($P''_{O_2} = 10^{-9}$ atm)

Eq.[31] is preferable for this cell to calculate the p-type electronic conductivities, while his calculation was made by eq.[22], since the sequence of oxygen partial pressure for his cell may be

$$P_{\oplus} \gg P'_{O_2} \gg P_{\oplus\ominus} \gg P''_{O_2} \gg P_{\ominus}.$$

In summary, the values of p-type electronic conductivities given in his TABLE 1 would be somewhat inaccurate. On the other hand, his values obtained by the following permeability measurement cell at the temperature range from 1615 to 1900 K would be accurate

O_2 (P'_{O_2} = 1 atm)	$ZrO_2(CaO)$ solid electrolyte tube	$N_2 - O_2$ ($P''_{O_2} = 5.2 \times 10^{-1}$ to 5.4×10^{-4} atm)

The sequence of oxygen partial pressure for this cell may be

$$P_{\oplus} \gg P'_{O_2} > P''_{O_2} \gg P_{\oplus\ominus}.$$

Alcock and Chan[4] have used the following cell to measure the permeability from 1674 to 1873 K;

O_2 (P'_{O_2} = 1 atm)	ZrO_2(CaO) solid electrolyte tube	CO/CO_2 (P''_{O_2} = 0.5 to 10^{-2} atm)

The inside of the zirconia tube was filled with pure oxygen at one atmospheric pressure and the pressure drop inside the tube was recorded on a manometer connected to the zirconia tube. They calculated the total quantities of oxygen which was transmitted through the tube from the inner volume and the change in pressure. Consequently, the oxygen pressure inside the tube had not been kept constant during the permeability measurements. In other words, the steady-state condition was not kept in their experiments, though they used the steady-state equation.

The permeability measurement by Palguev et al[3] was carried out for the following cell at the temperature from 1173 to 1523 K

O_2 (P'_{O_2} = 0.01 to 1 atm)	ZrO_2(CaO) solid electrolyte tube	Vacuum (P''_{O_2} = unknown)

Their experimental technique was similar to that used by Alcock and Chan[4] and their analysis was based on unsteady state condition[12]. They reported the 1/4 power dependence of P'_{O_2} on oxygen permeability. Though their calculation of p-type electronic conductivities was made by the following equation

$$\sigma^{\circ}_{\oplus} = 4 F^2 L J / RT, \qquad [32]$$

eq.[22] may be preferable for the calculation of p-type electronic conductivity.

Quite the same kind of discussion would be applicable for the analysis of oxygen permeability reported by Heynes and Beekman[7], and Kitazawa and Coble[5].

4.3.4. Cell(II)

The sequence of oxygen partial pressure for cell(II) is

$$P_{\oplus} \gg P'_{O_2} \gg P_{\oplus\ominus} \gg P''_{O_2} \gg P_{\ominus}.$$

Representative experimental results for this cell are shown in Fig.4.7. Quite linear behavior was observed. Calculated values of oxygen flux from eq.[1] are summarized in TABLE 2. The effect of oxygen partial pressure, P''_{O_2}, on the permeability is shown in Fig.4.8. A good linear relationship between oxygen permeability and $P''^{-1/4}_{O_2}$ is observed as predicted from eq.[31].

4.3.5 Calculation Of P-type And N-type Electronic Conductivities

The p-type electronic conductivity at $P_{O_2} = 1$ atm, $\sigma^{\circ}_{\oplus}$, was calculated from eq.[22] for cell(I). For the case of cell(II), the slope and intercept of the lines in Fig.4.8 should give $(RT\,\sigma^{\circ}_{\ominus} / 4F^2 L)$ and $(RT\sigma^{\circ}_{\oplus}/4F^2L)$, respectively.

TABLE 2a Results of calculation of oxygen permeability at various temperature and various oxygen partial pressure with cell(II).

No.	$-\Delta h/\Delta t$ $(cm\ s^{-1}) \times 10^2$	Atmospheric Pressure, P (atm)	$\dot{n}_{O_2}$(total) $(mol\ s^{-1}) \times 10^7$	J_{O_2} $(mol\ cm^{-2}\ s^{-1}) \times 10^8$	$P''^{-1/4}_{O_2}$ $(atm^{-1/4})$
1662 K					
1	4.00	0.996	4.13	1.05	636
2	4.65	0.996	4.80	1.23	766
4	3.00	1.001	3.11	0.795	334
5	3.40	1.007	3.54	0.906	447
6	3.70	0.999	3.40	0.869	556
13	3.32	0.993	3.40	0.869	556
14	3.08	0.993	3.17	0.810	394
15	2.94	0.993	3.03	0.773	288
16	2.04	0.992	2.10	0.536	191
17	2.27	0.999	2.35	0.600	220
18	2.91	0.996	3.00	0.767	269
19	4.01	0.997	4.14	1.06	501
20	3.73	0.997	3.85	0.984	632
21	3.86	0.996	3.98	1.02	605

TABLE 2b Results of calculation for oxygen permeability at various temperature and various oxygen partial pressure with cell(II) (continued)

No.	$-\Delta h/\Delta t$ $(cm\ s^{-1}) \times 10^2$	Atmospheric Pressure, P (atm)	$\dot{n}_{O_2}$ (total) $(mol\ s^{-1}) \times 10^7$	J_{O_2} $(mol\ cm^{-2}\ s^{-1}) \times 10^8$	$P''_{O_2}{}^{-1/4}$ $(atm^{-1/4})$
1662 K					
22	2.95	0.999	3.05	0.780	209
23	3.01	0.999	3.11	0.795	272
1719 K					
7	5.70	0.999	5.90	1.51	361
8	6.70	0.997	6.92	1.77	590
24	4.97	0.997	5.13	1.31	305
25	6.65	0.997	6.87	1.76	518
27	4.56	0.999	4.71	1.20	192
28	6.44	0.997	6.66	1.70	430
29	6.26	0.997	6.47	1.65	347
30	7.44	0.995	7.44	1.90	566
31	7.22	0.995	7.99	2.04	616

TABLE 2c Results of calculation for oxygen permeability at various temperature and various oxygen pressure difference ith ell(II) (continued)

No.	$-\Delta h/\Delta t$ ($cm\ s^{-1}$) x 10^2	Atmospheric Pressure, P (atm)	$\dot{n}_{O_2}$(total) ($mol\ s^{-1}$) x 10^7	J_{O_2} ($mol\ cm^{-2}\ s^{-1}$) x 10^8	$P''_{O_2}{}^{-1/4}$ ($atm^{-1/4}$)
1719 K					
32	7.63	0.995	6.14	1.62	320
33	6.14	0.995	5.80	1.48	256
34	5.64	0.992	4.79	1.22	164
35	4.79	0.991			
1771 K					
36	6.20	0.999	6.41	1.64	122
37	8.85	1.000	9.17	2.34	232
38	11.4	1.000	11.8	3.02	308
39	12.4	1.000	12.8	3.28	420
40	14.3	1.000	14.8	3.78	481
47	8.38	0.995	8.65	2.21	173
48	10.4	0.999	10.6	2.71	262

TABLE 2d Results of calculation for oxygen permeability at various temperature and various oxygen pressure difference with cell(II) (continued)

No.	$-\Delta h/\Delta t$ $(cm\ s^{-1}) \times 10^2$	Atmospheric Pressure, P (atm)	$\dot{n}_{O_2}$(total) $(mol\ s^{-1}) \times 10^7$	J_{O_2} $(mol\ cm^{-2}\ s^{-1}) \times 10^8$	$P''^{-1/4}_{O_2}$ $(atm^{-1/4})$
1771 K					
49	11.8	0.992	12.1	3.10	371
50	13.2	0.993	13.6	3.47	453
51	7.06	0.993	7.26	1.86	107
52	8.30	0.993	8.54	2.18	139
1820 K					
41	10.1	1.003	10.5	2.68	76
42	11.6	1.003	12.0	3.08	96
43	14.0	1.003	14.5	3.71	126
44	14.7	1.003	15.3	3.90	146
45	9.20	1.003	9.55	2.44	62
46	13.1	1.003	13.6	3.48	106

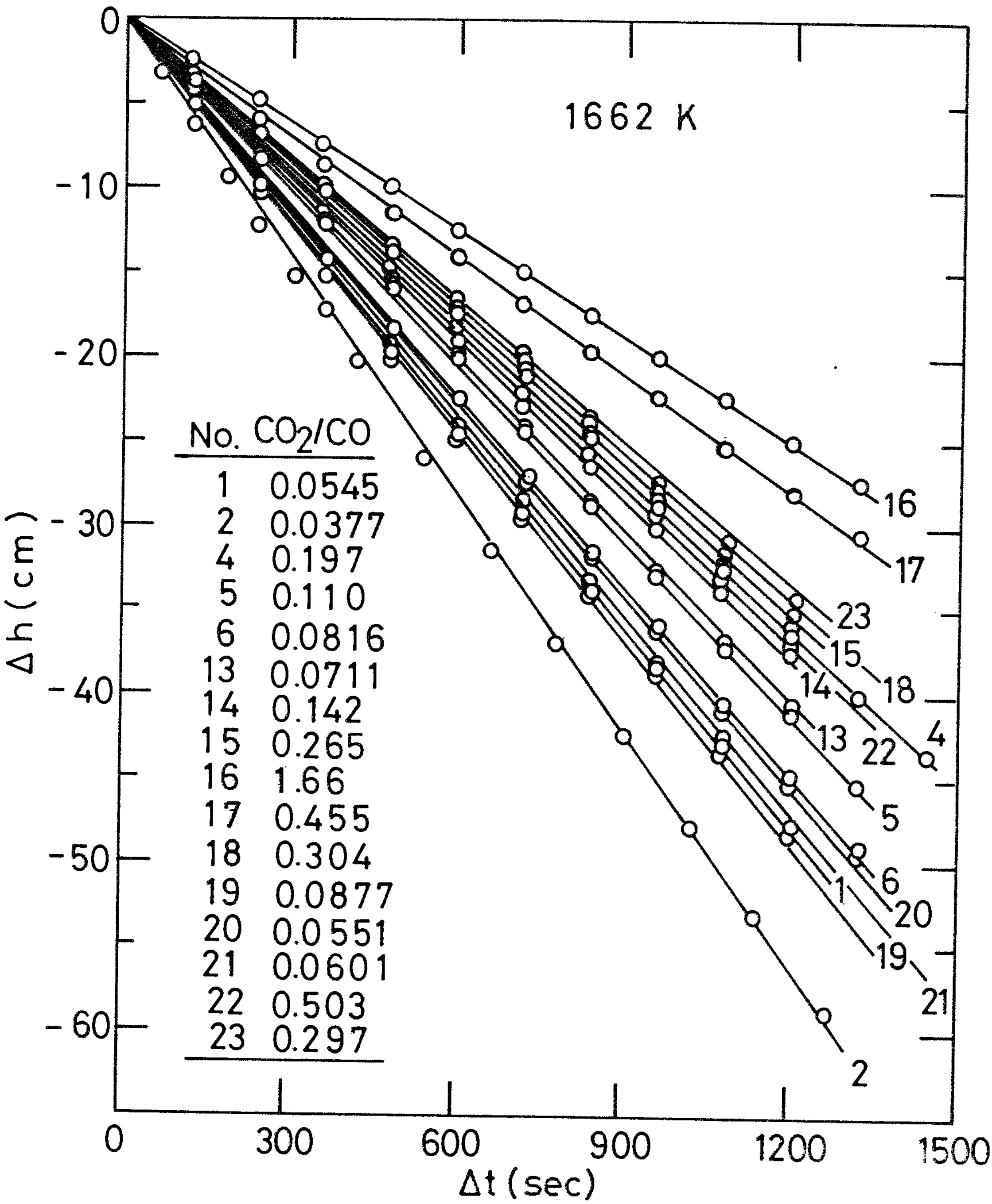

Fig.4.7a Experimental results for cell(II).

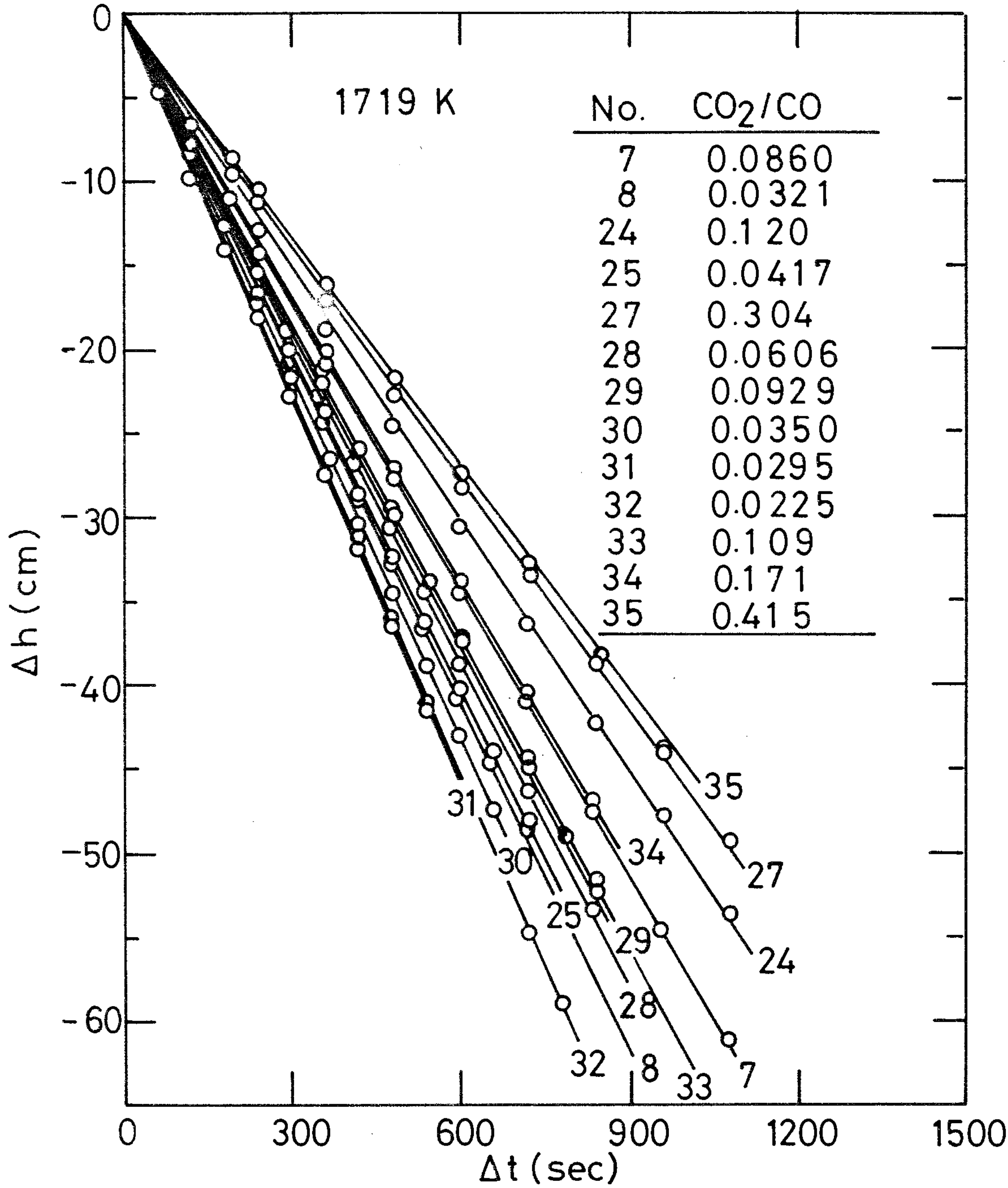

Fig.4.7b Experimental results for cell(II).

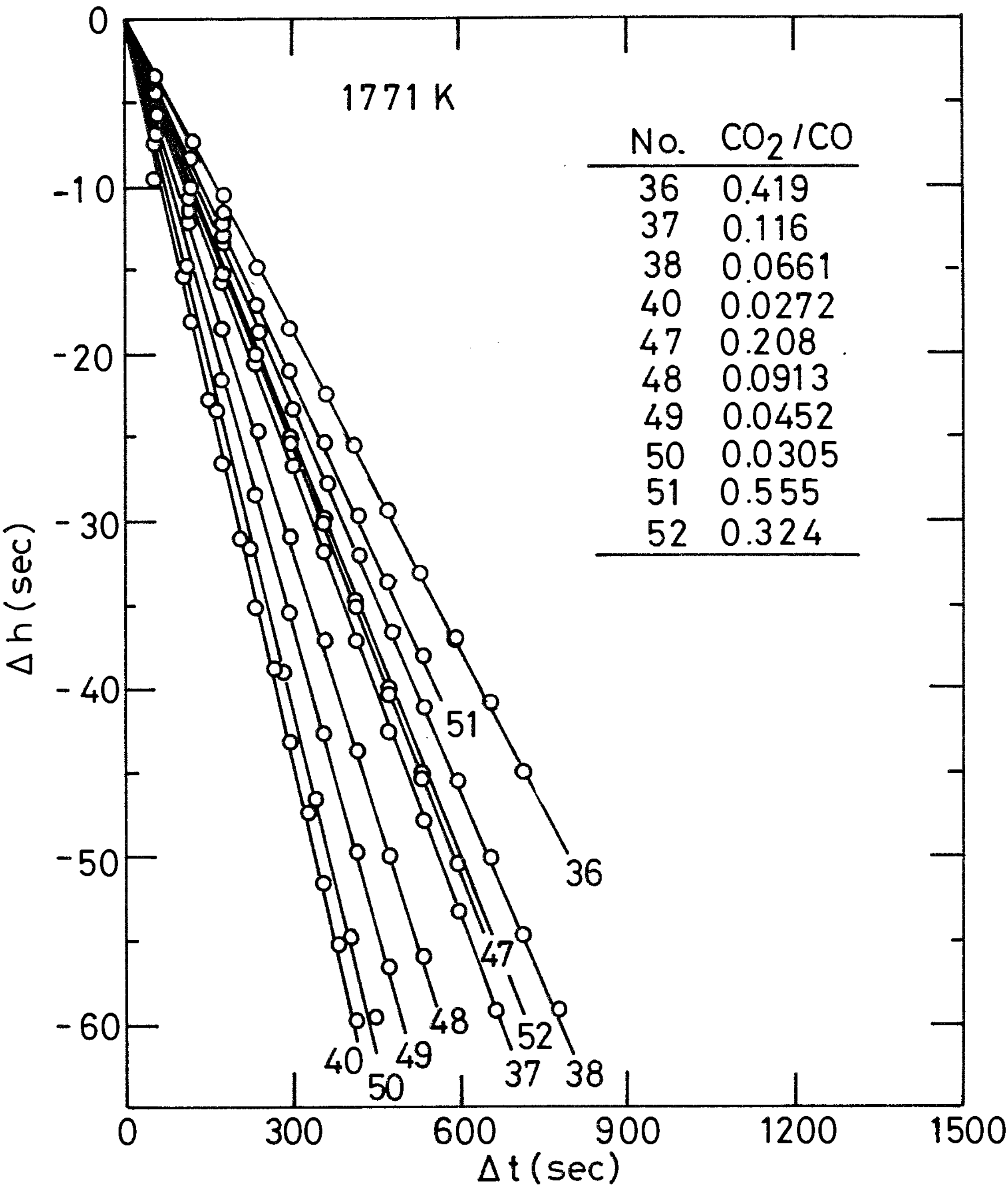

Fig.4.7c Experimental results for cell(II).

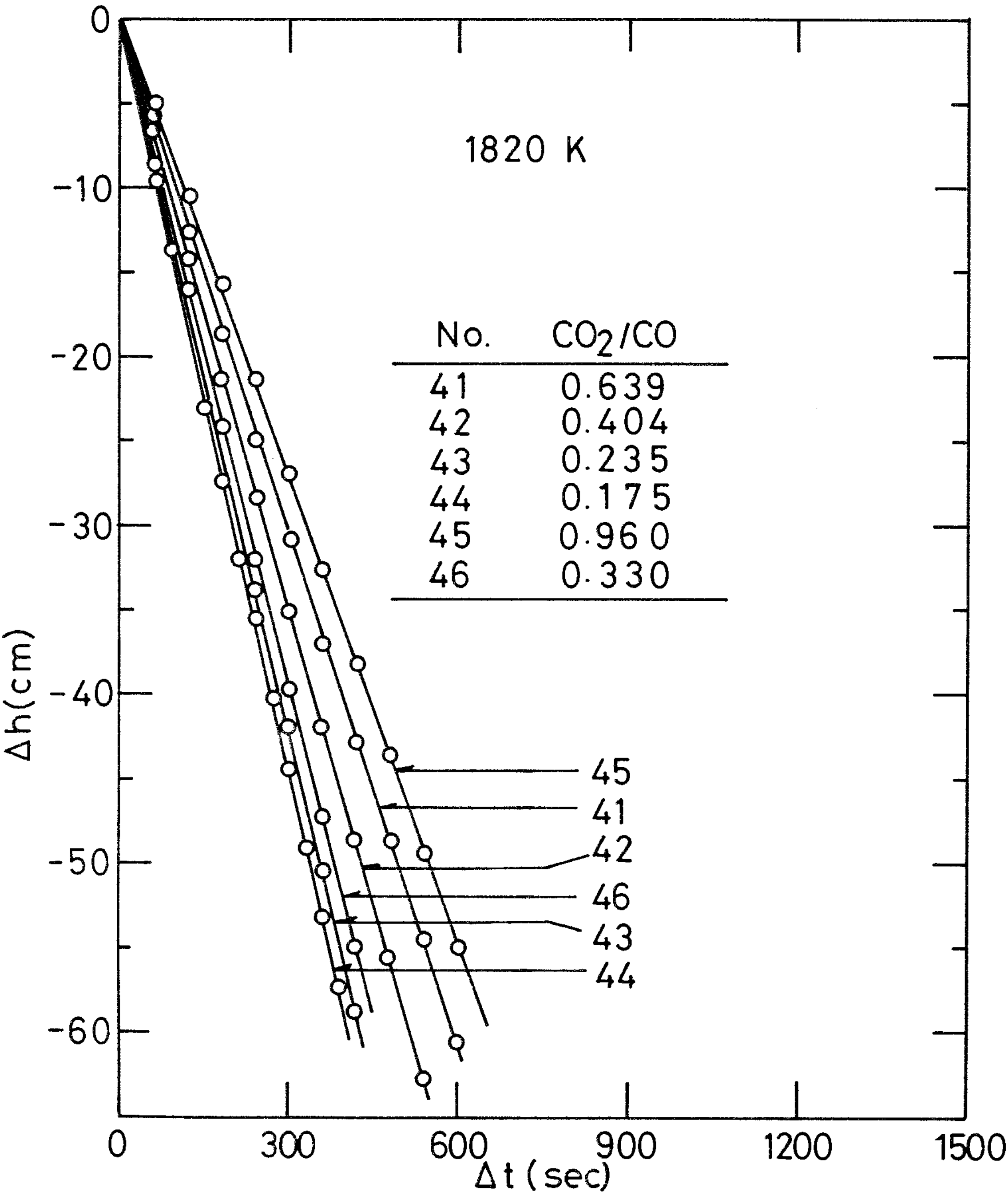

Fig.4.7d Experimental results for cell(II).

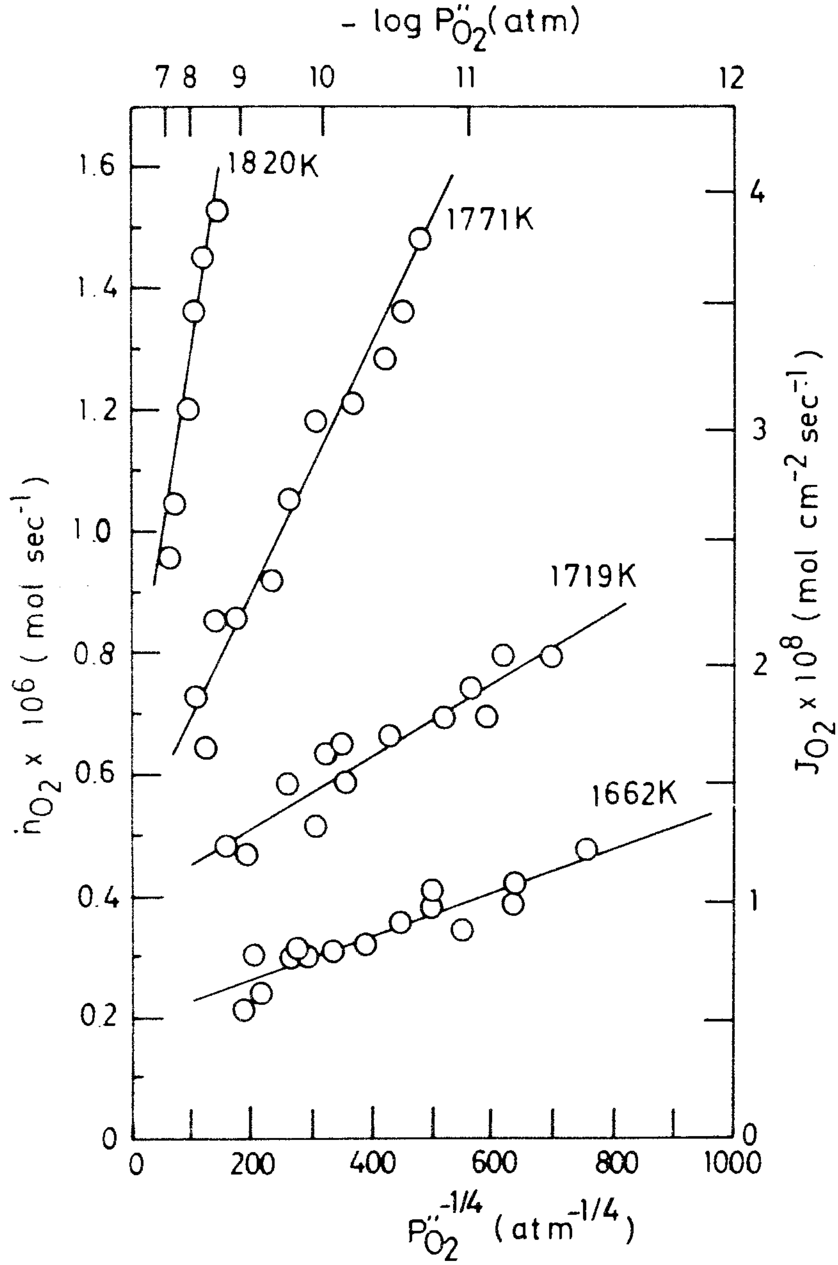

Fig.4.8 Oxygen partial pressure dependence of oxygen permeability for cell(II)

The results for $\sigma^{\circ}_{\oplus}$ are shown in Fig.4.9. Values reported by Fischer [2], Friedman et al.[13], and Hartung and Möbius[9] are for commercial zirconia tube, while the high values of Patterson et al.[14] are for high-purity electrolyte. The present results obtained by cells(I) and (II) are shown in good agreement with each other. The temperature dependence of $\sigma^{\circ}_{\oplus}$ was calculated as

$$\log \sigma^{\circ}_{\oplus} = 0.28 - 5100\ (T/K)^{-1} \qquad [33]$$

from cell(I),

$$\log \sigma^{\circ}_{\oplus} = 2.05 - 7600\ (T/K)^{-1} \qquad [34]$$

from cell(II).

The results for $\sigma^{\circ}_{\ominus}$ are shown in Fig.4.10. The values of Friedman et al.[13], and Patterson et al.[14], for commercial ZrO_2 + 3 to 4 wt pct CaO and high purity ZrO_2 + 15 mol pct CaO, respectively were obtained by means of d-c polarization method[15]. On the other hand, the experiments by Scaife et al.[16] and Etsell and Flengas[17] were based on coulometric titration method[18] and the conductivity measurements. Temperature dependence of the n-type electronic conductivity at P_{O_2} = 1 atm, $\sigma^{\circ}_{\ominus}$, obtained in the

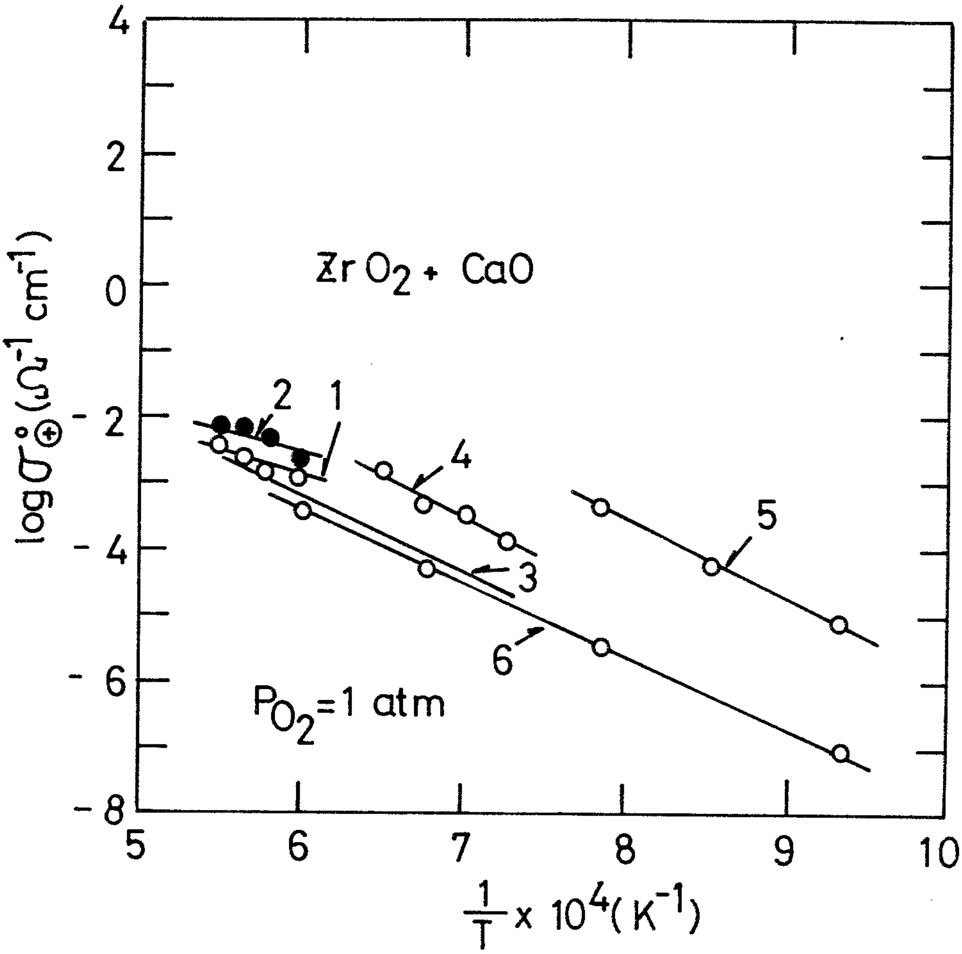

Fig.4.9 The p-type electronic conductivity at P_{O_2} = 1 atm, $\sigma_{\oplus}^{\circ}$, as the functions of reciprocal temperature.

1. Present study by cell(I).
2. Present study by cell(II).
3. Fischer
4. Friedman et al.
5. Patterson et al.
6. Hartung and Möbius.

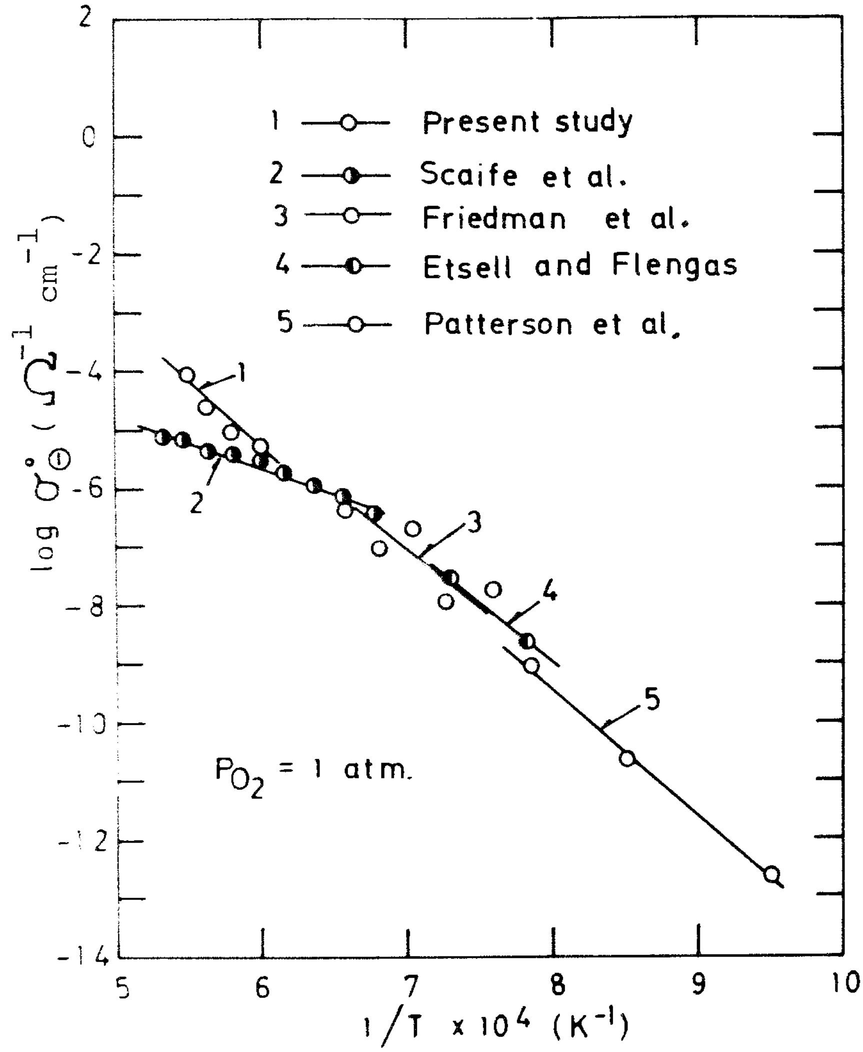

Fig.4.10 The n-type electronic conductivity at P_{O_2} = 1 atm, $\sigma^{\circ}_{\ominus}$, as a function of reciprocal temperature.

present study with cell(II) was represented as

$$\log \sigma^{\circ}_{\ominus} = 8.81 - 23600\ (T/K)^{-1}. \qquad [35]$$

4.3.6. Calculation Of The Parameters, $P_{\oplus}$ And $P_{\ominus}$

For the practical application of solid electrolyte in a solid-oxide galvanic cell as a device for monitoring oxygen in liquid steel, the parameters, $P_{\oplus}$ and $P_{\ominus}$, give more usefull information than the p-type and n-type electronic conductivities. These parameters can be calculated by combining available ionic conductivity(19) and the p-type and n-type electronic conductivities obtained in the present study. The results of calculation for $P_{\oplus}$ are shown in Fig.4.11. The temperature dependence of $P_{\oplus}$ was calculated as

$$\log P_{\oplus} = -\ 0.87 + 15400\ (T/K)^{-1} \qquad [36]$$

from cell(I),

$$\log P_{\oplus} = 2.65 + 6500\ (T/K)^{-1} \qquad [37]$$

from cell(II).

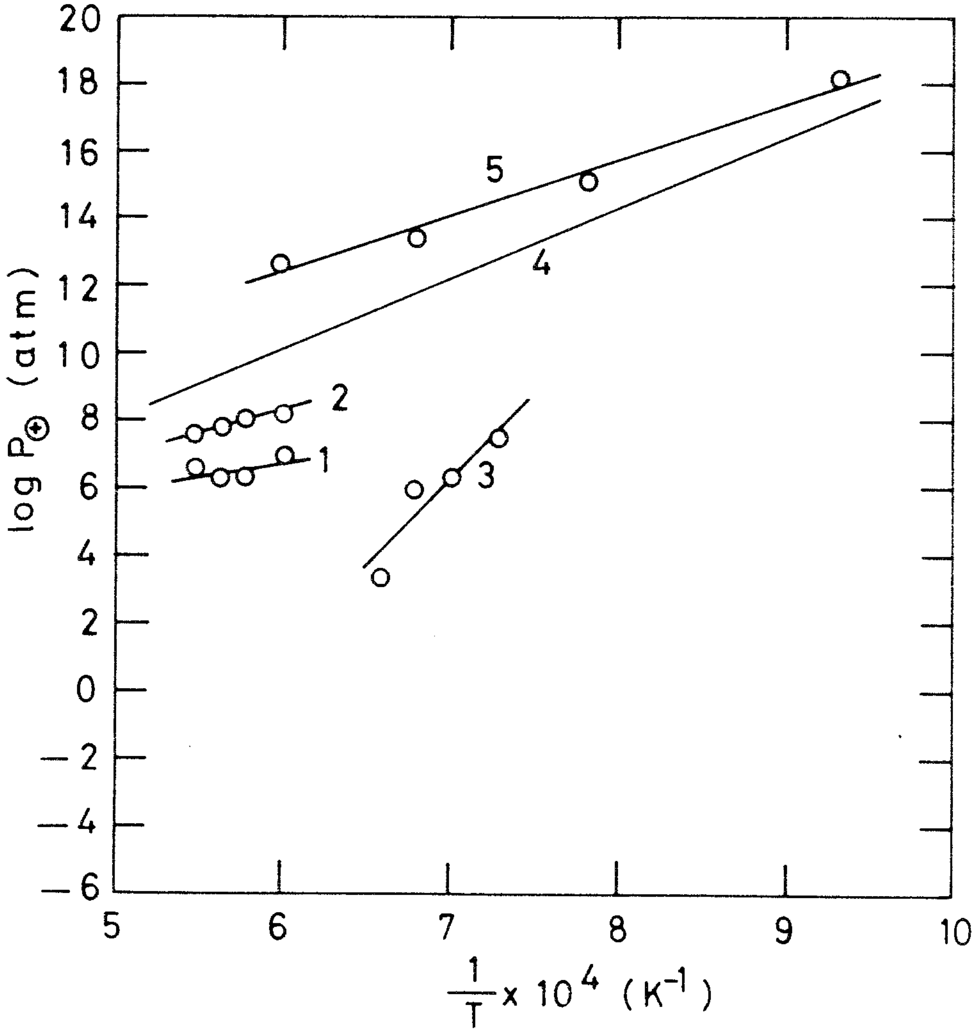

Fig.4.11 The parameter, $P_\oplus$, as a function of reciprocal temperature

1. present study by cell(II)
2. Present study by cell(I)
3. Friedman et al.
4. Patterson
5. Hartung and Möbious

The present results obtained by cell(I) and cell(II) are shown in fair good agreement with each other. The disagreement between the present results and those by Hartung and Möbious[9] would be attributed to the difference in impurities. Patterson[20] has made a comprehensive survey of literature concerning the conduction properties of calcia-stabilized zirconia and has provided an estimate of $P_{\oplus}$. His analysis was based on permeability measurement by Smith et al.[1] for commercial zirconia tube supplied from Zirconia Corporation of America, and the conductivity measurement by Patterson et al.[14] for high-purity zirconia. In other word, he assumed that the ionic conductivity of commercial zirconia tube was equal to that reported for high purity materials; this assumption might not be valid. No obvious reason except for the difference in the ionic conductivity can be found for the disagreement between the present results and those by Friedman et al[13]. The extrapolation of their values to steelmaking temperature yields $\log P_{\oplus} = -3.5$ at 1873 K. This value of -3.5 means that the Pt/air reference electrode is not suitable as the reference electrode of oxygen sensor for steelmaking. This is contrary to the fact[21.22]. The results by Friedman et al[13] would be inaccurate.

The results of calculation for P_θ are shown in Fig.4.12. Janke and Fischer[23,24], Scaife et al.[16], and Etsell and Flengas[17] utilized the coulometric titration method[18], which is rapid and should be accurate as pointed out by Etsell and Flengas[17]. Disagreement between the present results and those by Janke and Fischer[23,24] would be attributed not only to the difference in impurities in the commercial zirconia tubes but also to different experimental technique used. Errors in the present study with cell(II) would arise from the uncertainty of effective permeation area and ionic conductivity (Appendix-C).

The low P_θ values reported by Scaife et al.[17] and Richards et al.[25] are for high purity electrolyte. The extrapolation of the values reported by Friedman et al.[15] to steelmaking temperatures yields log P_θ = - 9.0. In their experiments, commercial ZrO_2 + 3 to 4 wt pct CaO solid electrolyte was used. Consequently, their high values would be attributed to the presence of significant amounts of monoclinic ZrO_2 in the electrolyte. According to Kumar et al.[26], monoclinic ZrO_2(tetragonal above 1273 K) would be predominantly electronic conductor.

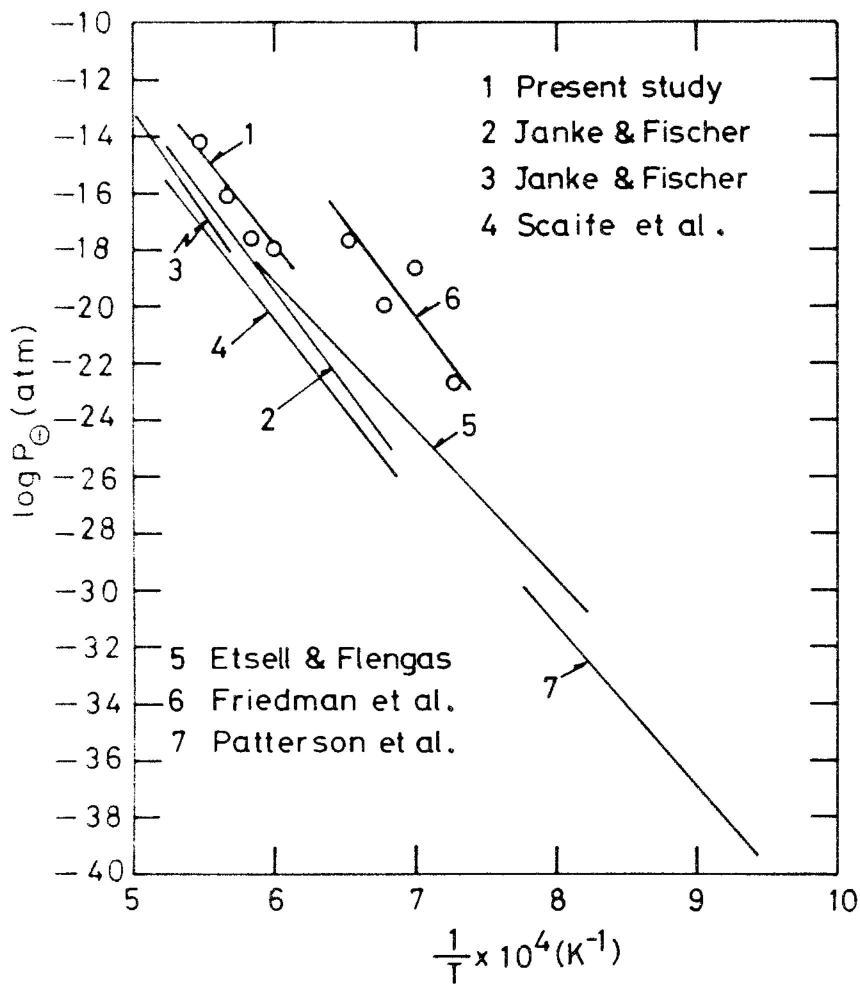

Fig. 4.12 The parameter, P_{Θ}, as a function of reciprocal temperature.

Temperature dependence of log $P_{\ominus}$ obtained in the present study is represented as

$$\log P_{\ominus} = 24.12 - 70500\ (T/K)^{-1} . \qquad [38]$$

The results for $\sigma^{\circ}_{\oplus}$, $\sigma^{\circ}_{\ominus}$, $P_{\oplus}$ and $P_{\ominus}$ in the present study are summarized in TABLE 3.

TABLE 3a Experimental results for the p-type electronic conductivity and the parameter, $P_\oplus$, obtained by cell(I)/

Temp (K)	log σ_{ion} (ohm^{-1} cm^{-1})	log $\sigma^{o}_{\oplus}$ (ohm^{-1} cm^{-1})	log $P_\oplus$ (atm)
1673	- 0.825	$-2.88^{+0.04}_{-0.06}$	$8.18^{+0.16}_{-0.24}$
1723	- 0.705	$-2.77^{+0.02}_{-0.03}$	$8.26^{+0.08}_{-0.12}$
1773	- 0.605	$-2.56^{+0.01}_{-0.02}$	$7.82^{+0.04}_{-0.08}$
1823	- 0.505	-2.43 ± 0.02	7.70 ± 0.08

TABLE 3b Experimental results for the p-type and n-type electronic conductivities and the parameters, $P_{\ominus}$ and $P_{\oplus}$, obtained by cell(II).

Temp. (K)	log σ_{ion} ($ohm^{-1}\ cm^{-1}$)	log $\sigma^{\circ}_{\ominus}$ ($ohm^{-1}\ cm^{-1}$)	log $P_{\ominus}$ (atm)	log $\sigma^{\circ}_{\oplus}$ ($ohm^{-1}\ cm^{-1}$)	log $P_{\oplus}$ (atm)	log $P_{\oplus\ominus}$ (atm)
1662	-0.838	$-5.31^{+0.11}_{-0.15}$	$-17.9^{+0.44}_{-0.60}$	$-2.58^{+0.06}_{-0.07}$	$6.97^{+0.24}_{-0.28}$	-5.47
1719	-0.710	$-5.10^{+0.07}_{-0.10}$	$-17.6^{+0.28}_{-0.40}$	$-2.28^{+0.04}_{-0.05}$	$6.28^{+0.24}_{-0.28}$	-5.66
1771	-0.606	$-4.60^{+0.07}_{-0.08}$	$-16.0^{+0.28}_{-0.32}$	$-2.18^{+0.14}_{-0.19}$	$6.30^{+0.56}_{-0.70}$	-4.85
1820	-0.509	-4.04 ± 0.02	-14.1 ± 0.08	$-2.18^{+0.06}_{-0.07}$	6.68 ± 0.24	-3.71

4.4 Summary

Oxygen permeability of commercial calcia-stabilized zirconia has been measured from 1673 to 1823 K by the following cells

cell(I)

O_2 (P'_{O_2} = 1 atm)	$ZrO_2(CaO)$ solid electrolyte tube	N_2 - O_2 (P''_{O_2} = 0.39 to 10^{-3} atm)

cell(II)

O_2 (P'_{O_2} = 1 atm)	$ZrO_2(CaO)$ solid electrolyte tube	CO/CO_2 (P''_{O_2} = 10^{-7} to 10^{-12} atm)

The following conclusions can be drawn;

1) Oxygen permeability of calcia-stabilized zirconia is proportional to $(1 - P''^{1/4}_{O_2})$ for cell(I) and to $P''^{-1/4}_{O_2}$ for cell(II), respectively.
2) The temperature dependence of the p-type and n-type electronic conductivities and the parameters, $P_{\oplus}$ and $P_{\ominus}$ were obtained as

$$\log \sigma^{\circ}_{\oplus} = 0.28 - 5100\ (T/K)^{-1},$$
$$\log P_{\oplus} = -0.87 + 15400\ (T/K)^{-1},$$

from cell(I),

$$\log \sigma^{\circ}_{\oplus} = 8.81 - 23600\ (T/K)^{-1},$$
$$\log \sigma^{\circ}_{\ominus} = 2.05 - 7600\ (T/K)^{-1},$$
$$\log P_{\oplus} = 2.65 + 6500\ (T/K)^{-1},$$
$$\log P_{\ominus} = 24.12 - 70500\ (T/K)^{-1},$$

from cell(II).

3) The total oxygen permeability due to the p-type and n-type electronic conduction is given by

$$J_{total} = \frac{RT}{4\ F^2\ L} \left[\sigma^{\circ}_{\oplus} \left(P'^{\,1/4}_{O_2} - P''^{\,1/4}_{O_2}\right) - \sigma^{\circ}_{\ominus} \left(P'^{\,-1/4}_{O_2} - P''^{\,-1/4}_{O_2}\right) \right].$$

4) A new parameter, $P_{\oplus\ominus}$, would be convenient to discuss the specific case which arise from the above equation. In permeability measurement, the conditions for oxygen partial pressure at gas/ electrolyte interface which is characterized by the parameter should be taken into account.

4.5 References

1. A. W. Smith, F. W. Mezsadors and C. D. Amata ; J. Amer. Ceram. Soc., 49(1966),240.
2. W. A. Fischer ; in "Fast Ion Transport in Solid -- solid state batteries and devices", edited by W. van Gool, pp.503-512, North-Holland Publishing Co., Amsterdom, 1972.
3. S. F. Palguev, V. K. Gildermann and A. D. Neujimin; J. Electrochem. Soc., 122(1975), 745.
4. C. B. Alcock and J. C. Chan ; Can. Met. Quart., 11(1972), 559.
5. K. Kitazawa and R. L. Coble ; J. Amer . Ceram. Soc., 57(1974),288.
6. T. Takahashi, H. Iwahara and I. Ito., DENKI KAGAKU 38(1970), 288.
7. F. A. Kröger and H. J. Vink ; "Solid State Physics" vol.3, edited by F. Seitz and D. Turnbull, p.310, Academic Press, New York, 1956.
8. C. Wagner ; Z. Phys. Chem., B21(1933), 25.
9. R. Hartung and H. Möbius ; Z. Phys. Chem., 243(1970) 133
10. H. Schmalzried ; Ber. Bunsenges. Phys. Chem., 66 (1962), 572.

11. H. Schmalzried ; Z. Phys. Chem., 38(1963), 87.

12. R. M. Barrer ; "Diffusion in and through Solid", p.37, Cambridge University Press, New York, 1941, c.f. J. C. Crank ; "The Mathematics of Diffusion" p.78, Oxford University Press, London , 1957.

13. L. N. Friedman, K. E. Obreg, W. M. Boorstein and R. A. Rapp ; Met. Trans. , 4(1973),69.

14. J. W. Patterson, E. C. Bogren and R. A. Rapp ; J. Electrochem. Soc., 114(1967), 752.

15. C. Wagner ; Z. Elektrochem., 60(1956),4, 63(1959) 1027.

16. P. H. Scaife, D. A. J. Swinkels and S. R. Richards ; High Temperature Science, 8(1976), 31.

17. T. H. Etsell and S. N. Flengas ; J. Electrochem. Soc., 119(1972),1.

18. D. A. J. Swinkels ; J. Electrochem. Soc., 117(1970) 1267.

19. K. S. Goto ; Trans. Iron Steel Inst. Japan., 16 (1976),469.

20. J. W. Patterson ; J. Electrochem. Soc., 118(1971), 1033

21. W. A. Fischer and W. Ackermann ; Arch. Eisenhüttenw., 36(1965), 643.

22. W. A. Fischer and D. Janke ; ibid, 41(1970), 1027.

23. W. A. Fischer and D. Janke ; ibid, 46(1975)755.

24. D. Jakne and W. A. Fischer ; Arch. Eisenhüttenw. , 46(1975), 477.

25. S. R. Richards, D. A. J. Swinkels and J. B. Henderson ; Proc. Internat. Conf. Sci. Tech. Iron. Steel., Suppl. Trans. Iron. Steel Inst. Japan., 11(1971), 371.

26. A. Kumar, D. Rajedev and, and D. L. Doughlass ; J. Amer. Ceram. Soc., 55(1972), 865.

APPENDIX-A Permeation of nitrogen through zirconia tube used in the present study

Preliminaly experiments were done to test the selective permeation of the zirconia tube from 1703 to 1873 K. The inside of the tube was evacuated , and the outside was flushed with a stream of nitrogen or oxygen. Pressure increase in the tube was measured for about 20 minutes after turning off the stopcock. The results of these preliminary experiments are shown in Fig.A.1 As shown in this figure, permeation of nitrogen is negligible in comparison with that of oxygen. These results show that the oxygen permeability under the present condition is not due to Knudsen diffusion through pores, diffusion through grain boundaries and molecular diffusion through cracks.

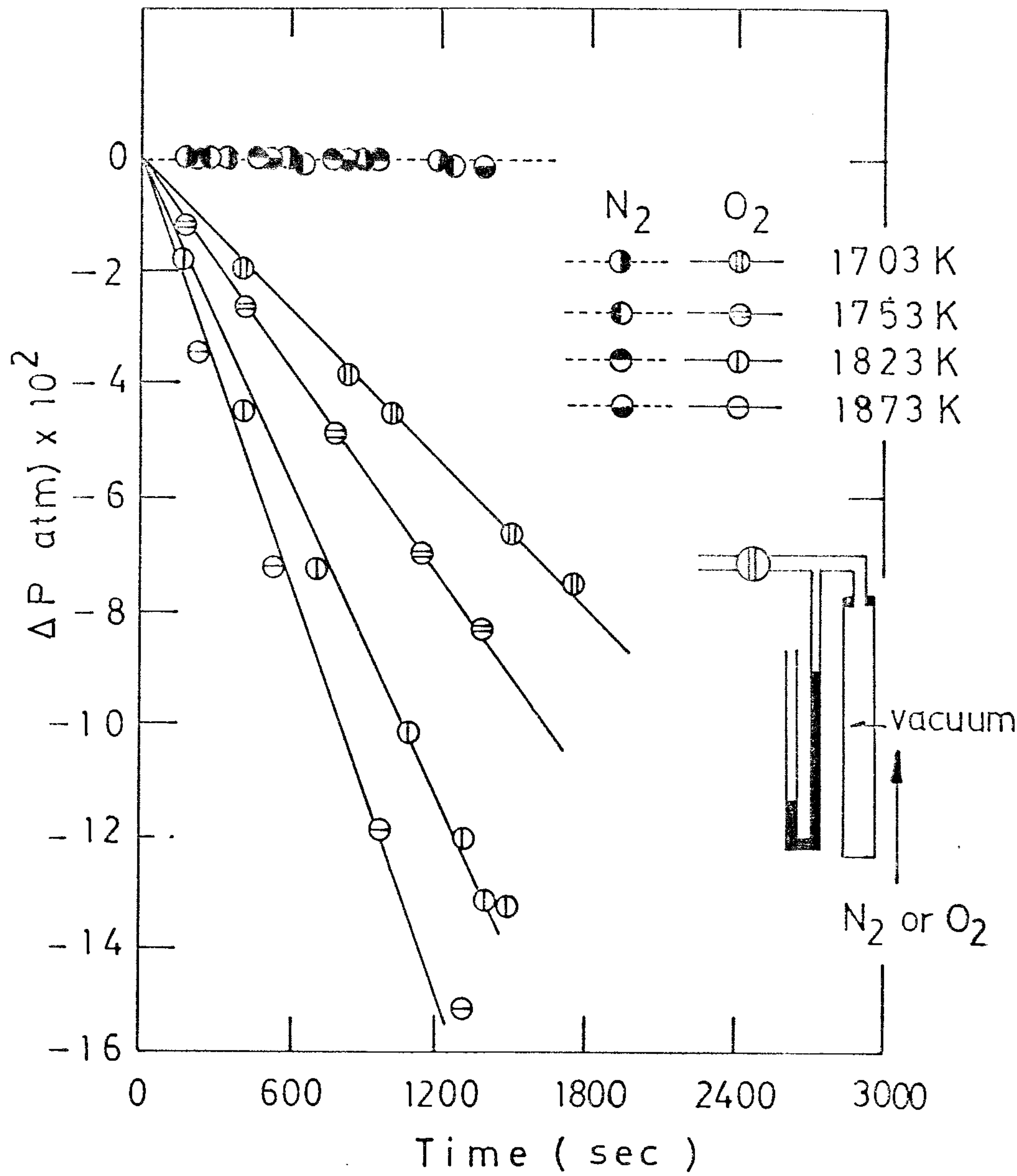

Fig.A-1 Pressure increase in the zirconia tube evacuated.

APPENDIX-B Calibration of effective permeation area for cell(I)

It is very difficult to measure the permeability at constant temperature because both the zirconia tube and the furnace have a temperature gradient in their axial direction. The temperature distribution in the SiC resistamce furnace is shown in Fig.B-1, which indicates that the distribution was nearly the same and homogeneous temperature zone of $\pm$ 5 K was about 40 mm long at each temperature. The contribution of homogeneous temperature zone to the total permeability could be calculated by eq.[B-1].

$$\frac{\dot{n}_{O_2}(\mathrm{h.t.z.})}{\dot{n}_{O_2}(\mathrm{total})} = \frac{\int_{X_1}^{X_2} [\exp(-\Delta Q/RT)/\exp(-\Delta Q/RT_\circ)]\, dX}{\int_{0}^{B} [\exp(-\Delta Q/RT)/\exp(-\Delta Q/RT_\circ)]\, dX}, \qquad \text{[B-1]}$$

where $\dot{n}_{O_2}$(h.t.z) is the permeability at homogeneous temperature zone of $\pm$ 5 K, $\dot{n}_{O_2}$(total) is the total permeability which can be calculated from eq.[1] of Chapter 4, B is the length of zirconia tube(cm), ΔQ is the apparent activation energy which can be

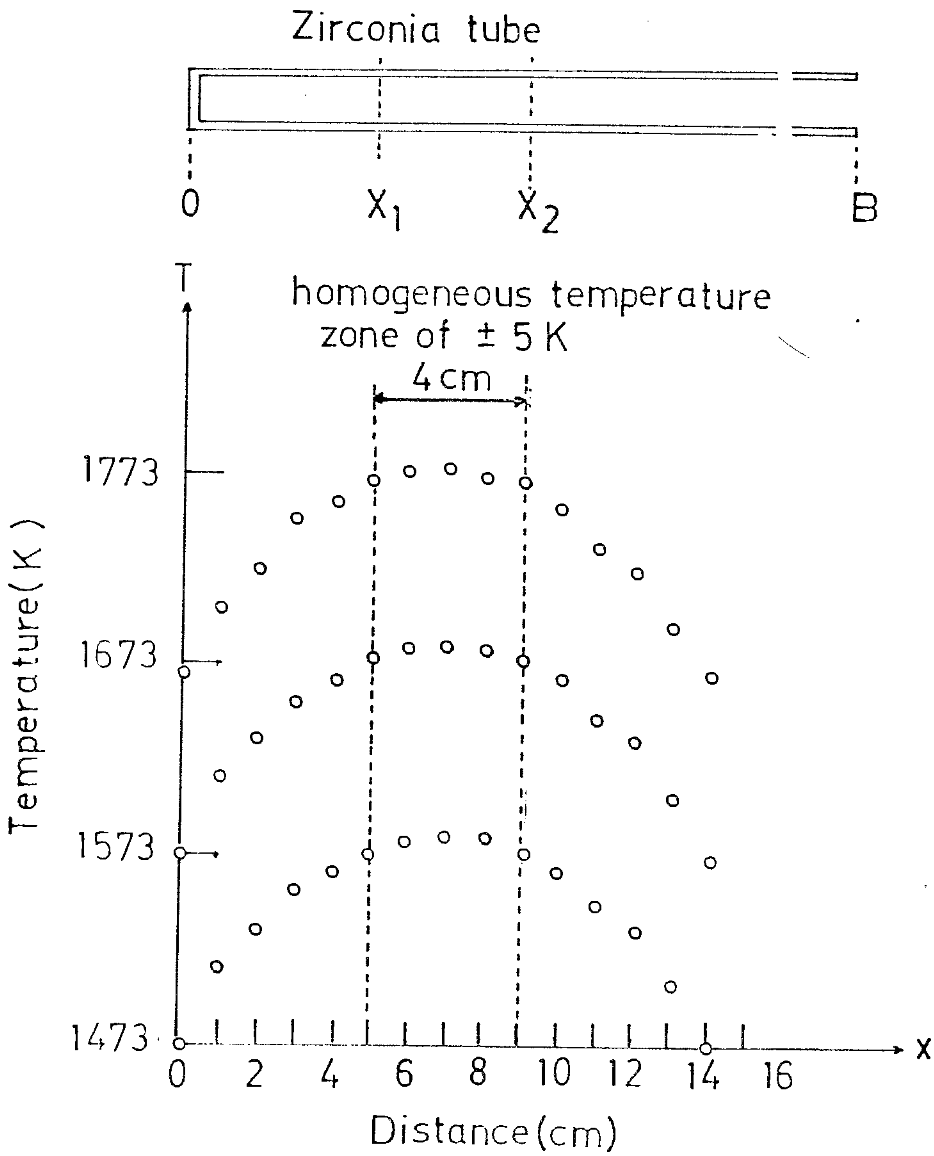

Fig.B-1 Temperature distribution in the SiC resistance furnace and the zirconia tube.

experimentally determined as described in 4.3.1 and assumed to be constant for the calculation of eq. [B-1], T_0 is the highest temperature in the homogeneous temperature zone and T is a function of distance X(cm). The value of $\dot{n}_{O_2}$(h.t.z.)/$\dot{n}_{O_2}$(total) was estimated to be 0.35 ± 0.03 from the graphical calculation by eq.[B-1]. So that the oxygen flux at homogeneous temperature zone can be calculated from eq.[B-2],

$$J_{O_2} = \dot{n}_{O_2} \times 0.35 \times \frac{\ln (r_2/r_1)}{(r_2 - r_1)\ 2\pi Y}, \qquad [B-2]$$

where r_2, r_1 and Y are outer radius of the zirconia tube, inner radius, and the length of homogeneous temperature zone of $\pm$ 5 K (cm), respectively. The effective permeation area, A, was calculated as

$$A = \frac{1}{0.35} \frac{2\pi(r_2 - r_1)\ Y}{\ln(r_2/r_1)} . \qquad [B-3]$$

APPENDIX-C Effective permeation area for cell(II)

The apparent activation energy of oxygen permeability for cell(I) would be explained by using eq.[22] of Chapter 4;

$$J_{O_2} = \frac{R\ T}{4\ F^2\ L}\ \sigma^{\circ}_{\oplus}\ (P'^{\ 1/4}_{O_2} - P''^{\ 1/4}_{O_2}) \qquad [22]$$

Eq.[22] can be rewritten as follows

$$\log J_{O_2} = \log \sigma^{\circ}_{\oplus} + \log (P'^{\ 1/4}_{O_2} - P''^{\ 1/4}_{O_2}) + \log \left(\frac{R\ T}{4\ F^2\ L} \right) \qquad [C-1]$$

Temperature dependence of the p-type electronic conductivity, $\sigma^{\circ}_{\oplus}$, would be represented as

$$\sigma^{\circ}_{\oplus} = (\text{const.}) \times \exp(-\Delta Q'/RT) \qquad [C-2]$$

Therefore, in a narrow range of temperature, the apparent activation energy of oxygen permeability for cell(I) would be nearly equal to $\Delta Q'$ of eq.[C-2].

On the other hand, the logarithm of eq.[31] yields

$$\log J_{O_2} = \log \left(\frac{R\,T}{4\,F^2\,L}\right)$$

$$+ \log \left(\sigma^{\circ}_{\oplus} P'^{\,1/4}_{O_2} + \sigma^{\circ}_{\ominus} P''^{\,-1/4}_{O_2} \right). \qquad [C-3]$$

Therefore, apparent activation energy of oxygen permeability for cell(II) can not be obtained. Consequently, similar calculation for the estimate of effective permeation area for cell(II) as that used for cell(I) would not be available. For convenience, the effective permeation area for cell(II) was assumed to be the same as that for cell(I). If the effective permeation area for cell(II) included an uncertainty of $\pm$ 30 %, the uncertainty of $\log P_{\oplus}$ and $\log P_{\ominus}$ would be $\pm$ 0.6.

APPENDIX-D Calculation of oxygen permeability by using Kirchhoff's law

The equilvalent electric curcuit for solid-oxide galvanic cell under open curcuit condiiton is shown in Fig.D-1. The solid-oxide galvanic cell can be considered to be short-curcuited by electronic resistance R_e. The theoretical e.m.f. of this cell can be expressed by

$$E = \frac{RT}{F} \ln \left(\frac{P'_{O_2}}{P''_{O_2}} \right)^{\frac{1}{4}} . \qquad [D-1]$$

When $P_{\oplus} \gg P'_{O_2} > P''_{O_2} \gg P_{\ominus}$,

the measured e,m.f. of this cell can be expressed by

$$E^* = \frac{RT}{F} \left[\ln \frac{P'^{\,1/4}_{O_2} + P_{\ominus}^{1/4}}{P''^{\,1/4}_{O_2} + P_{\ominus}^{1/4}} + \ln \frac{P''^{\,1/4}_{O_2} + P_{\oplus}^{1/4}}{P'^{\,1/4}_{O_2} + P_{\oplus}^{1/4}} \right] . \qquad [D-2]$$

From Kirchhoff's law, it can be easily deribed

$$E - E^* = I\, A\, R_{ion} , \qquad [D-3]$$

where I is leakage current density, A is cross-sectional area of electrolyte.

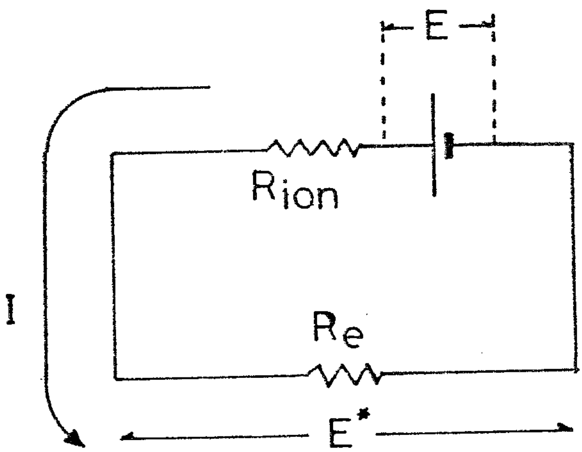

Fig.D-1 Equivalent electrical curcuit for solid-oxide galvanic cell involving solid electrolyte that exhibits mixed ionic and electronic conduction.

Therefore,

$$I = \frac{1}{A \cdot R_{ion}} \ (E - E^*)$$

$$= \frac{\sigma_{ion}}{L} \ (E - E^*) . \qquad [D-4]$$

The leakage current density is related to the oxygen permeability, J_{O_2},

$$4 F J_{O_2} = I. \qquad [D-5]$$

Introduction of eq.[D-5] into eq.[D-4] yields

$$J_{O_2} = \frac{\sigma_{ion}}{4 F L} \ (E - E^*) . \qquad [D-6]$$

Let us simplify the eq.[D-6] as follows

$$E - E^*$$

$$= \frac{RT}{F} \left\{ \ln \left[1 + \left(\frac{P_{\ominus}}{P''_{O_2}} \right)^{\frac{1}{4}} \right] - \ln \left[1 + \left(\frac{P_{\ominus}}{P'_{O_2}} \right)^{\frac{1}{4}} \right] \right\}$$

$$+ \frac{RT}{F} \left\{ \ln \left[1 + \left(\frac{P'_{O_2}}{P_{\oplus}} \right)^{\frac{1}{4}} \right] - \ln \left[1 + \left(\frac{P''_{O_2}}{P_{\oplus}} \right)^{\frac{1}{4}} \right] \right\} . \qquad [D-7]$$

Eq.[D-7] becomes

$$E - E^* = \frac{RT}{F}\left[\left\{\left(\frac{P'_{O_2}}{P_\oplus}\right)^{\frac{1}{4}} - \left(\frac{P''_{O_2}}{P_\oplus}\right)^{\frac{1}{4}}\right\} - \left\{\left(\frac{P'_{O_2}}{P_\ominus}\right)^{-\frac{1}{4}} - \left(\frac{P''_{O_2}}{P_\ominus}\right)^{-\frac{1}{4}}\right\}\right].$$

[D-8]

Sunstituting eq.[D-8] for eq.[D-6] yields

$$J_{O_2} = \frac{R\ T\ \sigma_{ion}}{4\ F^2\ L}\left[\left(\frac{P'_{O_2}}{P_\oplus}\right)^{\frac{1}{4}} - \left(\frac{P''_{O_2}}{P_\oplus}\right)^{\frac{1}{4}} - \left(\frac{P'_{O_2}}{P_\ominus}\right)^{-\frac{1}{4}} - \left(\frac{P''_{O_2}}{P_\ominus}\right)^{-\frac{1}{4}}\right]$$

$$= \frac{R\ T}{4\ F^2\ L}\left[\left(\sigma_{\oplus(P'_{O_2})} - \sigma_{\oplus(P''_{O_2})}\right) - \left(\sigma_{\ominus(P'_{O_2})} - \sigma_{\ominus(P''_{O_2})}\right]\right. \quad [D-9]$$

$$= \frac{R\ T}{4\ F^2\ L}\left[\sigma^\circ_\oplus\left(P'^{\frac{1}{4}}_{O_2} - P''^{\frac{1}{4}}_{O_2}\right) - \sigma^\circ_\ominus\left(P'^{-\frac{1}{4}}_{O_2} - P''^{-\frac{1}{4}}_{O_2}\right)\right].$$

[D-10]

APPENDIX-E Rate controlling step of permeability measurements for cell(I)

If the transport of oxygen from the inside of the zirconia tube to the outside for cell(I) was controlled by the rate of ionic diffusion through electrolyte and molecular diffusion through the outer gas phase, then the total transport rate of oxygen at a steady-state would be given by

$$J_{total} = \frac{R\ T}{4\ F^2\ L}\ \sigma^{\circ}_{\oplus}\ (P'^{\ 1/4}_{O_2} - P''^{\ 1/4}_{O_2}) \quad [E\text{-}1]$$

$$= (D/\delta\ RT)\ (P_i - P''_{O_2}) \quad [E\text{-}2]$$

where D is interdiffusivity of oxygen in $N_2 - O_2$ gas mixture, δ is the thickness of the laminar gas film, P_i is the oxygen partial pressure at the electrolyte/N_2-C interface, respectively. By using the diffusion theory of Hirschfelder et al , the interdiffusivity of oxygen was estimated to be 4.08 $cm^2\ sec^{-1}$ at 1823 K.

---

* R. B. Bird, W. E. Steward and E. N. Lightfoot; Transport Phenomena, p.511, John Willey and Sons Inc., New York, 1960

The value of δ can not exceed 0.35 cm(distance between the zirconia tube and the surrounding alumina tube). Therefore, the lowest value of (D/δ) is

$$D/\delta = 4.08/0.35 = 11.66 \text{ cm sec}^{-1}.$$

The calculated value of P_i from [E-2] with (D/δ) = 11.6 cm sec^{-1}, T = 1823 K, J_{total} = 6.93 x 10^{-9} mol cm^{-2} sec^{-1} and P''_{O_2} = 1 x 10^{-3} atm is 1.09 x 10^{-3}. Precisely, the transport of oxygen from the inside of the zirconia tube to the outside is controlled by the solid-state diffusion in the present study.

CHAPTER 5

GENERAL CONCULSION

1. The electromotive force measurements were performed for the determination of the standard free energies of formation of NiO, CoO and MoO_2 by using the following cells

cell(I) $Pt/air/ZrO_2(CaO)/Ni\text{-}NiO/Pt$,

cell(II) $Pt/Ni\text{-}NiO/ZrO_2(CaO)/ZrO_2(CaO)\,powder/co\text{-}CoO/Pt$,

cell(III) $Pt/Co\text{-}CoO/ZrO_2(CaO)\,powder/ZrO_2(CaO)/Mo\text{-}MoO_2/Pt$,

cell(IV) $Pt/air/ZrO_2(CaO)/Mo\text{-}MoO_2/Mo$.

The results are represented as

$$\Delta G^\circ(NiO)/kJ\ mol\text{-}NiO^{-1} = -\ 230.7 + 0.08489\ (T/K) \pm 0.4$$

from 973 to 1723 K,

$$\Delta G^\circ(CoO)/kJ\ mol\text{-}CoO^{-1} = -\ 229.0 + 0.06832\ (T/K) \pm 0.4$$

from 1473 to 1723 K,

$$\Delta G^\circ(MoO_2)/kJ\ mol\text{-}MoO_2^{-1} = -\ 576.1 + 0.1692\ (T/K) \pm 0.15$$

from 1273 to 1723 K,

$$\Delta G^\circ(MoO_2)/kJ\ mol\text{-}MoO_2^{-1} = -\ 509.6 + 0.1297\ (T/K) \pm 0.3$$

from 1723 to 1923 K.

2. The activities of oxygen in liquid iron, nickel and iron-nickel alloys were determined from 1773 to 1873 K by using the following cells

cell(I) $Mo/Mo-MoO_2/ZrO_2(CaO)/\underline{O}(in\ Fe)/Mo$,

cell(II) $Mo/Mo-MoO_2/ZrO_2(CaO)/\underline{O}(in\ Ni)/LaCrO_3/Pt$,

cell(III) $Mo/Mo-MoO_2/ZrO_2(CaO)/\underline{O}(in\ Fe-Ni)/Mo$.

The standard free energy changes for the solution of gaseous oxygen into liuqid iron and nickel were determined as

$$\Delta G°(O\text{-}Fe)/kJ\ mol^{-1} = -\ 84.5 - 0.0017\ (T/K) \pm 1.2$$

from 1823 to 1873 K,

$$\Delta G°(O\text{-}Ni)/kJ\ mol^{-1} = -\ 81.8 + 0.0084\ (T/K) \pm 1.2$$

from 1773 to 1873 K.

The activity coefficient for oxygen in liuqid iron-nickel alloys were determined as

$$\log f_O(Fe) = -\ 0.2[\%O] + (0.006 \pm 0.002)[\%Ni] + (7 \pm 8) \times 10^{-5}\ [\%Ni]^2 + 0.004[\%O][\%Ni]$$

or

$$\log f_O(\mathrm{Ni}) = -\ 0.6[\%O] + (0.024 \pm 0.002)\ [\%Fe] + (1 \pm 0.8) \times 10^{-4}[\%Fe]^2 - 0.004[\%O][\%Fe].$$

at 1873 K.

3. The oxygen permeability of solid-oxide electrolyte that exhibits mixed ionic and electronic conduction is given by

$$J_{O_2} = \frac{RT}{4\ F^2\ L}[\ \sigma^{\circ}_{\oplus}(P'^{\ 1/4}_{O_2} - P''^{\ 1/4}_{O_2}) - \sigma^{\circ}_{\ominus}(P'^{\ -1/4}_{O_2} - P''^{\ -1/4}_{O_2})].$$

The new parameter, $P_{\oplus\ominus}$, was introduced to discuss the oxygen permeability for specific case. This parameter shows the specific oxygen pressure at which the p-type and n-type electronic conductivities are equal. The oxygen permeability measurements can be used for the determination of the p-type and n-type electronic conductivities.

4. The conduction properties of calcia-stabilized zirconia used in the present study were determined as the functions of temperature as follows

from cell(I)

$$\log \sigma^{\circ}_{\oplus} = 0.28 - 5100\ (T/K)^{-1},$$

$$\log P_{\oplus} = -0.87 + 15400\ (T/K)^{-1},$$

from cell(II)

$$\log \sigma^{\circ}_{\oplus} = 8.81 - 23600\ (T/K)^{-1},$$

$$\log \sigma^{\circ}_{\ominus} = 2.05 - 7600\ (T/K)^{-1},$$

$$\log P_{\oplus} = 2.65 + 6500\ (T/K)^{-1},$$

$$\log P_{\ominus} = 24.12 - 70500\ (T/K)^{-1}.$$

Acknowledgements

The author would like to express his greatest thanks to Professor Doctor Toshisada Mori who guided the author to the study of this problem and has given the constatnt encouragement, discussions and suggestions through the cource of this study.

The author wishes to express his gratitude to the following persons, since without any help of them, this study could not have the present form; Professor Hiroshi Majima, Professor, Joichiro Moriyama, Professor Yoshio Kondo, Professor Zensaku Kozuka, Assistant Professor Kimio Fujimura, Dr. Toshio Oishi, Assistant Professor Eiji Ichise, Dr. Akira Moro-oka, Assistant Professor Zenichiro Takehara, Professor Shiro Yoshizawa, Professor Kiyohiko Fujita, Mr. Moto-o Yasuda, Mr. Shin-ichi Miki, Mr. Hiroshi Takeshita, Mr. Yoshiyuki Morimoto, Mr. Yoshio Ishihara, Mr. Takashi Kanazawa, Miss Hisae Owaki and his wife Yoriko C. Iwase.

Financial support by Sakkokai Foundation is also gratefully acknowledged. This work was financially supported by the Ministry of Education.

Papers concerning the present thesis

1. M. Iwase, K. Fujimura and T. Mori
   Thermodynamic study on liquid lead-silver alloys
   J. Japan Inst. Metals. 39(1975)1153. (in Japanese)
2. M. Iwase and T. Mori
   Electrochemical Measurement of oxygen in liquid iron
   Metal-Slag-Gas Reactions and Processes,
   edited by Z. A. Foroulis ans W. W. Smeltzer
   Electrochem. Soc. Inc., Princeton, 1975, p.885
3. M. Iwase, K. Fujimura and T. Mori
   Electrochemical Measurement of oxygen in inert gas
   J. Japan Inst. Metals. 39(1975) 952. (in Japanese)
4. M. Iwase, S. Miki and T. Mori
   Thermodynamic study of liquid $PbO-GeO_2$ slags by means of solid-oxide galvanic cell
   J. Chem. Thermodynamics, vol.11, 1979, in press.
5. M. Iwase, S. Miki and T. Mori
   Electrochemical Measurment of oxygen in liquid nickel
   J. Chem. Thermodynamics, vol.11, 1979, in press.

6. M. Iwase, S. Miki, H. Takeshita and T. Mori
Electrochemical measurement of oxygen in liquid iron-nickel alloys at 1873 K
J. Chem. Thermodynamics, vol.11, 1979, in press.

7. M. Iwase and T. Mori
Oxygen permeability of calcia-stabilized zircoia
Met. Trans. 9B (1978), No.3, p.365.

8. M. Iwase and T. Mori
Oxygen permeability of calcia-stabilized zirconia at low pxygen partial pressuress
Met. Trans. 9B (1978), No.4, in press.

9. M. Iwase, M. Yasuda and T. Mori
Free energy of formation of MoO_2 from EMF measurement
Electrochimica Acta, vol.24, 1979, in press.

10. M. Iwase and T. Mori
Oxygen permeability od solid-oxide eletrolyte and its influence on the electrochemical measurement of oxygen in liquid steel
Proceedings of the 3rd International Iron and Steel Congress, held at Chicago, April 16-20, 1978 in press.

11. M. Iwase and T. Mori
Problems in oxygen sensor for steelmaking
Preprints of the 3rd Germany-Japan Seminor, held at Düsseldorf, April 27,28, 1978, p.385.

12. M. Iwase, K. Fujimura and T. Mori
Thermodynamic study of liquid lead-silver alloys
by means of solid-oxide galvanic cell
Trans.Japan Inst, Metals. 19(1978),377.

13. M. Iwase and T. Mori
Problems in Oxygen Sensor for Steelmaking
Trans. Iron. Steel.Inst. Japan., vol.19, 1979, in press

14. M. Iwase, M. Yasuda, S. Miki and T. Mori
A Thermodynamic Study of Liquid Tin-Silver Alloys
by means of Solid-Oxide Galvanic cell
Trans. Japan Inst. Metals., vol.19, 1978,p.654.